STUDY OF SMOOTH MUSCLE CELL DIFFERENTIATION MEDIATED BY EPIGENETIC MECHANISMS

DISSERTATION ZUR ERLANGUNG DES
DOKTORGRADES DER NATURWISSENSCHAFTEN (DR. RER. NAT)
DER FAKULTÄT FÜR BIOLOGIE UND VORKLINISCHE MEDIZIN
DER UNIVERSITÄT REGENSBURG

vorgelegt von
Benjamín Isaías de la Cruz Thea
aus
San Luis, Argentinien

im Jahr 2022

Das Promotionsgesuch wurde eingereicht am:

25.02.2022

Die Arbeit wurde angeleitet von:

Dr. Melina Mara Musri
Universidad Nacional de Córdoba, Argentinien

Prof. Dr. Gunter Meister
Universität Regensburg, Deutschland

Unterschrift:

Dedication

I want to dedicate this thesis to Cristina Thea and Wilfredo de la Cruz†. For teaching me to think critically, to question myself. For supporting me unconditionally in my decisions. For giving me the confidence to get here. Because without them I wouldn't exist and because thanks to them I am who I am.

Acknowledgments

First of all I want to thank my mother Cristina Thea and my father Wilfredo de la Cruz†. They are not only responsible for my existence, but also the source of my critical thinking and curiosity, two attributes necessary to do any research work. Secondly to my brother Jeremías, who has always been a great inspiration for all my personal developments for as long as I can remember. Thirdly, I would like to thank Melina Musri, who has not only been my thesis director, but also a great teacher inside and outside the laboratory, and a very important emotional support throughout these years.

Of course I also want to thank my advisory committee, Dr. Vivas and Dr. Milesi, for accompanying me throughout these years in the development of this work. A special mention also goes to my co-director, Dr. Meister, who opened the doors of his laboratory to me at the University of Regensburg. At this point I would like to include those people who made my stays at the UR a real wonder. First of all, to my friend Hung Ho, who was my guide and unconditional help during my stays in the UR. Secondly to Carolin Apfel, coordinator of the international exchange program at UR, who helped me inside and outside the University to make my experience in Germany as great as it was. Many thanks to Franzi, Eva, Balu, Daniele, Johannes Graf, Johannes Danner, Norbert, Gerhard, Marcus, Jan, Claudia, Tiana, Alice, Hannes, Simone, Kevin, Michi, Julia, Dani, Astrid, Corinna, Birgitt, Sigi, and to all those people who contributed to a greater or lesser extent to making the UR feel like home in Germany. Many thanks to my Latin friends in Bavarian lands, Tatiana, Ingrid, Roman, Eder, Seba.

I do not want the contribution of the people of the Ferreyra Institute to go unnoticed, researchers and interns, technical support staff and secretaries. Both in academia and outside of it. Many heartfelt thanks to each and every one of the members of the IMMF. Special mentions to my colleagues and laboratory partners. It would not have been possible without you, thank you very much Victoria Pisano, Lautaro Natali, Ximena Volpini, Micol Ruiz and Romina Scolari.

I also want to thank the National University of Córdoba, for being my home for tertiary and postgraduate studies, as well as CONICET, for giving me the opportunity to work in the national scientific system through the doctoral fellowship.

In this sense, I would like to thank the University of Regensburg and the DAAD for the financial support received during the stays in Germany.

Last but not least. I want to thank all my family and friends. Some special mentions go to Gastón Thea, Emiliano Luna, Maximiliano Güelpa, Pablo Ayala, Fernando Vanoli, Juan Diego Pinotti, Emilia Calcagno, Guillermo Morera, Tomás Dupetit, Facundo Robino, Manuel Novillo, Alejandro Ferreiro, Agostina Lorca, Daihana Argibay, Alejandro Enet, Ignacio Santillán, Andrés Issaly, Andrea Bonino, Giovana Galfrascoli, Leandro García, Tobías Rojas and Ignacio Giménez.

To close, a special thank that cannot be missing: To my partner and unconditional support for the last few years, Andrea Guzmán. Thank you very much for joining me on this journey.

This thesis work was carried out thanks to the economic financing of the National Council for Scientific and Technical Research (CONICET), the Secretary of Science and Technology of the National University of Córdoba (SECyT-UNC) and the Ministry of Science and Technology of the province of Córdoba by the Argentine Republic; and the University of Regensburg and the German Academic Exchange Service (DAAD) through its International PhD program at the University of Regensburg (iPUR) on behalf of Germany.

Abstract

Smooth muscle cells (SMC) retain remarkable plasticity, which allows them to switch between a contractile differentiated and a proliferative de-differentiated phenotype in response to environmental cues. The alteration of this process constitutes a key factor in the development of cardiovascular diseases, highlighting the relevance of its study. A large body of evidence has shown that long non-coding ribonucleic acids (lncRNAs) regulate a number of physiological and pathological processes, yet little is known about the role of these molecules in SMC biology. Furthermore, RNA modifications have emerged as a new layer of post-transcriptional regulation in recent years. In particular, it has been shown that N6-methyladenosine (m^6A) participates in several fundamental biological processes, including cell fate decisions at different developmental stages. One of the main ways by which it regulates these processes is through the recognition of messenger RNAs (mRNAs) that contain this modification, by proteins that possess the YTH domain. In particular, the YTHDF2 reader has been implicated in the destabilization of modified RNAs, through the recruitment of the CCR4-NOT deadenylation complex. The objective of this thesis was to evaluate the participation of long non-coding RNAs in the phenotypic modulation of human SMC and to analyze the role of the m^6A deposition, reading and removal machinery in this process. By the use of RNA deep sequencing, several regulated lncRNAs were identified during an in vitro model of human pulmonary artery SMC differentiation. The characterization of a specific candidate was carried out, and it was given the name "***D**ifferentiation **A**nd **G**rowth **A**rrest related lnc**R**NA*" (*DAGAR*). A marked increase in DAGAR was observed during cell-to-cell contact-induced SMC differentiation which was shown to be necessary for this process. *DAGAR* expression decreased both during tumor necrosis factor (TNFα)-induced SMC dedifferentiation, and in total RNA isolated from pulmonary arteries of chronic obstructive pulmonary disease (COPD) diagnosed patients compared to non-smoking controls. *DAGAR* silencing promoted a decrease in the expression of SMC markers, indicating defects in the conversion of these cells into a differentiated phenotype, which was concomitant with an increase in proliferation. Pull-down of *DAGAR* by the use of 3' biotinylated DNA probes complementary to its sequence (raPOOLs, siTOOLs), followed by mass spectrophotometry, evidenced its

interaction with proteins of the m^{6}A methylation machinery. In correlation with these data, experiments of m^{6}A immunoprecipitation (IP) from total RNA showed that *DAGAR* was m^{6}A modified. Furthermore, *DAGAR* expression significantly increased after YTHDF2 silencing in both MRC5 lung fibroblasts and SMC. In addition, a marked decrease in not only YTHDF2, but also YTHDF1 and YTHDF3 was found during SMC differentiation. Immunoprecipitation of YTHDF2 followed by RNA deep sequencing (RIP-Seq) showed a specific enrichment of transcripts associated with SMC identity and biology, such as the smooth muscle myosin heavy chain (*MYH11*) and members of the TGFβ, PDGF and VEGF pathways, among others. Strikingly, YTHDF2 silencing in SMC promoted an increase in the expression of SMC specific markers. We conclude that SMC phenotype is regulated by the long non-coding RNA *DAGAR* and by the modulation of the m^{6}A reader protein YTHDF2.

CONTENT INDEX

Abbreviations

ACTA2: Smooth muscle alpha actin

ATP: Adenosine triphosphate

C643: Human thyroid carcinoma cell line, *Cellosaurus 643*

CALD: Caldesmon 1

CDK1: Cyclin-dependent kinase 1

cDNA: Complementary DNA

CNN1: Calponin 1

COPD: Chronic Obstructive Pulmonary Disease

CRISPR: Clustered Regularly Interspaced Short Palindromic Repeats

DMEM: Dulbecco's Modified Eagle Medium

DMSO: Dimethyl Sulfoxide

DNA: Deoxyribonucleic Acid

EDTA: Ethylenediaminetetraacetic acid

EndoMT: Endothelial-to-Mesenchymal Transition

FBS: Fetal Bovine Serum

FTO: Demethylase named "Fat mass and obesity related"

gRNA: Guide RNA

HEK293: Human embryonic kidney 293 cells

hPAEC: Human Pulmonary Artery Endothelial Cells

hPASMC: Human Pulmonary Artery Smooth Muscle Cells

iPSC: Induced Pluripotent Stem Cells

lncRNA: Long non-coding RNA

m^{6}A: N6-methyladenosine

METTL3: N6-methyladenosine methyltransferase

MF: Myofibroblast

miRNA: MicroRNA

MRC5: Human fetal lung fibroblast cell line named MRC5 (*Medical Research Council 5*)

mRNA: Messenger RNA

MRTF: Myocardin-related Transcription Factor

MYH11: Myosin Heavy Chain 11 (Smooth muscle)

MYOCD: Myocardin

PCR: Polimerase Chain Reaction

PDGFRB: Receptor type B of the Platelet Derived Growth Factor

RISC: RNA-induced silencing complex

RNA: Ribonucleic Acid

RNAi: Interference RNA

rRNA: Ribosomal RNA

RT-qPCR: Retrotranscription and Quantitative Polymerase Chain Reaction

SMAD: Family of genes that belong to the TGFβ pathway named "Small worm phenotype – Mothers Against Decantaplegic" as reference to the SMA protein from *Caenorhabditis elegans* and MAD protein from *Drosophila melanogaster*, due to their homology

SMC: Smooth muscle cell / Smooth muscle cells

SRF: Serum Response Factor

TGFβ: Transforming Growth Factor Beta

TNFα: Tumor Necrosis Factor Alpha

tRNA: Transfer RNA

UPR: Unfolded Protein Response

WHO: World Health Organization

YTHDF1/2/3: Members 1/2/3 of the Family of proteins with YT512-B homology domain

Chapter 1
INTRODUCTION

1 Introduction

1.1 Cardiovascular diseases

According to a follow-up study carried out by the World Health Organization (WHO) over the last two decades (2000-2019), ischemic heart disease, heart attacks and chronic obstructive pulmonary disease (COPD) currently constitute the three main causes of death worldwide [1]. In particular, in Argentina, cardiovascular diseases top the list, only behind the large group of “non-communicable diseases”, of which they are also part. In 2016, according to the data collected by the WHO, the number of age-standardized deaths due to cardiovascular diseases in the Argentine Republic was 424.7 per 100,000 inhabitants [2]. For the current population of approximately 45,000,000 inhabitants, this means a total of more than 190,000 deaths per year.

The prevalent and widespread occurrence of these pathologies highlights the importance of understanding the mechanisms underlying vascular homeostasis and its relationship with the development of cardiovascular pathologies.

Most of these non-communicable diseases comprise the development of a process called vascular remodeling, which is defined as a structural alteration of the vessel wall in response to changes in long-term hemodynamic conditions [3, 4].

1.2 Vessels and vascular remodeling

In humans, blood vessels are widely distributed within the body, forming extensive networks and accumulating more than 100,000 km in their total length [5]. This is partly due to the great branching and diversity of structures and sizes that they can adopt. The vessels are formed during embryogenesis in a process known as vasculogenesis. Cells of the mesoderm denominated hemangioblasts and embryonic nucleated erythrocytes form the so-called "blood islets" that will give rise to the endothelial (located towards the external side) and hematopoietic (towards the internal side) progenitor populations respectively. These proto-vessels form the primary capillary plexus from which the primary cardiac tube will be derived, by fusion of vessels, which will give rise to the heart. During the maturation of the vasculature, smaller caliber proto-vessels such as arterioles and venules are covered by mural cells, also known as pericytes. In the case

of capillaries, the amount of surrounding pericytes is negligible, although they still play important roles in their gating. These cells share many characteristics with smooth muscle cells (SMC), end express common markers such as smooth muscle alpha actin (ACTA2) and platelet-derived growth factor receptor beta (PDGFRB). Although they are believed to have a common progenitor, pericytes express a limited repertoire of contractile proteins and lack calponin (CNN1) or caldesmon (CALD), both of which are involved in the contraction of vascular SMC [6]. The concentric deposition of SMC of various origins will lead to the maturation of the main arteries and veins of the cardiovascular system. During this process, vascular SMC are recruited and differentiated from cellular progenitors of various embryonic origins. For example, the SMC that cover the aortic arch are derived from the neural crest and those responsible for bulging the pulmonary arteries come from the pleural mesothelium, while the thoracic and abdominal aortic sections are covered by SMC differentiated from the mesodermal somites, and the splanchnic mesoderm , respectively [7].

In the adult, blood circulation is complete and occurs from the heart, to the large-caliber arteries, which are thick, elastic and highly muscular, and serve as a guide to the main areas to be irrigated. It is for this reason that they are also called elastic or conductive arteries. In this group we can find the aorta, the pulmonary arteries and the carotids. From them, the blood continues through the medium-caliber arteries, also called distributing muscular arteries, to the target organs and their arterioles, to then branch into a large capillary plexus and thus finally deliver oxygen and nutrients to the cells of the tissue. The exchange of substances from the capillaries occurs through a complex regulation of permeability and diffusion mechanisms by endothelial cells and pericytes. Terminal arterioles, also known as pre-capillary arteries, divide into meta-arterioles and blood flow through them is controlled by pre-capillary sphincters made up of pericytes. After diffusing the oxygen and nutrients, the blood circulates towards post-capillary venules and continues through medium and large caliber veins, to return to the heart and be sent to the lungs where it is re-oxygenated. From the lungs it returns to the heart and the cycle begins again.

The characteristic structure of a blood vessel depends on its size and the function it performs. In particular, large and medium caliber veins and arteries have three layers or tunics: the external or adventitia, consisting mainly of fibroblasts and elastic fibers;

the media, made up of smooth muscle cells, and also elastic fibers in the case of arteries; and the intima, represented mainly by a monolayer of endothelial cells called the endothelium, together with its basal lamina. As arteries and veins decrease in caliber, the thickness of the wall and the proportion of elastic proteins in them also decrease. In the penultimate instance are the arterioles, which have only some surrounding smooth muscle cells or pericytes; and the venules which are also encompassed by some pericytes. Finally, capillaries constitute the connection point between both groups of vessels, and are represented by endothelial cells and their basal lamina, shared with a few surrounding pericytes.

In the present research work, primary smooth muscle cells derived from human pulmonary arteries were studied. These arteries are highly muscular and their SMCs are particularly interesting to investigate, since the alteration of their homeostasis during pulmonary vascular remodeling constitutes one of the main factors involved in the development of pulmonary diseases such as COPD and pulmonary hypertension [8-11].

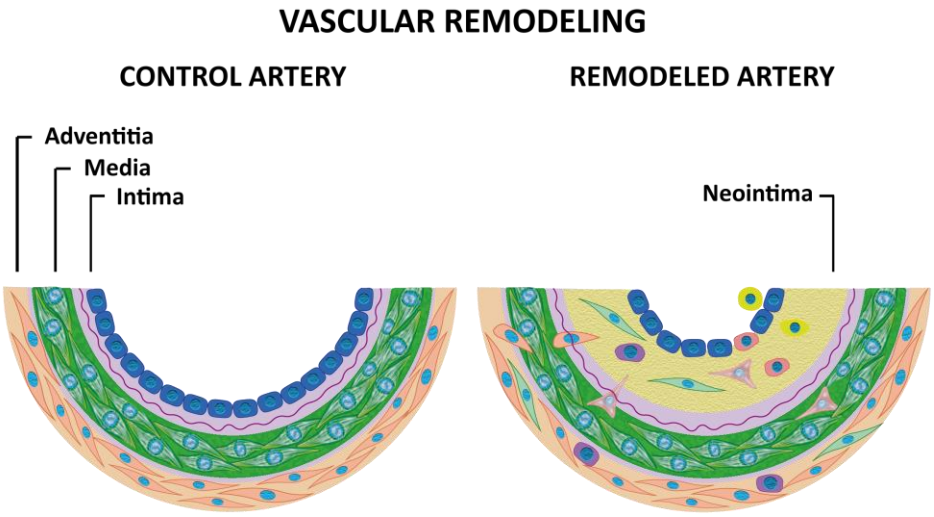

Figure 1. Vascular remodeling. Structural alteration. Representative schematic of a healthy artery (left) and a remodeled artery (right). A thickening of the arterial wall can be observed, constituting a new layer called neointima, populated by different cell types from different origins.

It should be noted that although vascular remodeling may constitute a normal and reversible physiological process, as occurs with exposure to high altitude for a prolonged period of time, hereinafter is referred to as "vascular remodeling" to the pathological and irreversible structural alteration of vessels (Figure 1). During the development of this process, the internal caliber, or "vessel lumen" decreases, while the total thickness

of the vessel can remain either constant or increase. This causes an augmentation of the peripheral resistance, which leads to the increase in local blood pressure and the reduction of gas exchange. This phenomenon generates localized changes in blood flow, hypoxia and inflammation, which are both the cause and consequence of vascular remodeling at the local level taking part of a positive feedback loop, thus exacerbating the thickening of the vessel wall. These structural changes are mediated by the proliferation and migration towards the intima of cells from various sources that in general express alpha smooth muscle actin and originate the neointima. Among the cell types that invade the intima, it has been described the participation of circulating and local progenitor cells, fibroblasts differentiated into myofibroblasts, endothelial cells that have undergone a process of transition from endothelium to mesenchyme or Endo-MT (Endothelial to Mesenchymal Transition) and SMC that have undergone a phenotypic switch, among others (Figure 2)[12]. The neointimal thickening is usually accompanied by the thickening of the media or, in the case of arterioles, by a muscularization process, significantly increasing the number of SMC lining the vessel and thus making gas exchange difficult.

The signaling mechanisms involved in vascular remodeling have not yet been fully elucidated.

It is widely accepted that dysfunction of the mechanisms that control both the differentiation and maintenance of the cell phenotype in the artery are key factors involved in the development of this process. Therefore, during the progress of vascular remodeling there is an increased cell proliferation, cell dedifferentiation, cell transdifferentiation and excessive synthesis of extracellular matrix [12-17].

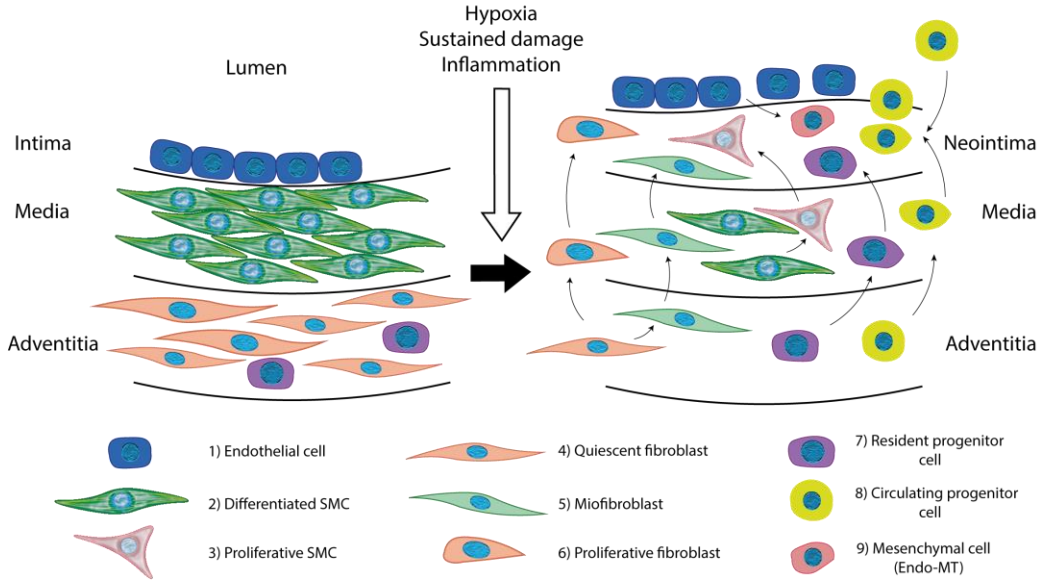

Figure 2. Cell processes involved in the development of vascular remodeling. Cells involved. In conditions such as chronic hypoxia, sustained vascular damage or chronic inflammation, numerous cell types undergo changes in cell phenotype and show an increase in proliferation, contributing to the formation of the neointima and vascular remodeling. Some of the cells that contribute to this process are depicted in the diagram. Endothelial cells (1) can undergo a process called Endothelial to Mesenchymal Transition (9). Differentiated smooth muscle cells (SMCs) (2) can undergo phenotypic modulation and re-enter the cell cycle, acquiring a highly synthetic and proliferative phenotype (3). The quiescent fibroblasts of the adventitial layer (4) have the ability to differentiate into myofibroblasts (5), as well as to migrate in a proliferative state (6). Other sources, such as resident (7) or circulating (8) progenitor cells have been reported, however their contribution to neointima formation appears to be relatively low.

1.3 Smooth muscle cells (SMC)

SMC, which make up the medial layer, play an important role in maintaining the structure and function of the arterial wall. These cells are highly plastic and have an intrinsic mechanism of phenotypic change that in a normal physiological environment allows them to respond to microenvironmental cues through the integration of different signals [18]. This physiological mechanism of differentiation-dedifferentiation is called "**SMC phenotypic swtich**" [19]. Dedifferentiated SMC exhibit high expression of extracellular matrix proteins and a low level of contractile proteins. In addition, dedifferentiated SMC display high proliferation and migration rates [18]. The terms "differentiated" and "contractile phenotype" on the one hand and "dedifferentiated" or "proliferative phenotype" on the other are used synonymously. Although this phenomenon was described in a large number of *in vitro* studies, it has recently been shown *in vivo* that in response to sustained vascular damage, SMC undergo an

irreversible phenotypic change with increased proliferation and migration. In addition, through lineage tracing studies, it has been shown that SMC not only undergo a conversion into dedifferentiated phenotypic stages, but also, SMC can transdifferentiate, acquiring markers of other different cell types, including those of macrophages, mesenchymal stem cells, osteo-chondroblasts, etc. [20].

1.4 Fibroblasts

Fibroblasts are tough, flexible cells that make up the interstitium, known as connective tissue. In turn, these are the main cells in charge of wound repair. This ubiquitous cell type plays an important structural role in the vessels under physiological conditions, providing flexibility and resistance, as well as in the development of pathologies [13]. Similar to what occurs with SMC, dysregulated proliferation and migration, differentiation into myofibroblasts (MF), together with the excessive synthesis and deposition of extracellular matrix proteins are the main ways in which fibroblasts contribute to the development of vascular remodeling [21-26]. Fibroblasts are capable of modulate their phenotype between proliferative/migratory and quiescent/polarized states in response to different stimuli, such as damage, cell contact or nutrient availability [26, 27]. In addition, they have the ability to transdifferentiate into other cell types, or acquire specific characteristics, depending on their origin and location (reviewed in [13]). In the same way, other cell types can be transdifferentiated to "mesenchymal" cells, obtaining characteristics similar to those of fibroblasts, such as the transformation of endothelial cells into mesenchyme or endothelial to mesenchymal transition (Endo-MT or En-MT) [28]. Fibroblasts express a repertoire of proteins typically expressed by SMC, such as TAGLN or ACTA2. These fibroblasts with muscular characteristics are known as myofibroblasts (MF). MF can originate from mesenchymal stem cells, as well as from pericytes or SMC [19, 29, 30]. However, due to the multiplicity of origins, MF are not considered as a cell type *per se*, but rather a functional state of the cell [19]. MF present a response similar to SMC when treated with TGFβ, inducing the expression of SMC markers [31, 32] or after treatment with PDGF, which increases their proliferation and migration [33, 34].

1.5 Signaling pathways involved in SMC differentiation

Smooth muscle cells have a complex network of signaling pathways that modulate the expression of key genes for the development of their physiological cellular activity within the tissue. The main characteristic of SMC in a differentiated state is its contractility. This is possible due to the development of a cytoskeleton rich in contractile proteins [15]. In particular, the smooth muscle myosin heavy chain (MYH11) has been described and remains to date as the most specific marker of this cell type [35]. The filaments of these proteins give the smooth muscle cell the ability to respond to mechanical forces applied to its structure, and in the particular case of arterial smooth muscle, to the regulation of vessel tone and blood pressure. In a normal physiological environment, these cells are in a quiescent state, with negligible rates of proliferation. However, faced with damage to the vasculature, smooth muscle cells and local fibroblasts modulate their phenotype in order to contribute to vessel repair. Unlike other cell types such as striated muscle cells, cardiomyocytes or neurons, which complete an irreversible process of differentiation, SMC retain a functional plasticity that allows them, in response to specific stimuli, to exit the quiescent state, disintegrate the fibrillar proteins of their contractile cytoskeleton and return to a proliferative and migratory phenotype (reviewed in [18, 30]), which is particularly useful for the repair of such an important structural tissue as the arterial wall.

This phenotypic plasticity is finely regulated by a complex network of interacting signaling pathways (Figure 3). Chronic exposure to factors that induce their phenotypic modulation causes the mechanisms of differentiation and proliferation to be pathologically disturbed, which generate vascular alterations that often undergo

positive feedback loops, triggering the development of serious vascular pathologies.

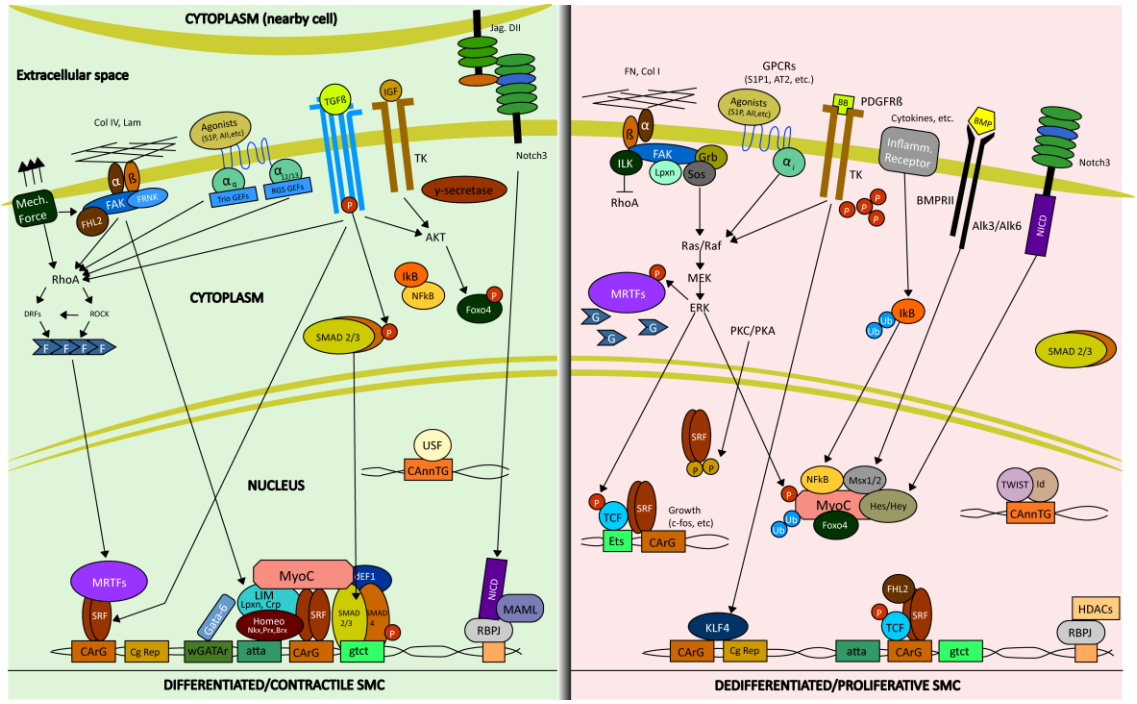

Figure 3. Signaling pathways involved in smooth muscle cell (SMC) differentiation. The different signaling cascades can be seen in differentiated (left) or proliferative (right) CML. Modified from [30].

The differentiation process in SMC requires the binding of the serum response transcription factor (SRF) to serum response elements (SRE) present in *cis* in the promoter region of most SMC-specific genes. These elements called CArG boxes have the sequence CA(A/T)$_6$GG. More than one CArG box can be observed in most SMC genes, which act cooperatively to induce transcription [36, 37].

SRF expression and function is not restricted to SMC [38] and therefore requires contextual cues to assist its action. Regulation of SRF activity depends on the proteins it associates with. In smooth muscle cells, its activity is mainly mediated by myocardin-related transcription factors (MRTF-A and MRTF-B), the GATA family of transcription factors (GATA6 in particular) and NkX, as well as by cofactors, mainly myocardin (MYOCD) [39].

The zinc finger transcription factors of the GATA family interact with DNA in consensus A/T GATA A/G (WGATAR) sequences. Factors GATA4/5 and 6 are essential for the development of the cardiovascular system [40], however, GATA6 is the only one that is expressed in SMC of the medial layer of arteries [41]. GATA6 regulates SMC phenotype in vivo by promoting the expression of MYH11, smooth muscle alpha actin (ACTA2) and calponin (CNN1) [42]. In addition, it directly regulates the progression of the cell cycle,

ergo proliferation [43]. After vascular damage, recovery of GATA6 expression levels prevents increased proliferation and hyperplasia of the intima [42].

Of the transcription cofactors with which SRF interacts, in particular, MYOCD has been widely considered the master regulator of SMC differentiation, since MYOCD overexpression is capable of inducing the transcription of most of the SMC specific genes in related cell types [44], in particular those that encode proteins important for the cytoskeleton and its contractile capacity, such as ACTA2, MYH11, CNN1, CALD and transgrelin (TAGLN) [36]. To accomplish this task, MYOCD behaves as a transcriptional co-activator, forming a complex with SRF and binding to specific promoters that contain SREs. Its importance in the differentiation of SMC is such that transgenic mice lacking this protein die at embryonic day 10.5, with defective vascular SMC phenotypes [45]. However, its expression is not sufficient for the induction of the complete differentiation plan of SMC from multipotent stem cells [46], being therefore a necessary but not sufficient condition for the differentiation of SMC. This fact reveals that we still do not know which is the master gene governing the differentiation of this cell type, in case it exists, or if the mechanisms involved In SMC lineage commitment are different than those observed for terminally-differentiated cell types.

Numerous regulatory mechanisms have been reported for MYOCD, its main inducers are the transforming growth factor beta (TGFβ), angiotensin II (Ang II) and the family of genes with homology to RAS member A (RhoA) [47-49]. Its main inhibitors are the platelet-derived growth factor BB (PDGFBB) and the inflammation-related factor NFkB [50, 51]. In addition, its function is dependent on the expression of isoforms generated by alternative splicing. In cardiac muscle and proliferative SMC, a type of canonical mRNA molecule is produced that codes for the full form of myocardin by skipping exon 2a. In differentiated cells, the inclusion of this exon introduces an in-frame stop codon which produces a truncated form of MYOCD that does not have the site of interaction with MEF2, which is involved in activation of cardiac gene transcription. This variant that includes exon 2a has a stronger effect when activating the promoters of specific SMC genes [52]. It has been observed that this phenomenon is mediated by the RBPMS protein (RNA Binding Protein with Multiple Splicing) and antagonized by the QKI protein (Quaking Homolog, KH Domain RNA Binding) [53].

Another regulatory mechanism for MYOCD and its associated factors (MRTFs) is the binding to glomerular actin through its RPEL domain, which contains tandem repeats of the RPEL motif [54]. In MRTFs, this binding prevents their nuclear localization and therefore blocks their activity. When the RhoA-dependent actin polymerization, induced by angiotensin II (ANG II), sphingosine-1-phosphate (SP1), TGFβ, Ca2 +, BMP2 or cell tension is activated [55], G-actin is rapidly depleted from the cytoplasm and allows MRTFs to be transported into the nucleus [56], where they form MRTF/SRF complexes and bind to consensus CArG elements in promoters of genes important for contractility such as ACTA2 and TAGLN [36, 37, 57, 58]. Meanwhile, MYOCD remains in the nucleus since it does not have a high affinity to G-actin. In the case of MYOCD, the RPEL domain binds to Arp5, a protein that prevents the binding of the MYOCD/SRF complex to SMC specific promoters, by interacting with the CArG domains through its C-Terminal region [59].

Post-translational modifications can also affect MYOCD activity, it has been observed that glycogen synthase kinase 3b (GSK3B) and extracellular signal-regulated kinase (ERK) phosphorylate it [60, 61], which results in reduced expression of SMC markers.

The decrease of MYOCD has been observed in several models of vascular damage, and the induction of its expression prevents the formation of neointima in carotid arteries of mice after injury [62, 63].

Of the inducers of MYOCD, the TGFβ signaling pathway is of vital importance in the differentiation of SMC. The ligand TGFβ1 is synthesized as a latent form (LTGFβ) that is activated via proteolytic cleavage by endoproteases such as FURIN [64]. The active ligand binds to type II TGFβ receptors (TGFβRII) with the help of the beta-glycan TGFβRIII [65]. This triggers the formation of tetrameric heterocomplexes with the type I TGFβ receptor called ALK5, which induces their phosphorylation. Activation of ALK5 promotes endocytosis of receptors in vesicles containing the SARA protein (SMAD Anchor for Receptor Activation), which is capable of binding SMAD proteins [66]. Recruitment and phosphorylation of SMAD2/3 heteromeric complexes occurs in these vesicles. After interaction with SMAD4, the SMAD2/3/4 complex translocates into the nucleus where it activates transcription by direct binding to DNA in functional elements called SBE

(*Smad-Binding Element*) on specific promoters, or through interaction with other transcription factors. SMAD6 and SMAD7 negatively regulate TGFβ signaling, since they compete for binding to SMAD4 and their interaction with TGFβ receptors mediates their degradation [67]. At the nuclear level, there are TGFβ control elements called TCE (*TGFβ Control Element*) with the consensus sequence G(A/C)GT(T/G)GG(T/G)GA in several promoters of specific SMC genes and its deletion has been shown to inhibit the transcription of the TAGLN gene [68]. In the same line, TGFβ1 increases SRF binding to CArG boxes and induces SMC gene expression [69].

In this way, the complex network of interactions between the different signaling pathways that regulate phenotypic expression in this cell type is glimpsed. During wound healing under physiological conditions, cell contact is of vital importance at the time of phenotypic modulation. The Notch signaling pathway plays a crucial role in SMC homeostasis and vascular development [70]. In mammals, there are 4 transmembrane Notch receptors (NOTCH1/2/3/4), of which NOTCH3 is preferentially expressed in SMC. The ligands for this receptor are the transmembrane Jagged 1/2 and delta-like 1/3/5 receptors. Upon cell-to-cell contact, the activation of the NOTCH3 receptor leads to the release of the intracellular domain of Notch (NICD), allowing its interaction with RBPJ (Recombination signal-binding protein for immunoglobulin kappa J region). The NICD-RBPJ complex stimulates the expression of genes related to contractility in SMC, in particular ACTA2, MYH11 and microRNAs-143/145 [71-74]. Conversely, while NICD is anchored to the NOTCH3 receptor, RBPJ recruits histone deacetylases (HDACs) for the repression of target genes [75].

Taking into account the aforementioned signaling pathways, it is evident that it is possible to trigger cell differentiation through cell-cell interaction, both by tension in the cell membrane, which promotes the activation of RhoA and the consequent translocation of MRTFs to the nucleus; as well as through the activation of Notch signaling with the formation of the NICD-RBPJ complex and subsequent activation of its target genes.

A large number of smooth muscle-specific promoters, including TAGLN [76], MYH11 [77] and ACTA2 [78, 79] contain E-box binding sites, with sequence CAnnTG. This motif preferentially binds homo or heterodimeric bHLH proteins (basic Helix Loop Helix)

[80] and the SNAIL family of transcription factors. In particular, bHLH proteins can inhibit or stimulate the transcription of SMC-specific genes that contain E-boxes. USF (Upstream Stimulatory Factor), E2-2, E12 and HEB stimulate the expression of ACTA2 [81] while ID and Twist decrease the expression of ACTA2 and TAGLN [82, 83]. It has also been described that some of them interact directly with MYOCD and can inhibit the expression of SMC marker genes, among them we can mention HERP1/HEY2, MSX1 and MSX2 [73, 84]. In addition, the SNAIL family of transcription factors can bind to E-Boxes, in this sense our laboratory has reported that SNAI2 promotes a proliferative phenotype in SMC [85].

The phenotypic regulation of SMC is largely mediated by factors that suppress SMC gene expression. The factors that regulate phenotypic modulation after vascular damage *in vivo* are not yet fully known, however PDGF-BB has shown to play an important role in this process.

Although there are 4 variants of PDGF (A, B, C and D), the active ligand is composed of homo or heterodimers (only formed by A and B) of it. There are two types of receptors, both of the tyrosine-kinase type, alpha (PDGFRA) and beta (PDGFRB), the latter being the one with the highest affinity for PDGF-BB (reviewed in [86]). PDGFRB is expressed in smooth muscle cells, being often used as a marker of this cell type, as well as pericytes. During angiogenesis, that is, the generation of new vessels in the adult, the endothelial cells that have formed the proto-vessel secrete PDGF-BB, which allows the recruitment of SMC and surrounding pericytes [87]. Activation of the PDGFRB receptor in these cell types induces phenotypic modulation, proliferation, and chemoattractant migration toward secreting endothelial cells to promote lining of the developing vessel. Phenotypic modulation after PDGF-BB-induced vascular damage is mediated by the expression of the transcription factor KLF4 or 5 (Krüppel-Like zinc Finger 4/5) [50]. KLF4 represses genes which are important for SMC differentiation such as MYOCD and TAGLN [88]. Furthermore, PDGFRB activation triggers the RAS/RAF/MEK/ERK signaling cascade, activating the expression of SRF-dependent developmental genes, while inducing phosphorylation and consequent inactivation of MYOCD and MRTFs [89].

As mentioned at the beginning of the introduction, one of the most important factors in vascular pathogenesis is the decrease in gas exchange, that is, hypoxia. It is

widely known that the activation of hypoxia-inducible transcription factors (HIF-1 and HIF-2) mediates the development of both venous and arterial vascular pathologies [90-92]. In particular, the development of pulmonary hypertension is directly associated with hypoxic conditions [16, 93]. During the development of diseases that involve remodeling of lung tissue, such as asthma or pulmonary hypertension, angiogenesis plays a key role. During hypoxic events, the transcription factor HIF-1, composed of a heterodimer of HIF-1α and HIF-1β, is stabilized and translocates into the nucleus, where it binds to hypoxia response elements (HRE) in promoter regions of target genes. The vascular endothelial growth factor (VEGF) is the main stimulator of angiogenesis, and is induced in response to hypoxia [94, 95]. VEGF mediates increased permeability and proliferation of endothelial cells (reviewed in [96]), which in turn secrete mitogenic and pro-migratory factors such as PDGF-BB and induce activation of smooth muscle cells by this pathway. Hypoxia has also been documented to directly induce vascular SMC proliferation through the induction of the transcription factor FoxM1 in a HIF-2α-dependent manner [97]. This factor is significantly increased in lung tissue from patients with idiopathic pulmonary hypertension. Through studies with experimental models of pulmonary hypertension and with the use of transgenic mice with constitutive expression or with inducible silencing of FoxM1, its participation in the regulation of SMC proliferation and pulmonary vascular remodeling was revealed. It has also been observed in recent studies that FoxM1 can be induced through factors secreted by the endothelium during angiogenic processes, such as PDGF-BB and endothelin (ET-1), among others [98].

Chronic inflammatory states, such as smoking and chronic metabolic pathologies including obesity and diabetes are usually associated with sustained vascular damage, and have direct consequences on SMC homeostasis [85, 99]. Inflammation-induced phenotypic change is mediated not only by the loss of positive signals, but also by multiple supplemental repressor pathways of differentiated SMC-specific genes. In this sense, it has been shown that KLF4 and SP1 are involved in the silencing of SMC-related contractile filament genes [50]. Remarkably, numerous transcriptional pathways that induce the transition of epithelial cells to mesenchymal cells (EMT) share common molecular mechanisms with the phenotypic change of SMC.

In human umbilical vein endothelial cells (HuvECs), the TNFα induced EndoMT is

dependent on the activation of the TGFβ pathway and SMAD2/3 signaling. This activation induces the expression of the type I receptor TGFβ ALK5, as well as activin A and integrin alpha V and therefore TAGLN expression is induced together with the acquisition of a mesenchymal phenotype [100]. TGFβ signaling through activin A is typical of cells in a multipotent state, and therefore can be considered as a phenotypic regression by endothelial cells [101].

In smooth muscle cells, TNFα induces a dedifferentiated state with a significant decrease in differentiated SMC markers, as well as an increase in proliferation and migration [102]. This has been shown to occur through partially overlapping pathways with PDGF-BB [103]. The decrease in the expression of SMC marker genes, such as TAGLN, MYH11 or ACTA2, after treatment with TNFα is dependent on the induction of KLF4 expression through the binding of the transcription factor SP1 to the promoter region of KLF4 [102], similar to what occurs after treatment with PDGF-BB. Furthermore, TNFα induces the expression of a repertoire of genes involved in both pro-inflammatory signaling and remodeling of the extracellular matrix, which are also known inductors of dedifferentiation and proliferation of SMC themselves [14, 104]. The pro-migratory effects induced by PDGF-BB and TNFα share signaling pathways dependent on phosphatidyl-inositol 3 kinase (PI3k) and the mammalian Target of Rapamycin (mTOR) [103]. However, these pro-migratory effects are partially additive, and the suppression of the PI3k and mTOR-dependent pathways decreases SMC migration by 50%, denoting the existence of other complementary signaling pathways that participate in this process.

An important difference between PDGF-BB and TNFα-induced activation lies in the ability of SMC to secrete their ligands. SMC are capable of secreting TNFα under specific stimuli, such as vascular damage and metabolic diseases with generalized chronic inflammation [105-107]. However, in the case of PDGF-BB, endothelial cells are responsible for producing and secreting the ligand, while SMC only express its receptor (PDGFRB). PDGF-BB signaling represents a recurrent physiological mechanism in the adult organism, associated with non-pathological angiogenic processes. This is a key aspect, since the dysregulation of PDGF-BB-mediated dedifferentiation is relevant in pathologies that particularly concur with endothelial dysfunction, while the dysregulation of TNFα signaling may be mediated by changes in the SMC themselves as

well as in other cells of the environment, or even in the whole organism and therefore represents a general mechanism of pathological dedifferentiation in SMC.

In the last decade, it has been established that the processes that control the cellular phenotype are finely modulated by heritable mechanisms of gene expression regulation. These mechanisms do not produce changes in the genetic code, therefore they are called **epigenetic** [108], and are mediated by post-translational modifications of histones (methylation, acetylation or other modifications at specific sites) [109]; DNA methylation [110]; chromatin remodeling [111]; the control of gene expression through **non-coding RNAs [108] and posttranscriptional modifications of RNA [112]**.

1.6 Non-coding RNAs

Although the importance of the genes that transcribe for translatable mRNA does not go unnoticed, in humans only 2% of the genome has coding elements. This copious difference suggests the importance of non-coding genes in the genome. In fact, it has been observed that the amount of non-coding elements is associated with the complexity of the organism [113], advocating the regulatory importance of these sequences. In particular, regions that are transcribed and do not code for proteins are called noncoding RNAs (ncRNAs). As a first general classification of these RNAs, we can divide them into those that fulfill general functions or "housekeeping ncRNAs" and those that have regulatory functions or "regulatory ncRNAs". The first group has been intensively studied and is represented by RNAs that accomplish vital functions in the cell, such as ribosomal RNAs (rRNA) and transfer RNAs (tRNA), involved in protein synthesis [114, 115]; the small nuclear RNAs (snRNAs) that participate in the process of intron cutting and exon splicing [116], the small nucleolar RNAs (snoRNAs), that participate in the deposition of modifications in other housekeeping RNAs [117]; and telomerase RNA that participates in telomere maintenance [118]. The second large group comprehends regulatory RNAs, which are classified into long or small non-coding RNAs depending on whether or not they exceed 200 nucleotides (nt) respectively. Among the small RNAs, we can mention mainly three groups: microRNAs (miRNAs), small interference RNAs (siRNAs) and RNAs that interact with piwi (piRNAs). However, certain groups of non-coding RNAs can be classified into both long and small, since they

have great variability in their length, such as promoter-associated transcripts (PATs), enhancer RNAs (eRNAs) and circular RNAs (circRNAs) (Reviewed in [119]).

In the last two decades, progress has been made in the field of small non-coding RNAs, particularly with regard to the biology and function of microRNAs, which are 21 nucleotide transcripts that regulate gene expression through their partially complementary binding to mRNA. The binding of miRNA to its target mRNA in its 3 'UTR (Untranslated region) promotes the recruitment of the double-stranded RNA silencing complex called RISC (RNA Induced Silencing Complex) which mediates the inhibition of translation and/or degradation of the target molecule [120]. This mechanism plays important roles in SMC differentiation (reviewed in [30], Section 6.7). Consequently, the alteration in the expression of specific miRNAs has been found associated, both by our group (Section 6.7) and by others, with the development of vascular diseases [121-125].

On the other hand, long non-coding RNAs (lncRNAs) are less described in the literature, and they lack a clear scheme of classification, since they can perform various functions, both at the nuclear and cytoplasmic levels [126]. For example, lncRNAs located in the nucleus can regulate transcription by guiding or sequestering transcription factors [127], guiding histone modifying complexes and/or chromatin remodelers to the corresponding sites on the chromosome [128] or act as enhancer RNAs. [129]. Other studies have shown that lncRNAs can regulate nucleocytoplasmic transport of transcription factors [130] or alternative splicing of pre-mRNAs [131]. In the cytoplasm, lncRNAs can regulate the stability of messenger RNA and its translation [132], act as a sponge for microRNAs [133], as mediators of protein complexes [134] or produce peptides with specific functions. Some other regulatory functions also include stabilization of RNA-protein complexes [135], specific phosphorylation of proteins, and activation of signaling pathways [136]. In addition to all the aforementioned, some lncRNAs can be circularized after splicing (Circular lncRNAs) and also act as miRNAs sponges [137] or regulate the maturation of ribosomal RNAs (rRNAs) [138]. Finally, some lncRNAs are released in exosomes or microvesicles, possibly fulfilling a facilitating function of cell-to-cell communication [139, 140]. In recent years, numerous lncRNAs involved in the phenotypic switch process have been documented, some of which include ANRIL, SMILR, SENCR, and MYOSLID [128].

For example, the overexpression of ANRIL inhibits the phenotypic switch of SMC

and prevents the development of arteriosclerotic plaque *in vivo* [141, 142], while the decrease of SENCR promotes proliferation and migration [143]. The expression of SMILR induces proliferation through regulation of centromere F protein messenger RNA (CENPF) [144, 145] and MYOSLID has been described to enhance the vascular SMC differentiation program [136]. Other recently described lncRNAs such as FOXC2-AS1 and NR2F1-AS1 [146] decrease their expression during SMC differentiation, although after their silencing there is a decrease in the expression of marker genes that code for contractile proteins and therefore are necessary for the correct differentiation of SMC. Some other lncRNAs involved in SMC homeostasis have been documented [139, 147], however the mechanisms underlying their effects on SMC differentiation are not fully understood. Recently, some regulatory mechanisms have been reported. For example, GAS5 is able to bind to an RNA-binding SMAD element (rSBE) and prevent the interaction of SMAD with the promoter region of specific SMC genes. This mechanism is capable of regulating SMAD-dependent TGFβ activity and therefore SMC differentiation [148]. The functions and mechanisms of lncRNAs described to date in vascular SMC are summarized below.

Tabla 1.6.1. LncRNAs with known functions in vascular smooth muscle cells. The name of the lncRNA, its function according to the reference publication, the effect of its silencing and the proposed mechanism are detailed.

lncRNA	**Function**	**Silencing effect**	**Mechanism**	**Ref.**
AC105942.1	Inhibits proliferation	Unknown	Its overexpression decreases the expression of hnRNPA2B1	[149]
AK124326	Inhibits ARHGAP42 transcription	Increases the acetylation of H3K9 and the binding of Pol-II to the ARHGAP42 gene	Interact with and facilitate MYOCD activity	[150]
AL355711	Promotes SMC migration and the development of arteriosclerosis through ABCG1 / MMP3	Inhibits ABCG1 transcription	Unknown	[151]
ANRIL	Increases proliferation and survival. Increases NOX1 expression	Decreases ROS expression and phenotypic transition	Regulates the miR-7 / FGF2 pathway; Regulates the miR-181a / SIRT1 pathway; It functions as a chaperone for the binding of WDR5 and HDAC3, which in turn increases the expression of NOX1	[152-154]
BANCR	It promotes proliferation and	Unknown	Its overexpression activates the JNK pathway	[155]

	migration. Increases in response to TNFα			
CASC2	Inhibits proliferation, migration, and de-differentiation. Induce apoptosis. Decreases vascular remodeling and ACTA2 in a hypoxia-induced pulmonary hypertension model	Unknown	Unknown	[156]
CDKN2B-AS1	It inhibits proliferation and induces apoptosis after treatment with ox-LDL. Inhibits the PI3K / AKT pathway	Unknown	MiR-126-5p sponge; induces PTPN7	[157]
CRNDE	It is induced after treatment with PDGF-BB and in a carotid balloon lesion model. Act on the PDGF-BB pathway	Inhibits proliferation, migration, and dedifferentiation after PDGF-BB treatment	Unknown	[158]
GAS5	Inhibits proliferation and induces apoptosis. Modulates TGFβ / SMAD3 signaling	Attenuates apoptosis. Induce EZH2, inhibit RIG-I	Sponge for miR-21, inhibits Akt	[148, 159, 160]
GIVER	Promotes oxidative stress and proliferation in rat aortic SMC	Attenuates the expression of genes related to oxidative stress (NOX1) and inflammation (IL6, CCL2 and TNFα)	Unknown. Interacts with the NONO protein. Its overexpression decreases the acetylation of H3K9 and the enrichment of Pol II in the NR4A3 promoter	[161]
H19	Increase proliferation, migration and survival.	Reduces the growth of aneurysms *in vivo* . Suppresses proliferation and induces apoptosis of SMC treated with ox-LDL	Sponge for let-7 miRNA family; Induce the expression of HIF1α; Regulates miR-148b / WNT / β-CATENIN	[162-164]
HAS2-AS1	Regulates the expression of hyaluronic acid, reduces migration	Unknown	Inhibits HAS2 transcription	[165, 166]
HCG18	Inhibits proliferation and dedifferentiation. Induce apoptosis. Decreases after PDGF-BB treatment	Reduces TAGLN, ACTA2 and SMTN. Increase SPP1 and TPM1	Interact with FUS	[167]
HIF1A-AS1	Inhibits proliferation through increased TGFβ1	Unknown	Increases TGFβ1	[168]

HOTAIR	Reorganization of the extracellular matrix	Induce apoptosis and suppress type I and III collagens	Unknown	[169]
LINC00341	Promotes proliferation and migration	Suppresses proliferation and migration	MiR-214 sponge; induces FOXO4	[170]
LINC01278	Inhibits proliferation and dedifferentiation	Induce proliferation and dedifferentiation	MiR-500b-5p sponge; Induce ACTG2	[171]
LincRNA-p21	Suppresses proliferation and induces apoptosis	Dysregulates target genes of the P53 pathway. Induces neointima formation *in vivo*	It is induced by p53. Interacts with MDM2, an E3-Ub ligase and de-represses P53	[172]
LIPCAR	Promotes proliferation, migration and phenotypic change of SMC	Unknown	Unknown. Its overexpression induces CDK2, PCNA, MMP2 and MMP9. P21 expression decreased	[173]
lncRNA 430945	Promotes proliferation and migration of vascular SMC in arteriosclerosis	Decreases proliferation and migration in response to ANGII	Induce the expression of ROR2	[174]
lncRNA-ES3	Promotes calcification and senescence of human aortic SMC in response to glucose	It increases the expression of miR-34c-5p. Decreases calcification of SMC.	Regulates miR-34c-5p; induces BMF	[175]
LOC285194	Inhibits proliferation and migration	Induce proliferation and migration	Unknown	[176]
LOXL1-AS	It promotes proliferation and survival of human aortic SMC. It is increased in patients with thoracic aortic aneurysm	Unknown	Induce the expression of lncRNA GIVER	[177]
MALAT1	Increases proliferation and migration through activation of the Akt pathway	Decreases proliferation and migration	Regulates the miR-150-eIF4E / Akt pathway	[178]
MEG5	Decreases proliferation and apoptosis in SMC treated with ox-LDL	Induce proliferation and inhibit apoptosis	MiR-361-5p sponge; induces ABCA1	[179]
MIAT	Induce de- and trans-differentiation	Decreases proliferation and migration; increases apoptosis	Increases KLF4 transcription	[180]
MiR143HG/CARMN	Gene that contains the 143/145 microRNAs, maintains the contractile phenotype	Increases neointima formation	Unknown	[181]

MRAK048635_P1	Unknown It appears to be important in maintaining the contractile phenotype.	Promotes migration and proliferation, decreases apoptosis	Unknown	[182]
MYMSL	Unknown It is induced by MYOCD and decreases in phenotypic modulation	Decreases the synthesis of extracellular matrix	Unknown	[183]
MYOSLID	Amplifies the differentiation program	Decreases the formation of actin fibers, blocks the translocation of MLK1 to the nucleus. Inhibit TGFβ-dependent phosphorylation of SMAD2	Unknown	[136]
NEAT1	Promotes proliferation and survival in response to oxidative damage	Reduces proliferation, survival and induction of inflammation in response to H_2O_2	Prevents miR-30d-5p from degrading its target gene, ADAM10	[184]
PVT1	Promotes phenotypic change, apoptosis and induces remodeling of the ECM by MMP2 and MMP9	Decreases apoptosis, ECM changes and pro-inflammatory cytokines detected in serum	Unknown. Works as miRNA sponge in other cell types	[185]
SAMMSON	Decreases proliferation	Unknown	Its overexpression inhibits the maturation of miR-130a	[186]
SENCR	Decreases migration and proliferation	Increase proliferation and migration	Regulates miR-4731-5p / FOXO3a pathway	[187-189]
SMILR	Increase proliferation	Decreases proliferation	Interacts with the CENPF mRNA	[145]
SNHG16	It promotes proliferation and migration of human aortic SMC. It is induced in atherosclerosis.	Decreases the proliferation and migration induced by treatment with PDGF-BB	MiR-205 sponge, induces SMAD2	[190]
SOX2OT	Decreases proliferation	Increases proliferation and decreases apoptosis; decreases MYH11	MiR-330-5p sponge; induces MYH11	[191]
TUG1	It promotes proliferation and migration in response to PDGF-BB in human aortic SMC. Induce proliferation and survival in SMC treated with ox-LDL	Decreases the proliferation and migration induced by treatment with PDGF-BB. Reduces growth and enhances apoptosis in response to ox-LDL treatment	MiR-216a-3p sponge; induces SMURF2; Regulates miR-382-5p	[192, 193]
TYKRIL	Promotes proliferation and survival of SMC of human pulmonary arteries with	It decreases proliferation and increases apoptosis in *exvivo* studies of human arterial SMC with idiopathic pulmonary	Interacts with the N-terminal region of TP53 and prevents its interaction with P300	[194]

	pulmonary hypertension	hypertension. Decreases PDGFRB expression		
XIST	Promotes proliferation. Inhibits apoptosis	Decreases proliferation and induces apoptosis	MiR-1264 sponge; induces WNT5A / β-CATENIN	[195]
XR007793	Promotes proliferation and migration in rat models of hypertension and balloon injury	Induce ACTA2 and TAGLN	MiR-23b sponge, induces FOXO4	[196, 197]

1.7 RNA modifications

In recent years, the regulation of RNA expression, stability, and function by post-transcriptional modifications has flourished as a promising research subject. Similar to DNA and proteins, RNA can be posttranscriptionally modified with a variety of more than 160 different modifications [198]. The set of all RNA modifications present in a cell is called the "epitranscriptome". The deposition of these modifications is carried out through specific enzyme complexes that have a high degree of conservation between species and whose alteration is involved in a large number of diseases [199]. The existence of the modifications m^6A, m^5C y m^1A has been known since the 1970s [200-202]; however, its participation in fundamental biological processes has only recently been explored. While the total number of known modifications is growing, little is known about their biology and function.

In Eukaryotes, the most prevalent internal modification is N6-methyladenosine (m^6A) [112]. This modification is involved in a number of important processes such as RNA decay [203, 204], intron splicing [205, 206], and translation [204], as well as stem cell differentiation [207, 208], stress response [209], among others.

The deposition and the function of this modification are controlled by three protein groups: the writers, involved in its deposition; the erasers, who are in charge of removing it; and the readers, which are those capable of recognizing the modification and determining the fate of the RNA molecule.

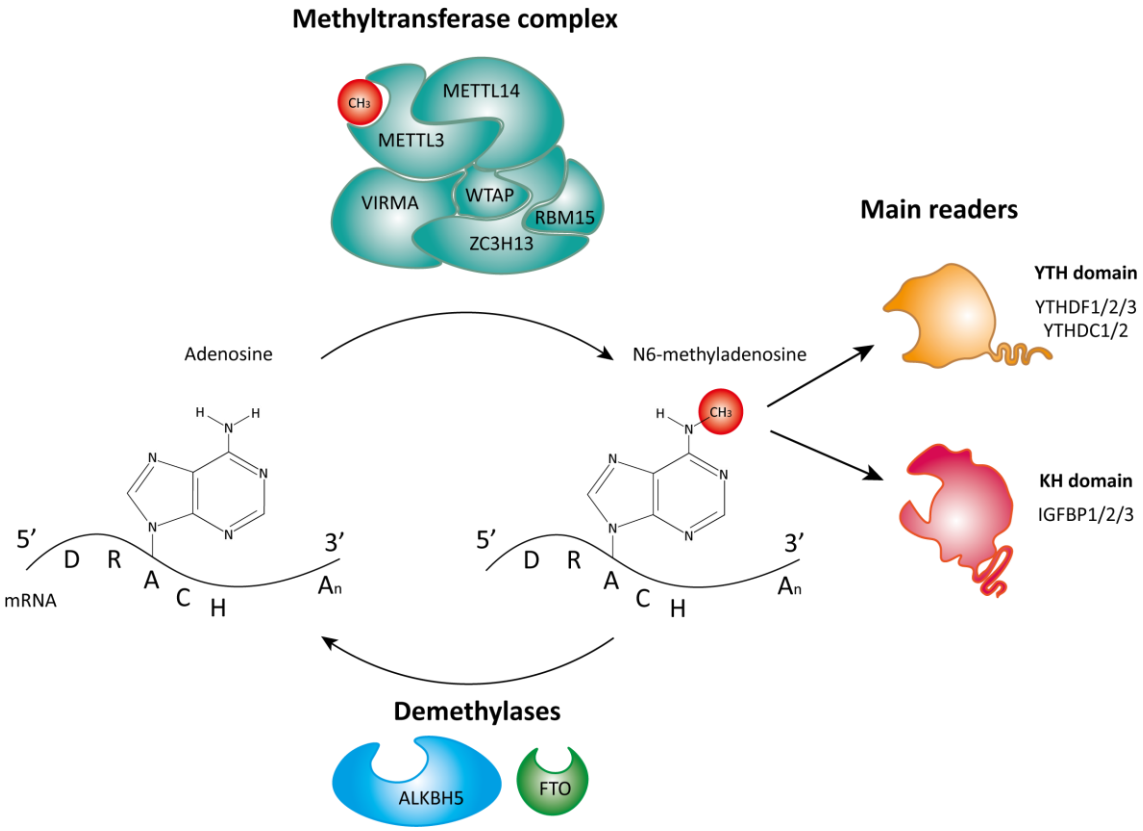

Figure 4. m⁶A methylation machinery. The main components involved in the biology of the N6-methyladenosine modification (m⁶A) are depicted. The substrate RNA molecule is recognized at specific sites with the consensus motif "DRACH" by the METTL3-dependent multiprotein methyltransferase complex, where the central "A" will be modified. Once the methylation has been deposited, it is recognized by reader proteins with the YTH domain, or alternatively by readers containing the KH domain. Interaction with the reader will determine the fate of the target molecule. The m⁶A modification can be removed by demethylases, mainly ALKBH5 and, to a lesser extent, FTO.

1.6.1 Deposition: Methyltransferase complex

The m^{6}A modification is deposited by a multiprotein enzyme complex that recognizes the specific motif "DRACH" in the target RNA, "A" being the base that is methylated (where D can be A or U; R represents a purine; and H can be A, U or C) [210]. This deposition occurs co-transcriptionally, since it is present in immature transcripts or pre-mRNAs [211]. Although not necessary for the splicing process, several of the methyltransferase complex proteins have been observed to regulate alternative splicing events, promoting exon skipping and intron retention in regions with particular characteristics [212].

For the occurrence of m^{6}A deposition, the presence of the catalytic nucleus of the methyltransferase complex is necessary, consisting of a heterodimer formed by METTL3/METTL14. Although their presence has been shown to be sufficient to methylate RNA *in vitro*, [213, 214] other proteins with important functions are required *in vivo*. Among those described so far, WTAP and VIRMA would perform regulatory

functions [215, 216]. WTAP mediates the nuclear localization of the complex, and the ablation of both VIRMA and WTAP significantly reduces the deposition of m^6A globally on the transcripts of the cell, in other words, on the transcriptome [215, 216]. The RNA-binding protein RBM15 and its homologue RBM15b have also been shown to interact with METTL3 through its binding to WTAP, and that RBM15 is an essential part of the methylation complex in Drosophila [217-219]. In this sense, it has been hypothesized that the function of RBM15 comprises the interaction with regions rich in uracils (U), through its RBM domain, recruiting the methylation complex to sites close to its consensus binding motif.

The ZC3H13 protein has recently been shown to be part of the methyltransferase complex [220, 221]. This zinc finger protein has been studied in both mice and Drosophila and it has been observed that it is necessary for the functional and efficient deposition of m^6A, as well as for the translocation of the methyltransferase complex to the nucleus. Studies in Drosophila suggest that this protein acts as a bridge between WTAP and RBM15. Finally, it has been proposed in different studies that the E3 ubiquitin-ligase CBLL1 is associated with this complex, although its role is still not entirely clear yet [218, 221, 222].

1.6.2 Removal: Demethylases

The modulation of this layer of transcriptional regulation has been proposed as a highly dynamic event, due to the existence of demethylases responsible for removing the methyl group in response to specific signals [207, 223, 224]. The existence of two m^6A demethylases has been described so far: Fat-mass and Obesity associated protein (FTO) and Alk B homolog *5* (ALKBH5) [223, 225].

Although the role of m^6A removal at the global transcriptomic level has been a matter of discussion for FTO, since its absence does not produce major changes in the general level of m^6A, it has been shown that it is capable of transcript demethylation. In particular, FTO demethylates those that have this modification at their 5 'end, functioning as a regulator of cap-independent translation. In this sense, it was recently shown that FTO demethylates HIF1α mRNA, leading to a decrease in protein expression through the modulation of YTHDC2 reader recognition and m^6A-dependent translation initiation [226].

On the other hand, ALKBH5 has a more global demethylase function and is considered the main protein involved in the removal of m^6A, since it was recently shown that the loss of ALKBH5 increases the prevalence of m^6A in the transcriptome [225]. In this line, it was observed that its silencing also affects the splicing process and the stability of specific transcripts in mouse germ cells, generating infertility as a consequence [225, 227].

However, other independent studies suggest that the m^6A modification is rather stable [228, 229], leading to the alternative hypothesis that although there is regulation by demethylation, this mechanism would not be the main modulator of this post-transcriptional pathway.

1.6.3 Reading and function

Taking into account the global stability of the m^6A modification, it is easy to understand why the reader proteins might be in charge of regulating the final effect that this modification will have on the target molecule [230]. Most of the proteins that recognize m^6A possess a particular protein domain called the YT512-B homology domain or YTH, which is highly conserved between species. The YTH domain is able to recognize and interact with m^6A through electrostatic charges and the formation of hydrogen bonds [231]. Two families of readers have this domain: YTHDC (1/2) and YTHDF (1/2/3) [232-235].

In particular, YTHDC1 is the only reader whose location is exclusively nuclear, while its counterpart YTHDC2 is found in both the nucleus and the cytoplasm. These proteins have a regulatory role in gene expression and alternative splicing, as well as in mRNA export to the cytoplasm, in the case of YTHDC1 [236, 237]; or on the efficiency of translation of determined mRNAs in germ lines, in the case of YTHDC2 [238-240]. It should be noted that there is a great difference in the conformation of the protein domains between both readers [241].

On the other hand, the YTHDF family of proteins represents a group of three proteins with similar size and structure, which can act individually or cooperatively, and have partially overlapping functions. YTHDF1 interacts with the Eukaryotic Translation Initiation Factor 3 (eIF3) and promotes cap-independent translation, and it has been

shown to modulate mRNA degradation [242]. YTHDF1 mostly recognizes modifications set at the 5' end [243], while YTHDF2 preferentially binds to m^6A that have been deposited in the 3' UTR region, and mediates the degradation of its target RNA through the recruitment of the CCR4-NOT deadenylation complex. This pathway determines that the half-life of the RNA molecules is shorter when they harbor the m^6A modification, regulating their abundance and consequently their translation [203, 244]. This posttranscriptional regulatory pathway controls a large number of genes, and has been proposed as a mechanism of transcriptional plan replacement during both mouse development [245], and induced pluripotent stem cells (iPSCs) differentiation into neurons [246]. In addition, it has been shown that under heat shock stress, YTHDF2 translocates into the nucleus, where it competes with FTO for binding to m^6A modifications located in the 5 'UTR region of specific mRNAs, thus avoiding its removal and promoting its cap-independent translation [243, 247]. Finally, YTHDF3 has overlapping functions with its two homologous family members, probably operating with them in a coordinated manner [204, 248]. In this sense, it has been observed that YTHDF3 mediates the degradation of lncRNAs in concert with YTHDF2 [204].

There are also unconventional m^6A readers, such as the IGFBP (1/2/3) family. These proteins interact with RNA through KH-type RNA-binding domains (K Homology domain). It has been observed that the consensus binding site for IGF2BP overlaps with the consensus motif of m^6A and that 80% of the transcripts bound to this site have m^6A. Although it has been described that recognition by IGF2BP increases the stability and translation of target RNA molecules, the functions and mechanisms associated with these unconventional readers have not yet been fully elucidated [249].

Taking into consideration that YTHDF2 is the main reader involved in the m^6A-mediated degradation of modified RNAs and therefore an important candidate to regulate changes in the transcriptional plan and that the present work is intended to investigate the regulation of the phenotypic plasticity of SMC, special focus will be placed on the YTHDF2 reader.

1.8 HYPOTHESIS AND OBJECTIVES

The **general objective** of this work is to contribute to the knowledge of the

molecular mechanisms involved in the phenotypic modulation of human pulmonary artery smooth muscle cells, with special interest in their regulation by epigenetic processes.

My **working hypothesis** is that the action of long non-coding RNAs, not yet described in the literature, as well as the degradation of RNAs regulated by the post-transcriptional modification of RNA N6-methyladenosine (m^6A) play a key role in the modulation of human pulmonary artery SMC phenotypic switch.

Specific objectives

Part I. Identification of candidate lncRNAs in primary cultures of human pulmonary artery SMC (hPASMC):

1.1. To identify differentially expressed long noncoding RNAs during hPASMC differentiation.

1.2. To analyze the expression of candidate genes in the different cell types that build up the artery.

1.3. To analyze the effect of loss of function of candidate genes on hPASMC differentiation.

1.4. To study the function of the candidates through the analysis of associated proteins (RNA binding proteins).

1.5. To analyze the expression of candidate genes in human pulmonary arteries with vascular remodeling.

Part II. Characterization of the N6-Methyladenosine-mediated RNA degradation machinery during hPASMC differentiation

2. 1. To characterize the expression of genes involved in the regulation of the RNA modification N6-methyladenosine throughout the differentiation of hPASMC .

2. 2. To analyze the consequences of the inhibition of the YTHDF2 reading protein during the differentiation of hPASMC.

2. 3. To identify target RNAs of YTHDF2 during hPASMC differentiation.

Chapter 2

MATERIALS AND METHODS

2 Materials and Methods

2.1 Differentiation model

A cell contact-induced SMC differentiation model previously employed in the laboratory was used [17, 85]. The model was performed as specified below: Proliferative human pulmonary artery smooth muscle cells (hPASMC) were plated at 70% confluence and extracted the next day (D0). At about 48 h later the cells reach confluence (D2) and begin the differentiation process. 96 h after confluence, the cells are polarized and show high expression of SMC markers (D6). (Figure 5)

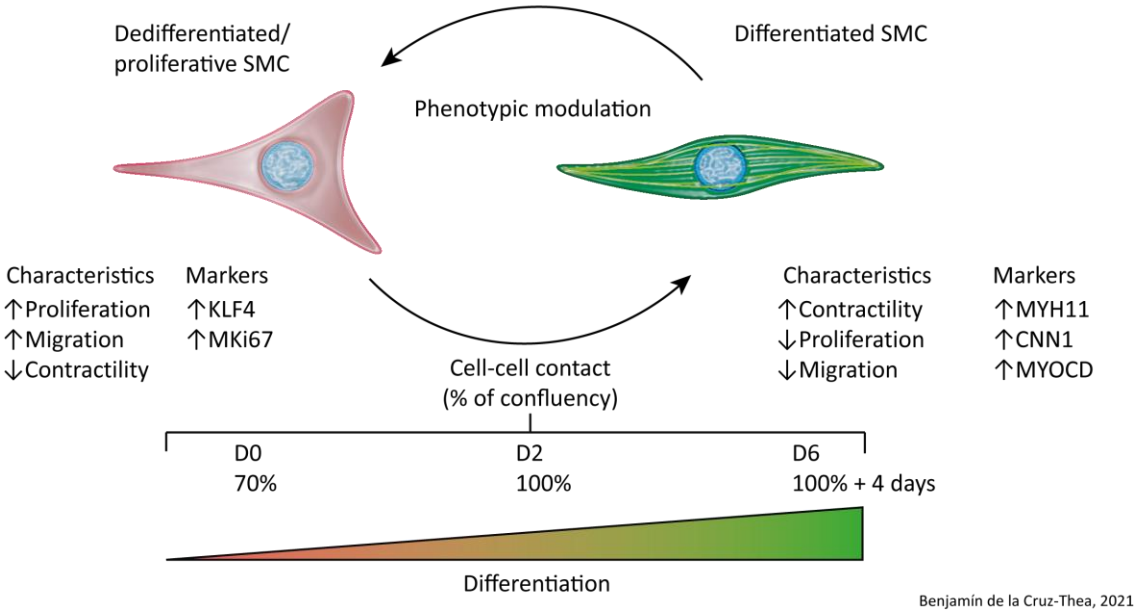

Figure 5. Differentiation model. Schematic view of the cell contact differentiation model in SMC. Under "Characteristics" the main associated functional changes are mentioned; under "Markers" are listed the most important marker genes whose expression increases in each condition. Up and down arrows indicate increase and decrease respectively. In a color gradient from red to green, the differentiation status of the cell is qualitatively indicated, so that after 4 days at maximum confluence the SMC are fully differentiated (green). Curved arrows indicate the possibility of conversion between proliferative (left) and differentiated (right) phenotypes.

2.2 Cell culture

All cells were cultured in incubators suitable for mammalian cell lines with 95% humidity, 5% CO2 and routinely tested for contamination with *Mycoplasma spp.*

2.2.1. Human Pulmonary Artery Smooth Muscle Cells (hPASMC)

Human pulmonary artery Smooth Muscle Cells (SMC) culture (hPASMC, Lonza Group, Switzerland) was performed using the medium proposed by the manufacturer (Lonza SM-bullet Medium, Lonza Group, Switzerland) supplemented with 10% Fetal bovine serum (FBS) (GIBCO, Thermo Fisher, USA). Cells were used between passages 4 and 8.

2.2.2. Human Pulmonary Artery Endothelial Cells (hPAEC)

Human pulmonary artery endothelial cells (hPAEC, Lonza Group, Switzerland) were cultured using the manufacturer's specific culture medium (Lonza Group, Switzerland) supplemented with 10% FBS (GIBCO, Thermo Fisher, USA). The cells were used in confluence.

2.2.3. Human lung fibroblasts (MRC5)

Human lung fibroblasts (MRC5, ATCC, USA) were cultured using Dulbecco's Modified Eagle Medium (DMEM) (SIGMA-Aldrich, Merck KGaA, USA) supplemented with 10% FBS (GIBCO, Thermo Fisher, EE .UU.).

2.2.4. Human anaplastic thyroid tumor cells (C643)

Human C-643 anaplastic thyroid tumor cells (RRID: CVCL_5969) (CLS, GmbH & Co. KG, Germany) were cultured using DMEM (SIGMA-Aldrich, Merck KGaA, USA) supplemented with 10% FBS (GIBCO, Thermo Fisher, USA).

2.2.5. Human kidney embryonic derived transformed cells (HEK293)

Transformed cells derived from human embryonic kidney cells HEK293 (RRID: CVCL_0045) (ATCC CRL-1573, USA) were cultured using DMEM (SIGMA-Aldrich, Merck KGaA, USA) supplemented with 10% FBS (GIBCO, Thermo Fisher, USA).

2.3 Pharmacological treatments

2.3.1 TNFα

Background: Tumor Necrosis Factor alpha (TNFα, *Tumor Necrosis Factor alpha*) is a pro-inflammatory cytokine that induces dedifferentiation and proliferation of SMC [85, 102, 103]. Because of this, the treatment of SMC with this cytokine facilitates the study of signaling cascades and gene expression changes associated with the

inflammation-mediated phenotypic modulation process. To evaluate this particular effect, cells are starved of fetal bovine serum (1% FBS) 24 h prior to the stimulation and until the end of the experiment.

Method: Differentiated smooth muscle cells (hPASMC D6, see section 2.1) were serum-starved (1% FBS) 24 h prior to the stimulation. Cells were treated for 48 h with 10 µg/ml of TNFα (R&D Systems, USA) in Sm-Bullet medium (Lonza Group, Switzerland) supplemented with 1% FBS.

2.3.2 RO-3306

Background: This drug occupies the binding site for adenosine triphosphate (ATP) in the cyclin-dependent kinase 1 (CDK1) molecule in a specific and reversible way, since the replacement of the stimulation medium by a basal one restores the capacity of CDK1 to bind ATP [250]. The inability of CDK1 to phosphorylate its target genes causes a blockage in the progression of the cell cycle in G2/M [251] and therefore represents a state of pharmacologically induced quiescence. The time and concentration used are optimized to avoid the induction of cellular apoptosis. It should be noted that the affinity of this inhibitor for CDK1 is widely greater than for CDK2 (by a factor of 10) and CDK4 (by a factor of 50), making it a sufficiently specific inhibitor for CDK1 at the concentrations used.

Method: Proliferative cells (at 70% confluence) were treated for 24 h with Ro3306 [250] at a final concentration of 10 µM (SIGMA-Aldrich, Merck KGaA, USA) in DMEM medium (SIGMA-Aldrich, Merck KGaA, USA) supplemented with 10% FBS (GIBCO, Thermo Fisher, USA). Treatment with the same volume of vehicle DMSO for 24 h was used as a control.

2.3.3 MG-132

Background: This small molecule (carbobenzoxy-Leu-Leu-leucinal) causes a powerful and reversible inhibition in the degradation of ubiquitinated proteins by the proteasomal pathway, through the blockade of the 26S proteasome subunit, without interfering with its ATPase or Isopeptidase activity [252, 253]. It induces cell death, so the treatments were carried out at moderate concentrations and on a time scale of a few hours.

Method: Confluent MRC5 cells were treated for 4 h with the proteasome inhibitor MG-132 at a final concentration of 20 µM (SIGMA-Aldrich, Merck KGaA, USA) in DMEM medium (SIGMA-Aldrich, Merck KGaA, EE .UU.) Supplemented with 10% FBS (GIBCO, Thermo Fisher, USA). Treatment with the same volume of vehicle DMSO for 4 h was taken as a control.

2.3.4 Brefeldin A

Background: Brefeldin A is a lactone derived from the fungus *Eupenicillium brefeldianum*. In mammalian cells, the main target of this compound is a guanine nucleotide exchange factor (GEF) called GBF1, which belongs to the family of the GEF Arf. This protein catalyzes the exchange of guanosine diphosphate (GDP) for guanosine triphosphate (GTP), allowing the activation of Arf1p GTPase. In a normal signaling cascade, it aids the recruitment of β-COP coat proteins to the Golgi membrane for the formation of loading vesicles targeting the endoplasmic reticulum (ER). This type of transport is involved in a type of autophagy [254]. Brefeldin A binds non-competitively to the complex formed between the exchange factor (GBF1) and the non-phosphorylated form of Arf1p GTPase (reviewed in [255]), so that the intermediate complex is stabilized, blocking the exchange and factor release. As a consequence, it is not possible to form transport vesicles between the Golgi and the ER, which subsequently leads to the fusion of both structures, triggering an unfolded protein response (UPR) or reticulum stress, which can result in apoptosis. This is why the treatment with Brefeldin A for the purpose of investigating this transport and autophagy pathway was carried out within a few hours timeframe.

Method: Confluent MRC5 cells were treated for 4 h with the retrograde transport inhibitor Brefeldin A at a final concentration of 10 µg/µl (SIGMA-Aldrich, Merck KGaA, USA) in DMEM medium (SIGMA-Aldrich, Merck KGaA, USA) supplemented with 10% FBS (GIBCO, Thermo Fisher, USA). Treatment with the same volume of vehicle DMSO for 4 h was taken as a control.

2.4 Transfection and silencing

2.4.1 siPOOLs

Background: RNA interference (RNAi) is an evolutionarily conserved RNA degradation mechanism. It was first described as an antiviral mechanism, however currently it is known for its role in the regulation of expression (reviewed in [256]). The RISC multiprotein complex recognizes double-stranded RNA, resulting either from the binding of the target molecule with small single-stranded RNAs, or from the entry of foreign double-stranded RNA (mainly from viruses). As a consequence, the complex is activated and the double-stranded molecule is cleaved. This degradation mechanism has been widely used for gene silencing for experimental purposes by introducing single-stranded RNA probes complementary to a portion of the target mRNA. This approach has the drawback of generating unwanted effects, due to the complementarity of the chosen probe with other mRNA molecules (*"off-target" effect*). This is why the siTOOLS company (Germany) developed the siPOOLs technique, which consists of a set of 30 small probes, complementary to different areas of the target molecule, which allow the silencing of the target gene at much lower concentrations. This approach reduces the incidence of secondary silencing by a factor of 30 for each probe, since the relative concentration of a “nonspecific” probe is 1/30 relative to the overall directed at the target molecule, represented by all the probes [257].

Method: SiPOOLs (siTOOLS®, Germany) against the sequences of *DAGAR* (at a final concentration of 20 or 40 µM for 48 h) and YTHDF2 (at a final concentration of 3 µM for 72 h), were transfected using OptiMEM serum-free medium (Gibco, Thermo Fisher, USA) and RNAiMAX lipofectamine (Invitrogen, Thermo Fisher Scientific, USA) according to the manufacturer's instructions. As a transfection control, siPOOLs (siTOOLS®, Germany) were used against random sequences (siCT), at the same concentration as the siPOOL of interest.

2.4.2 CRISPR-CAS9

Background: *Clustered Regularly Interspaced Short Palindromic Repeats* (CRISPR) and *CRISPR-associated protein* (Cas) constitute an adaptive defense system present in bacteria and viruses, which induces double-stranded (genomic) DNA breakage and activates error-prone *Non-homologous End Joining* (NHEJ) repair or homology-directed

repair (HDR). In the absence of a template DNA for repair, this occurs through NHEJ that causes insertions and/or deletions (indels) at the target locus, interrupting its sequence. When a donor template with homology to the locus to be repaired is used, the HDR mechanism is activated. In this case, it is possible to insert specific mutations. These mechanisms are used in molecular biology to make point mutations in the genome, with great specificity, allowing the creation of stable cell lines or transgenic animal models. The CRISPR/CAS9 system works through the transfection of a guide RNA (gRNA) (or through the transfection and interaction of a Crispr RNA and a trans-activating crispr RNA) that directs *Streptococcus pyogenes Cas9* (SpyCas9) to specific DNA sites where double chain breaking occurs (reviewed in [258]).

Method: C643 cells were used for the generation of stable knockout cell-lines specific for METTL3 (described in [259]) and for YTHDF2. The latter was created using CRISPR/Cas9 genome editing. Briefly, C643 cells were transfected with px459 v2.0-YTHDF2 gRNA1 using Lipofectamine 2000 (Thermo Fisher Scientific, USA), according to the manufacturer's instructions. After making a selection with puromycin, several clones were seeded as a single cell in 96-well culture dishes, and expanded to 6-well dishes. The decrease of YTHDF2 in the clones was tested by Western Blot with a specific antibody against YTHDF2. Three different clones were selected to perform the experiments.

2.5 PCR and Cloning

2.5.1 PCR

Background: *Polymerase Chain Reaction* (PCR) is a widely used technique in molecular biology. The PCR takes advantage of the capacity of polymerase enzymes resistant to high temperatures, that is to say, thermostable (Taq, Phusion, etc.) for the amplification of genetic material. For this, a thermocycler is used with a specific program of times and temperatures, specific primers corresponding to the region to be amplified, and deoxynucleoside triphosphate (dNTPs). The reaction begins with an initial denaturation at 98°C to allow denaturation of the double-stranded DNA. Following this, the binding of the primers to the DNA template occurs, typically at 60°C, although this temperature depends on the sequence of the primers used. Following this step, the

elongation of the DNA chain nucleated by the primers occurs, caused by the presence of the polymerase enzyme and the dNTPs. This is done cyclically, doubling the genetic material after each cycle of amplification.

Method: 50 ηg of DNA was used as a template for each sample. The reaction preparation was carried out as detailed in Table 2.5.1.1.

Table 2.5.1.1. Prepared for the PCR reaction. The components and volumes used in PCR reactions for cloning and sequencing are detailed.

Component	**Volume (µl)**
5x HF buffer solution	10
10 mM forward primer	2,5
10 mM reverse primer	2,5
10 mM dNTPs	1
DMSO	1,5
Phusion polymerase	0,5
Water (PCR Grade)	32
DNA	

Next, the DNA of interest was amplified using the program detailed in Table 2.5.1.2.

Table 2.5.1.2. Program used for PCR. The times, temperatures and cycles used for thermocycling during DNA amplification by PCR are detailed.

Time (s = seconds; m = minutes)	**Temperature (° C)**	**Cycles**
30 s	98	Initial
10 s	98	35
30 s	60	
1 m	72	
7 m	72	Final

After amplification, the PCR product was run on a 2% agarose gel in Tris saline buffer (TBS) with ethidium bromide (EtBr) at 120 V for 50 minutes. Molecular marker

was also run as a reference for the size of the amplicons. The gene material was observed briefly through a UV backlight. Amplicons with the characteristics corresponding to the desired product were excised from the gel and purified using the NucleoSpin® Gel and PCR Clean-up Kit system (Macherey-Nagel GmbH & Co. KG, Germany) according to the manufacturer's instructions. The purified material was cloned.

2.5.2 Cloning

The cloning system pGEM®-T Easy Vector System (Promega, USA) was used. The linearized pGEM-T vector has 3 'unpaired thymidine residues at its ends that can be used for cloning of PCR products. For this, first, 5 'adenosine residues were added to the purified PCR product by the reaction described in Table 2.5.2.1.

Table 2.5.2.1. Prepared for the adenosine addition reaction. The components and volumes used are detailed.

Component	**Volume (µl)**
Purified PCR product	15
Taq buffer solution (+ (NH4) 2SO4) (10x)	2
dATP (2 mM)	2
$MgCl_2$ (25 mM)	1
Taq DNA polymerase (5 U / µl)	0,2

Incubation was performed at 72°C for 30 minutes and then rapidly cooled to 4°C. The product was purified using the NucleoSpin® Gel and PCR Clean-up Kit (Macherey-Nagel GmbH & Co. KG, Germany) according to the manufacturer's instructions. The ligation reaction was then carried out and incubated for 1 h at room temperature. The composition of the reaction is detailed in table 2.5.2.2.

Table 2.5.2.2. Prepared for the ligation reaction of the insert to the pGEM-T Easy vector. The components and volumes used are detailed.

Component	**Volume (µl)**
PGEM®-T Easy Ligation Buffer Solution (2x)	5
Vector pGEM®-T Easy	1

Insert	3
T4 DNA ligase (5 U / µl)	1

The ligation product was then added to competent bacteria (strains capable of taking DNA from the environment) for transformation. It was allowed to stand for 10 minutes on ice. A brief heat shock for 45 seconds at 42°C was performed and. 30 µl of X-GAL (5-bromo-4-chloro-3-indolyl-β-D-galactopyranoside), a galactose analog, and 4 µl of the inducer of the expression of β-galactosidase, IPTG (isopropyl-β-D-1-thiogalactopyranoside) were added.

The compound X-GAL can be hydrolyzed by the enzyme β-galactosidase to galactose and 5-bromo-4-chloro-3-hydroxyindole. This last compound has a blue color that allows distinguishing between bacterial colonies that were part of the expression vector (without staining) from those that did not (blue), since the insertion of genetic material in the vector interrupts the expression sequence of β- galactosidase, preventing hydrolysis of X-GAL.

After the addition of X-GAL and IPTG, it was incubated between 2 and 3 minutes on ice, and 1 ml of LB culture medium without antibiotics was added. The preparation was incubated between 20 and 30 minutes at 37°C with shaking at 1200 rpm. It was centrifuged at maximum speed for 1 minute and 850 µl of supernatant was discarded. The bacterial pellet was resuspended in the supernatant and smeared with sterile loops on ampicillin agarose plates. Since the expression vector confers resistance to ampicillin, only those bacteria that integrated the plasmid are able to grow on the plate. Colonies were allowed to grow overnight in incubation at 37°C. Several colonies with the desired characteristics (without staining, with clonal growth and without nearby satellite colonies) were selected and recovered using sterile wooden toothpicks. Colonies were placed in test tubes with LB medium and incubated with shaking at 37°C until the desired optical density was obtained. The incubation period was between 8 and 24 h. Plasmid extraction and purification was performed using the NucleoSpin® Plasmid system, Mini kit for plasmid DNA (Macherey-Nagel GmbH & Co. KG, Germany) according to the manufacturer's instructions. Restriction enzymes digestions were performed to release

the insert from the vector and corroborate the presence and size of the insert prior to its shipment for sequencing by the Sanger method to Macrogen (Seoul, South Korea).

2.6 RNA extraction and RT-qPCR

Total RNA was extracted using TRIzol (Invitrogen, ThermoFisher, USA) according to the manufacturer's instructions. For qPCR experiments, isolation was performed using the NucleoSpin RNA column RNA extraction kit (Macherey-Nagel, GmbH & Co. KG, Germany). The amount of total RNA was evaluated by NANODROP2000. (NanoDrop Products, Wilmington, DE, USA).

Reverse transcription (RT) was carried out using 1 µg of total RNA. The *RevertAid First Strand cDNA Synthesis Kit* (Thermo Fisher, USA) reverse *transcription* system was used.

Next, the amplification was performed by quantitative real time polymerase chain reaction (qPCR) using the intercalating *SYBER GREEN* (SsoFast EvaGreen supermix, Bio-Rad Laboratories, USA), (Takyon EUROGENTEC, Belgium) in the CFX96 qPCR machine (Bio-Rad Laboratories, USA). The specific primers used for each gene are listed in the primer table (Section 6.1). The relative change in expression was calculated with the double delta Ct (2^(-△△Ct)) method [260, 261] normalized to the level of glyceraldehyde-3-phosphate dehydrogenase (GAPDH). Further statistical analysis is described in section 2.16 (Statistical analysis).

2.7 Northern Blot

2.7.1 Procedure

20 µg of Total RNA were used per condition. 20 µg of RNA in 2X *RNA loading buffer* were denatured at 65 ° C for 10 minutes. Subsequently 2.3 µL of 400 mM ethidium bromide were added. Electrophoresis was performed in 1X MOPS (3- (n-morpholino) propanesulfonic acid) buffer gels, 1% agarose and 2% formaldehyde. The run was carried out at a constant 70 V until the running front reached the middle of the gel. It was then increased to 110 V until the end of the run (until the run front was within an inch of the limit). Subsequently, the gel was incubated in motion in 50 mM sodium hydroxide (NaOH) for 30 minutes, 50 mM Tris pH 7.5 for 30 minutes and finally 20X SSC (0.3 M tri-

Sodium Citrate; 3 M Sodium Chloride) for 30 additional minutes. All incubations were carried out at room temperature (25°C).

The material was then transferred to a membrane using an array of plastics and Whatman filter papers (Whatman Plc, Maidstone, United Kingdom) that allowed the RNA fragments to migrate by capillary action from the gel to the membrane (Cytiva Ameshram™ Hydrobond™, Marlborough, USA) in an overnight incubation at room temperature.

Once the transfer was finished, the effectiveness of the method was verified using a UV transilluminator and the RNA-membrane *cross-link was carried out* by exposure to UV using a UV Stratalinker at 254 µm (Auto-crosslink at 1200 Joules).

The membrane was then placed in a hybridization bottle containing approximately 30 ml of *hybridization buffer* (5 × SSC; 20 mM NaPi pH 7.2; 7% SDS, 0.02% Albumin fraction V; 0 , 02% Ficoll 400; 0.02% polyvinylpyrrolidone K30) and a pre-hybridization was carried out for 30 minutes. Finally, the cDNA probe previously generated by PCR using the DAGAR primers (NB 1 and NB 2, Section 6.1) previously labeled (See section 2.7.2) was added and incubated overnight in a rotary oven at 60 °. C.

Membrane washing was performed by replacing the hybridization solution with wash buffer 1 (2X SSC + 0.1% SDS) for 15 minutes. Then the wash buffer 1 was changed for wash buffer 2 (0.5X SSC + 0.1% SDS) and incubated for 30 minutes; and finally a final wash was performed with wash buffer 3 (0.1X SSC + 0.1% SDS) for 30 minutes. All incubations were carried out in rotation at 60°C.

Subsequently, the preparation was removed from the bottle, the labeling and radioactivity level of the membrane were corroborated and it was placed to expose within a radiographic *cassette* against a radiographic exposure membrane for approximately one week. The Northern Blot was revealed using a Phospho Imager laser scanner (Bio-Rad Laboratories, USA).

2.7.2 Probe labeling

Probe labeling was performed using the *GE Healthcare Amersham™ Megaprime™ DNA Labeling System* Kit (Thermo Fisher, USA) according to the manufacturer's instructions.

Internal radioactive double labeling was used with [α-^{32}P] dCTP and [α-^{32}P] dATP.

2.8 RNA deep sequencing

RNA deep sequencing was performed in RNA derived from proliferative (D0) and confluent (D2) SMC (hPASMC, Lonza). lncRNA candidates were validated by RT-qPCR and the efficiency of differentiation in D2 was assessed by changes in the expression of marker genes.

1 µg of RNA derived from both proliferative (D0) and confluent (D2) SMC was used for library preparation with the *TrueSeq RNA preparation Kit system* (Illumina®, New England Biolabs, MA USA). For the RNA deep sequencing of the transcripts immunoprecipitated with YTHDF2 (RIP-YTHDF2) in proliferative SMC (D0) and at the beginning of differentiation (D2), RNA derived from 6 different conditions (Input, IgG control and YTHDF2 IP, for both conditions) was used to prepare libraries (*NEBNext® Ultra ™ II RNA Library Prep Kit for Illumina®*, New England Biolabs, MA USA). 3 µg of initial RNA was used for SMC D0 and 6 µg of initial RNA for SMC D2, since the expression of YTHDF2 is approximately 50% in SMC D2 with respect to D0. 10 million copies of 3 exogenous synthetic reference RNAs (*Spiking RNAs*) were added to each immunoprecipitated condition (RIP-YTHDF2, IgG), and 10,000,000 times the ratio of RNA concentration in input over RIP-YTHDF2 condition were added to the inputs (10000000*[RNA INPUT]/[RNA RIP-YTHDF2] copies) for both D0 and D2. RNA integrity was corroborated before and after DNAse I digestion, as well as at all points suggested by the manufacturer of the library generation system using Tape Station (Agilent, USA). Ribosomal RNA depletion was performed using the riboPOOL system (siTOOLS, Germany). Libraries were prepared according to the manufacturer's instructions. 5 extra cycles of PCR amplification were performed on the control immunoprecipitation (IgG) in the final step of library generation to ensure a sequenceable base. The data were then

normalized according to the exogenous reference RNAs. The sequencer used was a *Hi-Seq 2000* (Illumina®, New England Biolabs, MA USA).

Data normalization and statistical enrichment analysis was performed using R software [262]. More information in section 2.15 (Bioinformatic analysis).

2.9 Cytometry

S-phase cell determination was performed by Flow Cytometry (Fortessa, Becton Dickinson, Franklin Lakes, NJ USA) after staining with propidium iodide (Bromodeoxyuridine). Briefly, cells maintained in growth medium were permeabilized with 100% ethanol and incubated at -20°C for 30 minutes. Then, the cells were incubated with 10 mg/ml of RNAse A, and 1 mg/ml of propidium iodide for 30 minutes at 37 ° C in the dark.

2.10 RNA-protein affinity purification

Differentiated SMC (D6) were subjected to a cross-linking agent to preserve transient interactions between nucleic acids and proteins (4% formaldehyde for 10 minutes followed by 5 minutes of 1% glycine to stop the reaction); and then samples were lysed (see section 2.12) and sonicated for 20 minutes (Bioruptor, Diagenode™, Belgium) to obtain nucleic acid fragments of approximately 300-600 nucleotides. The raPOOL system (siTOOLS®, Germany) was then used following the manufacturer's instructions. Briefly, the lysate is incubated with a set of small biotinylated DNA probes directed against the *DAGAR* sequence, to be then precipitated using streptavidin-conjugated magnetic beads. The precipitate obtained was processed for protein extraction followed by acrylamide/bisacrylamide gel electrophoresis. The areas showing specific bands were cut out, purified and subsequently sent for analysis by mass spectrophotometry. Two negative controls were used: nonspecific probes in the same cell type (raPOOL anti Lac-Z in SMC) and specific probes for *DAGAR* in a cell type that does not express target RNA (raPOOL anti *DAGAR* in HEK293 cells).

2.11 Immunoprecipitation and precipitation of polyadenylated RNA

Background: This technique, widely used in molecular biology, consists in the precipitation of molecules of interest by using agarose *beads* (*Sepharose beads*) or *magnetic beads* (*Dynabeads magnetic beads*). In the case of polyadenlylated RNA precipitation, these beads are conjugated with polythymine tails, while for immunoprecipitations, they are conjugated with protein G. In the latter case, the conjugated beads have a high immunoglobulin binding capacity and can be coupled with specific antibodies, allowing their precipitation after they have interacted with their target molecules, dragging their antigen with them. In the case of agarose beads, precipitation is carried out by centrifugation, while in the case of magnetic beads a magnet is employed. In this work, this technique is used in conjunction with real-time PCR (RT-qPCR) for the detection of RNAs with the modification N6-Methyladenosine (m^6A) from a total RNA extract; as well as to describe the target RNA of an m^6A reading protein, through RNA deep sequencing of transcripts recovered from the immunoprecipitation of YTHDF2 in SMC. The methods used for both immunoprecipitations are detailed below.

2.11.1 RNA m^6A

Total RNA from SMC at D0 and D2 of differentiation as well as form fibroblasts MRC5 at proliferative and quiescent states was isolated by TRIzol (Invitrogen, ThermoFisher, USA) according to the manufacturer's instructions. 10 µg of purified anti-m^6A [263](Clone 9B7) were incubated with 6 µg of total RNA in 1 ml of RNA-IP buffer (50 mM Tris pH 7.5, 150 mM NaCl, 5mM EDTA, 0.5% NP-40, 10% glycerol) for 3 h at 4°C. 30 µl of magnetic beads (*Magnetic dynabeads,* Invitrogen, USA) or *Sepharose* beads (GE Healthcare, USA) were added and incubated for 2 additional h at 4°C. The preparations were washed three times with washing buffer (50 mM Tris pH 7.5, 300 mM NaCl, 5mM EDTA, 0.5% NP-40, 10% glycerol). For RNA isolation from the beads, 500 µl of TRIzol and 100 µl of Chloroform were used, which was then precipitated by Isopropanol. An anti-IgG antibody was used as a negative control for nonspecific binding to the heavy chains of the antibody.

2.11.2 YTHDF2 protein

Immunoprecipitation of RNAs associated with the YTHDF2 protein was performed in proliferative (D0) and confluent SMC, at the beginning of differentiation (D2) in triplicate. For cells in D0, 10 T75 bottles for adherent mammalian cell culture (Corning, USA) were pooled between 70% and 85% confluence, while for cells in D2 state (confluent cells), 3 T75 bottles were pooled for each replicate. Because the expression of YTHDF2 is decreased by approximately 50% in the D2 condition with respect to D0, twice the total protein was used in the D2 condition with respect to D0, to obtain a similar amount of RNA bound to the protein of interest in both conditions. Cell lysis was performed by incubation for 30 minutes at 4°C in 1 ml of lysis buffer solution (25 mM TrisHCL pH 7.5, 150 mM KCl, 2 mM EDTA, 1 mM NaF, 0.5% NP-40, 1 mM DTT and 500 µM AEBSF in milliQ water) and occasional mixing, followed by 30 minutes of centrifugation at 20,800 G. Prior to the start of immunoprecipitation, the total protein concentration was measured by spectrophotometry using the Bradford assay (Biorad, USA). The total protein concentration was adjusted by adding lysis buffer. 150 µl were separated as initial fraction (Input) for each sample: 50 µl for protein extraction and control Western Blotting and 100 µl were used to extract total RNA. 100 µl of magnetic beads (*Magnetic dynabeads*, Invitrogen, USA) conjugated with 12 µg of antibody were used for each immunoprecipitation. Of each ml of sample, 400 µl were incubated with the control antibody (anti-IgG) and 400 µl with the antibody against YTHDF2. From each immunoprecipitation (500 µl in total), half (250 µl) was used for protein extraction and control Western Blot; and the other half (250 µl) for RNA extraction, library preparation and subsequent deep sequencing. The conjugation of the magnetic beads with the antibodies was carried out overnight in PBS at 4°C in rotation. Incubation of the lysate with the conjugated beads was carried out in a lysate buffer solution for 3 h at 4°C in rotation. Then the magnetic beads were washed three times with washing buffer solution (50 mM Tris-HCl pH 7.5, 300 mM KCl, 1 mM MgCl2, 0.5% NP-40, 1 mM DTT and 500 µM AEBSF in milliQ water) and resuspended in 500 µl of lysis buffer. Of the total immunoprecipitation, 250 µl were separated, 750 µl of Trizol LS (Thermo Fisher, USA) was added and the RNA was extracted according to the manufacturer's instructions. The

remaining 250 µl was placed on a magnet to separate the beads with the immunoprecipitate, the supernatant was discarded and resuspended in 20 µl of lysis buffer. Then 5 µl of 5X *Laemmli Buffer* was added and the immunoprecipitate was incubated for 5 minutes at 95°C to continue with the Western Blot protocol. 30 µg of each input and the totality of the separated immunoprecipitates for this purpose were used for the run. Treatment with DNAse I was performed to eliminate genomic DNA. Samples were depleted from ribosomal RNA by using the riboPOOL system (siTOOLS, Germany) according to the manufacturer's instructions. The integrity of the RNA was corroborated in all steps of the protocol using the Tape Station system (Agilent, USA). This system was also used for precision measurements, necessary for the incorporation of exogenous reference RNAs (*spiking*) and in control steps of the library preparation protocol. Libraries for deep sequencing were prepared according to the instructions of the manufacturer of the NEBNext Ultra II RNA library Kit (Illumina®, New England Biolabs, USA).

2.11.3 Precipitation of polyadenylated RNA

Precipitation of polyadenylated RNA from total RNA using magnetic beads conjugated with polythymine (Oligo $(dT)_{25}$ Dynabeads, Invitrogen, USA) was performed to characterize the structure of the mature transcript of the candidate lncRNA.

For this, 5 samples of 75 µg of total RNA were used in 100 µl of water suitable for RNA (distilled, treated with diethylpyrocarbonate (DEPC), free of RNAses). For each sample, 100 µl of binding buffer (20 mM Tris-Hcl, pH 7.5, 1 M LiCl, 2 mM EDTA) was added. It was incubated at 65°C for 2 minutes to break down secondary structures and the preparation was immediately chilled on ice. 200 µl of total RNA was added to the 200 µl of previously washed beads. 1 mg of beads were washed and resuspended in 200 µl of binding buffer for this purpose. The preparation was mixed and incubated with continuous spinning on a mixer for 5 minutes at room temperature. Then, the tube was placed on a magnetized support for 1-2 minutes and the supernatant was removed and placed in a new tube and stored as a non-polyadenylated fraction (Poly A -). The tube with the beads was removed from the magnetic support and 200 µl of wash buffer B (10 mM Tris-HCl, pH 7.5, 0.15 M LiCl, 1 mM EDTA) was added. The beads were resuspended

in wash buffer B and separated again with the magnetic support. The supernatant was discarded and washed again by the same procedure. The pellet from the beads was resuspended in 20 µl of 10 mM Tris-Hcl and incubated at 75-80°C for 2 min to release the RNA from the magnetic beads and the tube was immediately placed on the magnet. The supernatant was transferred to a new RNAse-free tube. This fraction is enriched in polyadenylated RNA (Poly A +).

2.12 Protein extraction

Cells harvested using a cell scraper were washed with phosphate buffered saline (PBS) at 4°C twice to remove cell debris and then incubated with lysis buffer (25 mM Tris-HCl pH 7.5, 150 mM KCl, 2mM EDTA, 1mM NaF, 0.5% NP-40 in H2O milli Q, 1mM DTT, 500 µM AEBSF) at 4°C for 30 minutes with occasional mixing. Then the lysate was centrifuged at 16,000 G for 20-45 minutes and the supernatant was recovered in a new container. Protein quantification was performed by the Bradford Assay and the concentration was calculated by absorbance at 595 µM, normalized to the calibration curve performed with the absorbance of the control samples. The concentration was adjusted to the desired level by adding lysis buffer. Finally, 5X *Laemmli Buffer* was added and incubated at 95°C for 5 minutes. At this point the samples were used for gel electrophoresis or stored at -20°C.

2.13 Western blot

30 µg of total protein were used per lane. 10% sodium dodecyl sulfate polyacrylamide gel electrophoresis (SDS-PAGE) was performed. The run was carried out at 120V constant voltage for the stacking *gel* and at 180V for the resolving *gel*. The transfer was carried out with a semi-dry transfer chamber at constant intensity so that the milliamperes required would be twice the height of the gel multiplied by the width of the gel, in a time in minutes equivalent to the approximate weight in kDa of the protein that was you want to visualize. Nitrocellulose membranes (Cytiva, USA) were used. Blocking was performed for 30 minutes in movement with 0.1% TBS-T + 2.5% bovine milk. All the primary antibodies used were incubated overnight at 4°C in motion, and all the secondary antibodies used at room temperature for 1h in motion and

darkness. Glyceraldehyde-3-Phosphate-Dehydrogenase (GAPDH) was used as a loading control. The image analysis software Image J (*National Institute of Health, USA*) was employed to quantify the optical density of the signals.

The antibodies used are detailed in section 6.2 (Table 6.2.1)

2.14 Immunofluorescence

Cells previously plated in circular glasses coated with 0.2% gelatin placed in 24 well plates and cultured under previously described conditions were fixed for 20 minutes at room temperature using a fixing solution (4% paraformaldehyde in PBS pH 7.4). The permeabilization was carried out for 10 minutes at room temperature (RT) with a permeabilization solution (3% Bovine Serum Albumin (BSA) and 0.2% Triton x100 in PBS) and washed twice with the washing solution (0, 2% BSA and 0.1% Tween20 in PBS) between each step of the protocol. Incubation with the primary antibody solution (in washing solution) was carried out overnight (ON) at 4°C in a humid chamber. The antibodies used were anti-α-SMA, anti-CNN1 (DAKO, Cytomation, Carpinteria CA, USA) and anti-Ki67 (Novocastra®, Newcastle, UK). Secondary antibodies conjugated with fluorescein (Jackson Immuno Research, West Grove, PA, USA) and diluted in PBS, were incubated for 1h at room temperature (RT). PRO-LONG GOLD mounting medium (Thermo Fisher, CAT # P36930, USA) with DAPI staining for nuclei visualization, was used. The antibodies used are detailed in section 6.2 (Table 6.2.1).

2.15 Bioinformatic analysis

For data normalization, control and enrichment calculations, the R Studio software was used, including the following packages: dplyr [264], ggplot2 [265], EnsDb.Hsapiens.v86 [266], DOSE [267], clusterProfiler [268], ReactomePA [269], DESeq2 [270]. For the Human gene atlas database analysis of cell type gene set enrichment the Enrichr online platform (https://maayanlab.cloud/Enrichr/) [271, 272] was used, and the downloaded data tables were graphed and styled using the R Studio software (https://www.rstudio.com/). For quality control, the sample to sample distance was analyzed (Section 6.3, Figure 6.3.1) and multivariate principal component analysis (PCA)

were performed, showing an acceptable grouping between replicates, as well as an appreciable distance between treatments (Section 6.3, Figure 6.3.2). Then, the enrichment of target genes in YTHDF2 (RIP-YTHDF2) immunoprecipitation compared to IgG immunoprecipitation (RIP-IgG) was calculated. A list of genes specifically bound to YTHDF2 was obtained, using a stringent selection criterion detailed below: Adjusted p value less than 0.01; mean of *counts* greater than 5, expressed in at least 2 of the 3 replicates and a logarithm base 2 value of the *fold change* (log2FC) greater than 4. Then, the enrichment analysis was performed in YTHDF2 IP compared to the INPUT, in order to identify the main YTHDF2 target genes in each condition. For this, a criterion of adjusted p value less than 0.05 and a positive value of log2FC were selected. It should be noted that those genes that passed the nonspecific binding filter cannot be discarded as YTHDF2 target genes (significantly enriched in RIP-YTHDF2 *vs* RIP-IgG but not enriched with respect to the INPUT). However they were not included in the subsequent enrichment analysis, since the objective was to describe the main signaling pathways regulated by YTHDF2, with a high level of confidence.

2.16 Statistical analysis

In general, the applied statistical analyzes vary according to the nature of the data to be analyzed and are closely related to the applied experimental design. Some of the data presented do not have associated statistical analysis because they correspond to exploratory experiments, whose statistical significance does not affect the conclusions of the work. For those data that were statistically analyzed, the necessary assumptions were checked according to the applied model. The GraphPad Prism 8 program (San Diego, USA) was used for statistical analysis and graphing.

In general, the differential expression analysis by RT-qPCR was performed by analysis of variance (ANOVA) in experiments with three conditions (three levels of the "treatment" factor), as is the case of the differentiation curve in SMC (with three levels of the differentiation factor, corresponding to D0, D2 and D6). In this case, it is intended to demonstrate that there are changes in the mean of the response variable associated with genes of interest during the differentiation process (or between more than two conditions), and by means of multiple post-hoc comparisons (Tukey's test), to identify

the nature of this change (increase, decrease) between the different phenotypic states or treatments analyzed.

On the other hand, the comparison of two experimental groups (control and treated, or in the case of proliferative and confluent MRC5 cells), was carried out by means of Student's T-test. An example of these are loss-of-function analyzes, with two levels of the silencing factor, represented by control silencing (siCT) and specific silencing (siDAGAR / siYTHDF2).

Statistical analyzes on samples with n = 2 were performed using Student's T-test with Welch's correction (it does not assume equality of standard deviations) for comparison of two groups, or Brown Forsythe ANOVA with Dunnett's post-hoc multiple comparisons, to the analysis corresponding to 3 experimental groups. This is because the use of n <3 presents the impossibility of testing the assumptions, therefore only variables that can be assumed with normal distribution are analyzed, and it is not assumed that there is homogeneity of variances. Although these tests have a lower associated statistical power, they are the most appropriate statistical resource for comparing experiments performed in duplicate.

It should be noted that the analysis of data derived from RT-qPCR was carried out on the base 2 logarithmic transformation of the normalized relative expression (NRE), as suggested in [261]. The distribution of the NRE variable accumulates between 0 and 1 the values that imply a decrease in the expression, while the increases are distributed between 1 and infinity, hence in its nature it does not have a normal distribution. The logarithmic transformation of NRE has a normal distribution between –infinite and infinite, with mean 0 for NRE values equal to 1 (unchanged with respect to the control). The logarithmic transformation is performed in base 2 because the relative change observed between conditions doubles for each PCR cycle of difference in Ct (see section 2.6), as explicitly stated by the formula 2^(-ΔΔCT). It is for this reason that the graphic representation is made with the normalized relative expression, which intuitively represents the relative change observed in the expression of the gene of interest, even though the statistical analysis has been performed on the logarithmic transformation of the variable.

Chapter 3

RESULTS

3 Results

The results presented below have been subdivided according to the development of each specific objective, however, it should be noted that Part I and II are closely related, so subsequent experiments with special attention to the interrelation of both parts are included in part II.

3.1 Part I

3.1.1 Long noncoding RNAs differentially expressed during human SMC differentiation

An *in vitro* model of human pulmonary artery smooth muscle cell differentiation (hPASMC, Lonza), previously validated by our laboratory, was used to find differentially expressed lncRNAs during SMC differentiation [17, 85]. Proliferative (de-differentiated) and confluent cells (at the beginning of differentiation), named D0 and D2 respectively, were analyzed by RNA deep sequencing. Of the total of differentially expressed transcripts, 1470 represent coding genes and the remaining correspond to non-coding RNAs, of which 828 were classified as long non-coding RNAs (lncRNA) (Figure 6). The analysis of differential expression of genes in D2 with respect to D0 showed, as expected, an increase in the expression of genes related to the transforming growth factor beta (TGFβ) signaling pathway and with the formation of cytoskeleton elastic fibers, as well as a decrease in the expression of genes related to cell cycle progression (Figure 6A). In a consistent manner, modulation of RNAs that change during SMC differentiation was observed, denoted by the increase in alpha smooth muscle actin (ACTA2), Vitronectin (VTN), leiomodin 1 (LMOD1) and differentiation factor 5 (GDF5), among others, and the decrease in the expression of genes that encode extracellular matrix proteins (such as collagens and metalloproteinases) (Figure 6B).

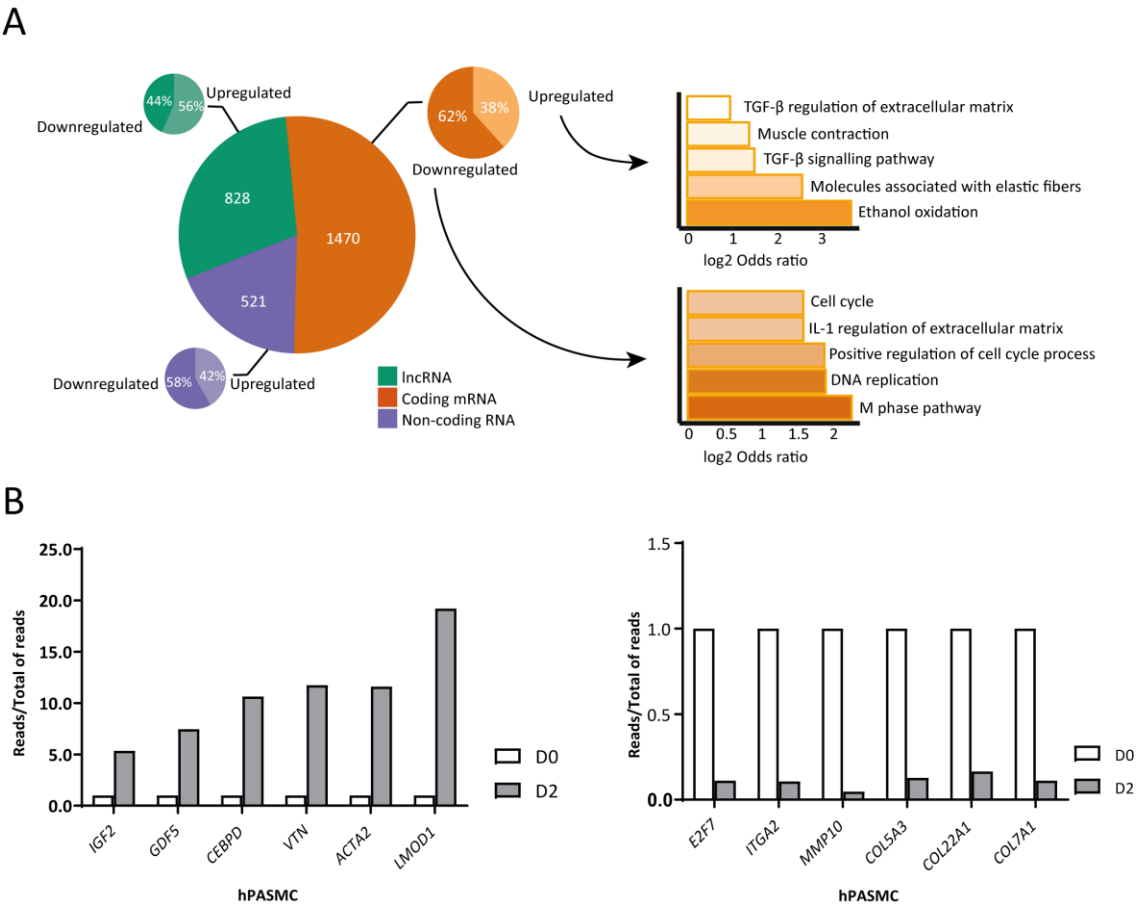

Figure 6. RNA deep sequencing in human pulmonary artery smooth muscle cells (hPASMC) in a proliferative state (D0, 70% confluence) or at the beginning of differentiation (D2, 100% confluence) A) Graphic representation of the different RNA classes and signaling pathways that were found regulated at the beginning of differentiation, analyzed by RNA deep sequencing in hPASMC D0 and D2. B) Differential expression of known genes that increase (left panel) or decrease (right panel) their expression during differentiation into smooth muscle cells.

3.1.2 Expression of candidate genes in the different cell types that build up the artery

The transcriptomic analysis revealed numerous lncRNAs that modify their expression during SMC differentiation. The main candidates were validated by RT-qPCR in the complete differentiation model. Furthermore, its expression in human pulmonary artery endothelial cells (EC) (hPAEC, Lonza) was analyzed to assess the specificity of the candidates in SMC compared to EC. No associated statistical analyzes are presented due to the exploratory nature of the experiment (Figure 7).

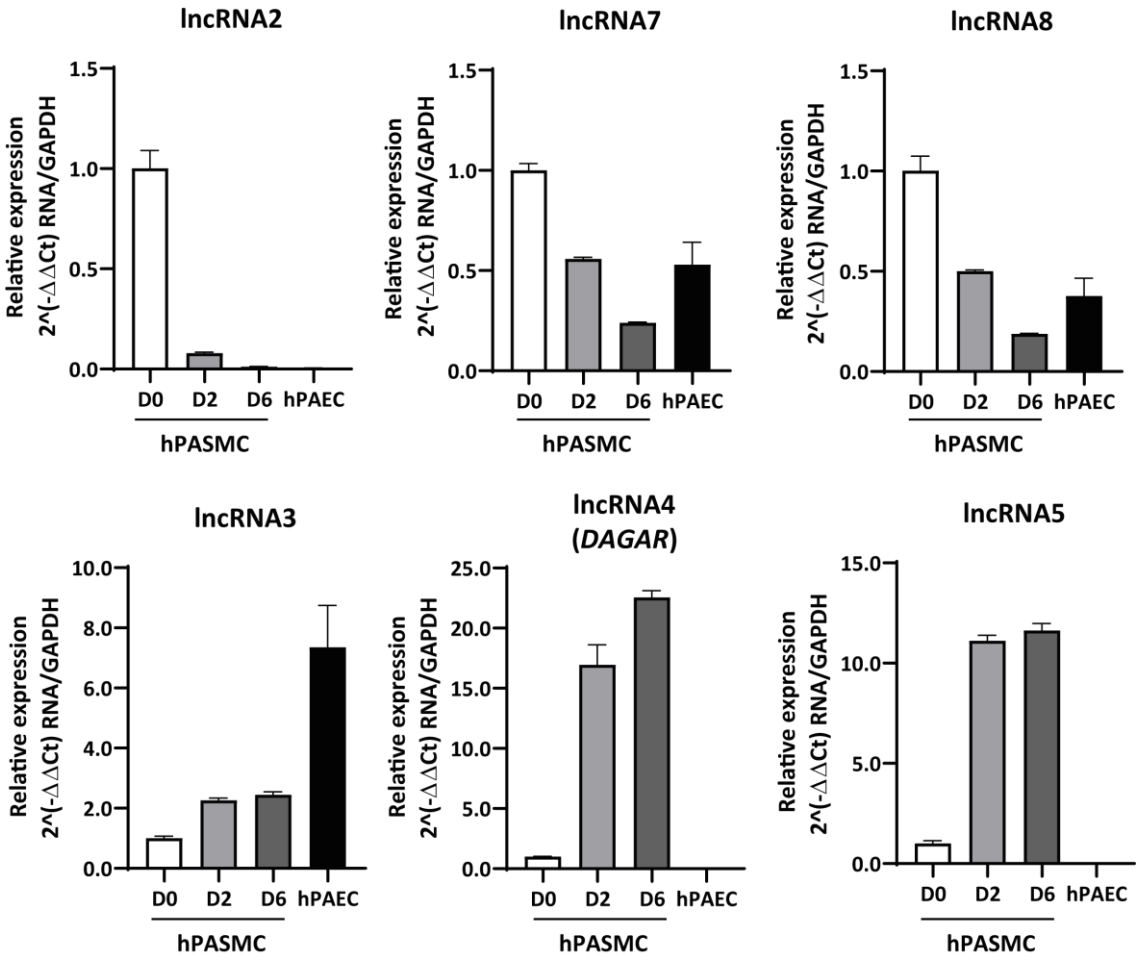

Figure 7. Normalized relative expression of candidate RNA during the differentiation process in human pulmonary artery smooth muscle cells (hPASMC) in proliferative/dedifferentiated (D0, cells at 70% confluence), at the beginning of differentiation (D2, cells 100% confluent) and differentiated (D6, 4 days after reaching confluence) states, and in human pulmonary artery endothelial cells (hPAEC), obtained by RT-qPCR.

3.1.2.1 Candidate selection

The candidate lncRNA (TCONS_00006193, CATG000061625.1 and hereinafter *referred to* as *DAGAR*) was selected for a deeper characterization, since a marked increase in its expression was observed during differentiation, surpassing all the candidates analyzed, while it was almost undetectable in proliferative SMC, and not detectable in hPAEC (Figure 7). *DAGAR* is encoded on chromosome 3, band 3p21.2 between the HEG1 and SLC128A genes. The FANTOM CAT database [273] describes 6 variants, including a short form of 194 nt and 5 long forms of 2938, nt, 3173 nt, 3386 nt, 3452 nt and 3674 nt (Figure 8). Its expression in MRC5 pulmonary fibroblasts was also analyzed, since it was the closest cell line available representing fibroblasts from the adventitia of pulmonary arteries. In these cells, the behavior of *DAGAR* was similar to that observed in SMC, being almost undetectable in proliferating cells, and showing a

marked increase after cell cycle arrest by different stimuli. The expression of *DAGAR* will be analyzed in detail in sections 3.1.2.2 & 3.1.2.3.

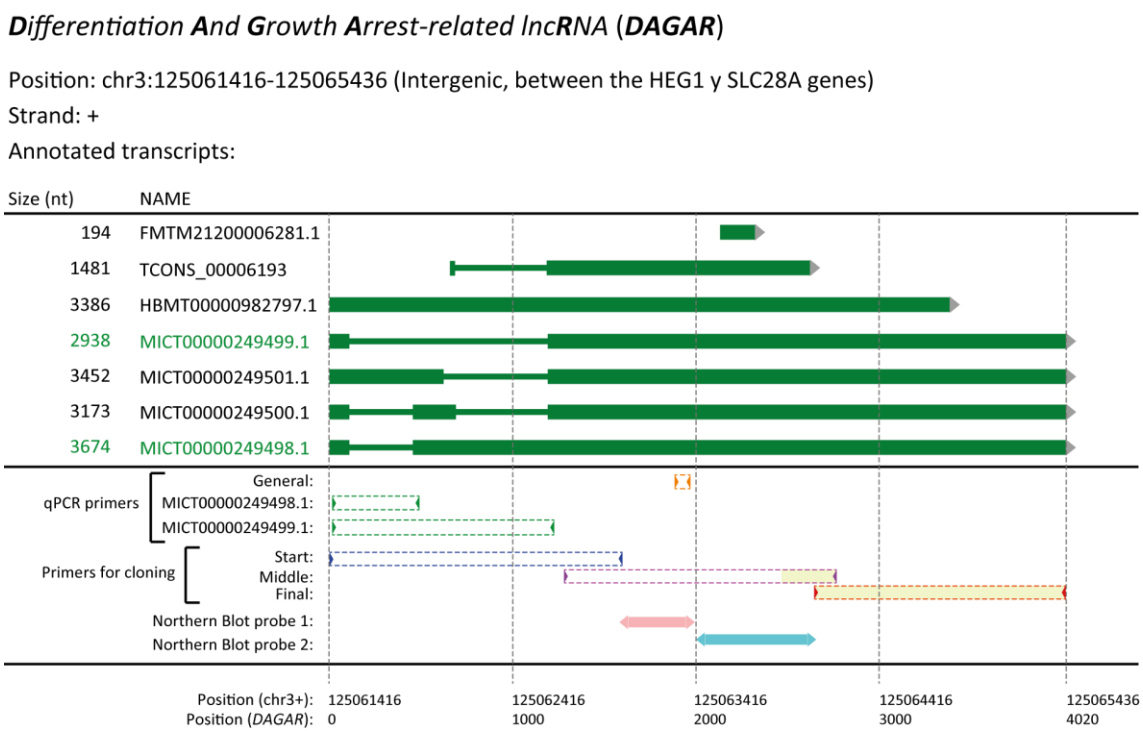

Figure 8. DAGAR locus and annotated variants. The different variants annotated in the available databases (FANTOM CAT and Genome Browser) are depicted. The sites of all primers used for RT-qPCR and cloning experiments are outlined, as well as the binding site for the Northern Blot probes. The name of the variants found in cloning and sequencing experiments is highlighted in green, and the area that was not sequenced in yellow.

3.1.2.2 Characterization of the mature transcript

Polyadenylated RNA precipitation from total RNA was performed in confluent MRC5 cells using polythymine conjugated beads (OligodT dynabeads, Invitrogen, USA). Then, the analysis by RT-qPCR was carried out in order to investigate the polyadenylation status of the mature *DAGAR* transcript. As a control of the technique, the RNA was run on an agarose gel and the intercalator ethidium bromide was used to stain nucleic acids. In the Figure 9 it can be observed that the fraction enriched in polyadenylated RNA (Poly A +) has less intensity in the 18S and 26S bands of ribosomal RNA (rRNA) compared to the initial fraction or the non-polyadenylated fraction. Although the consensus is that rRNA is not polyadenylated, there is a fraction of both subunits that have this modification, probably constituting an intermediate step in its degradation process [274]. The enrichment analysis over the initial fraction (*Input*) evidenced the presence of *DAGAR* in the polyadenylated RNA fraction.

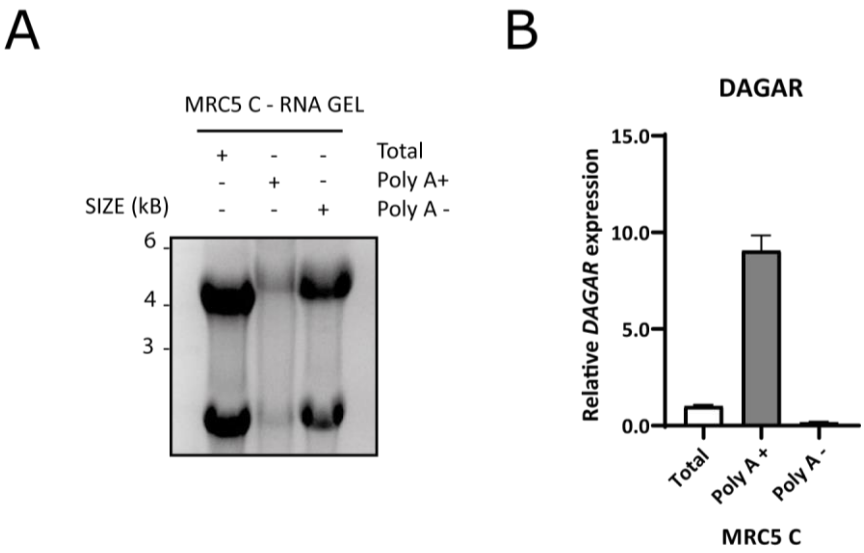

Figure 9. Precipitation of polyadenylated RNA. A) Agarose gel electrophoresis for visualization of RNA derived from confluent MRC5 cells. Three lanes are observed corresponding to the initial fraction (Total), Poly A + corresponding to the fraction precipitated with polythymine magnetic beads and Poly A- corresponding to the supernatant obtained after precipitation. Ribosomal rRNA depletion (non-polyadenylated) is observed in the Poly A + fraction. B) Enrichment relative to the total fraction analyzed by RT-qPCR for DAGAR. A marked enrichment is observed in the Poly A + fraction (n = 2).

RT-PCR experiments were performed followed by cloning and sequencing by the Sanger method (Technical details are described in section 2.5), allowing the identification of the variants that are expressed in SMC and MRC5 cells. Specific primers were used in the areas outlined (Figure 8). Cloning was achieved in the area with intronic variability (Start) and in the middle area of the transcript (Middle), however it was not possible to obtain the final fragment. The variants detected were MICT00000249498.1 and MICT00000249499.1, hereinafter *DAGAR-1* and *DAGAR-2* respectively. No fragments corresponding to the other variants were obtained. Furthermore, the expression of *DAGAR-1* and *DAGAR-2* in proliferative (D0) and differentiated (D6) SMC was analyzed by RT-qPCR, as well as after silencing by siPOOLs in SMC at the beginning of differentiation (D2). Both variants increased their expression in a similar way in SMC D6 compared to D0. A decrease in the expression of *DAGAR-1* and *DAGAR-2* in SMC D2 was also observed after the silencing of *DAGAR* by siPOOLs, denoting that the effects

and/or functions described cannot be attributed to a particular variant (Figure 10).

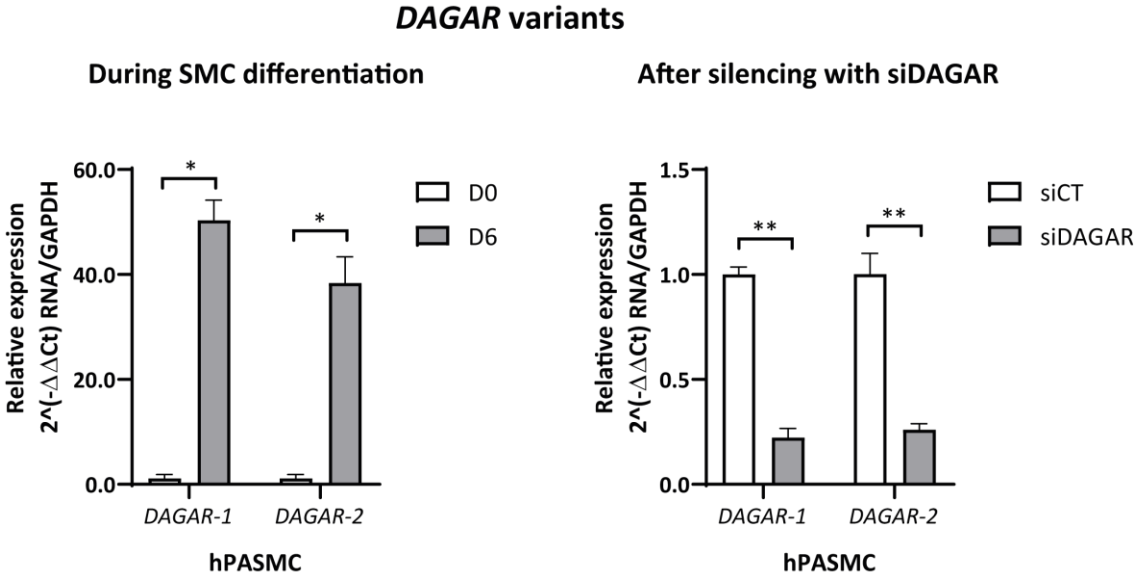

*Figure 10. Expression of DAGAR variants in smooth muscle cells. The normalized relative expression of the DAGAR-1 and DAGAR-2 variants is observed in human pulmonary artery smooth muscle cells (hPASMC) in proliferative / dedifferentiated (D0, cells at 70% confluence) and differentiated (D6, 4 days later) states. after reaching 100% confluence) (left panel, n = 2) and after silencing with siPOOLS against DAGAR (right panel, n = 2) in hPASMC by RT-qPCR with GAPDH as loading control. Analyzed by Student's t test with Welch correction on the base 2 logarithm of the normalized relative expression. p <0.05 *; p <0.01 **.*

In this sense, it was attempted to clone the different isoforms in expression vectors to work in a variant-specific manner. However, it was not possible to clone the final segment of the mature transcript (Figure 8, "Final" segment). Due to the technical difficulty that this represented, it was decided to work with primers that recognize both isoforms and presumably the effects reported for the silencing of *DAGAR* arise from the synergy of those corresponding to both variants.

3.1.2.3 Expression profile

DAGAR increased its expression significantly during SMC differentiation, observed by RT-qPCR (Figure 11A). The analysis of the signals obtained by *Northern Blot* using two probes complementary to different sectors of the transcript (Figure 8, Northern Blot Probes) made it possible to detect *DAGAR* in at least one of its variants, with a signal corresponding to approximately 3 kb (presumably *DAGAR-2*) that markedly increases its expression during differentiation (Figure 11 B), confirming the RT-qPCR data.

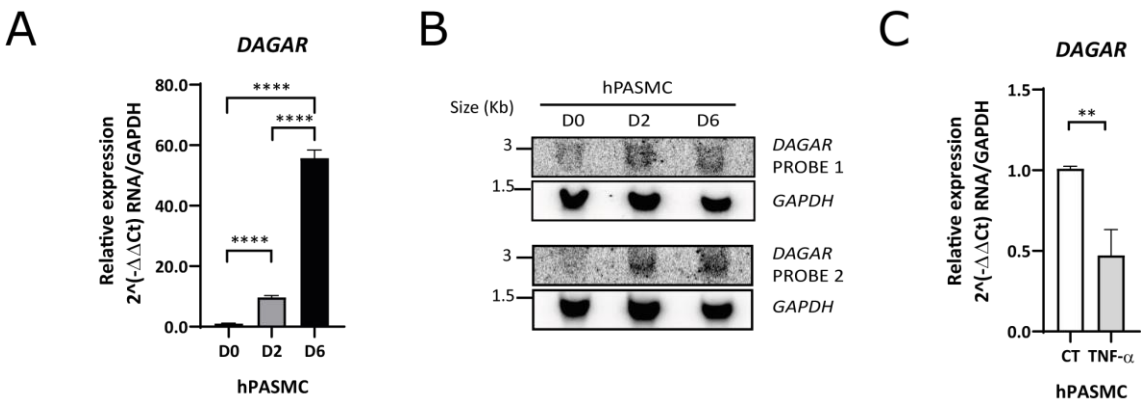

*Figure 11. Characterization of the expression of DAGAR in human pulmonary artery smooth muscle cells (hPASMC). A) Normalized relative expression (2^(-ddCT)) of DAGAR in human pulmonary artery smooth muscle cells (hPASMC) in proliferative/dedifferentiated (D0, cells at 70% confluence), at the beginning of differentiation (D2, 100% confluent cells) and differentiated (D6, 4 days after reaching confluence) states, by RT-qPCR, with GAPDH as loading control. A progressive increase in DAGAR expression is observed during differentiation (n = 3, Analyzed by one-way ANOVA on base 2 logarithmic transformation of normalized relative expression). B) Northern Blot of DAGAR with GAPDH as loading control. A marked increase is observed in the area corresponding to 3 kb (n = 2). C) Normalized relative expression of DAGAR after treatment with 10 ng/µ ofl TNFα relative to vehicle (CT) in hPASMC by RT-qPCR with GAPDH as loading control (n = 6). Data analyzed by Student's t test with Welch correction (does not assume equality of standard deviations) on the base 2 logarithm of the normalized relative expression. p <0.05 *; p <0.01 **; p <0.0001 ****.*

Interestingly, a decrease in *DAGAR* expression was observed after 48 h of treatment with 10 ng/µl of TNFα in SMC D6, a known inducer of dedifferentiation in SMC [17, 102, 103] (Figure 11 C). These data indicate that *DAGAR* expression is related to a quiescent-contractile phenotype in SMC.

A similar behavior was observed in MRC5 cells, with a significant increase in the expression of *DAGAR* after cell cycle exit, induced by different methods. Quiescence was induced by cell contact (48 h after reaching confluence, Figure 12 A), by serum starvation for 48 h (Figure 12 B) and by inhibition of CDK1 by 24 h treatment with the reversible inhibitor Ro3306 (Figure 12 C) [250]. Since this CDK1 inhibition is reversible after 24 h of recovery with normal medium (inhibitor withdrawal), DAGAR expression was tested in this condition and it was observed that *DAGAR* expression returned to basal levels. This data indicates that *DAGAR* expression decreases once cell proliferation has been restored, suggesting that its expression is inversely related to cell proliferation (Figure 12). However, *DAGAR* levels are markedly higher in SMC compared to MRC5 fibroblasts, which is why it was not possible to detect its presence by *Northern Blot* in this cell type.

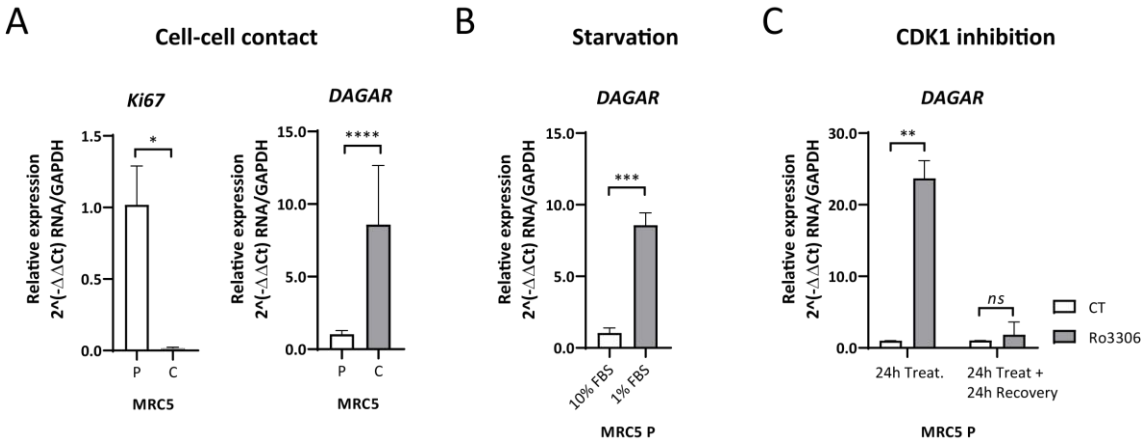

*Figure 12. Characterization of DAGAR expression in proliferative MRC5 lung fibroblasts and after cell cycle arrest under different conditions analyzed by RT-qPCR with GAPDH as loading control. Normalized relative expression is graphed. A) Quiescence induced by cell-to-cell contact. The expression of the proliferation marker Ki67 (n = 2) and DAGAR (n = 5) is observed in proliferative (MRC5 P, 70% confluence) and confluent (MRC5 C, 48 h after reaching 100% confluence) fibroblasts. Analyzed by Student's t test with Welch correction on the base 2 logarithm of the normalized relative expression. B) Expression of DAGAR in nutrient starvation-induced quiescence condition in MRC5 P (1% fetal bovine serum for 48 h) compared to standard growth medium (10% fetal bovine serum) (n = 3). Analyzed by Student's t test on the base 2 logarithm of the normalized relative expression. C) Expression of DAGAR in quiescence condition induced by treatment with 10 µM of Ro3306 for 24 h (left) and after 24 h of recovery in standard medium following treatment compared to vehicle-treated controls (left) or controls treated with vehicle followed by 24h recovery in standard medium (right) (n = 2). Data analyzed by Student's t test with Welch correction on the base 2 logarithm of the normalized relative expression. p <0.05 *; p <0.01 **; p <0.001 ***; p <0.0001 ****.*

3.1.3 Effect of DAGAR Loss of Function on Human SMC Differentiation

In order to evaluate the importance of *DAGAR* in the SMC differentiation process, loss of function experiments were performed using reverse transfection of *siPOOL* (siTOOLS, Germany) against the *DAGAR* sequence in SMC *in vitro*. The silencing efficiency was greater than 50%, evidenced by both RT-qPCR (Figure 13 A) and *Northern Blot* (Figure 13 B). The silencing of the candidate lncRNA caused defects in the differentiation process, denoted by a significant decrease in the mRNA levels of Myocardin (MYOCD), Calponin 1 (CNN1) and Transgrelin (TAGLN) (Figure 13A).

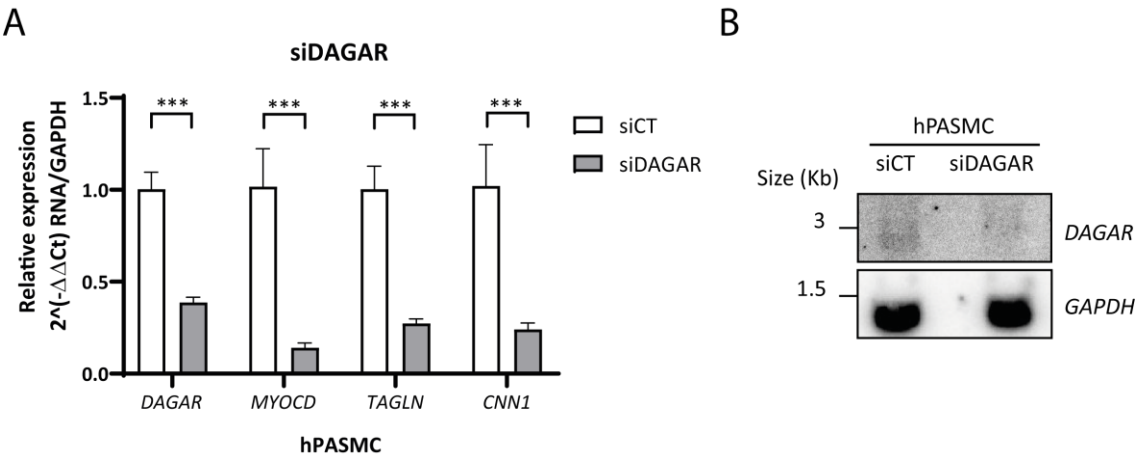

Figure 13. DAGAR silencing in human pulmonary artery smooth muscle cells (hPASMC) by siPOOLs. A) The normalized relative expression of DAGAR, MYOCD, TAGLN and CNN1 is observed after the silencing of DAGAR (siDAGAR) compared to the control siPOOL (siCT) by RT-qPCR with GAPDH as loading control. (n = 3). Data analyzed by Student's t test on the base 2 logarithm of the normalized relative expression. B) Representative Northern Blot after the silencing of DAGAR in siCT and siDAGAR conditions, showing the decrease of the band corresponding to DAGAR.

In correlation with these data, a decrease in the formation of elastic fibers of ACTA2 and CNN1 in cells transfected with siDAGAR compared to siCT was observed qualitatively by immunofluorescence (Figure 14).

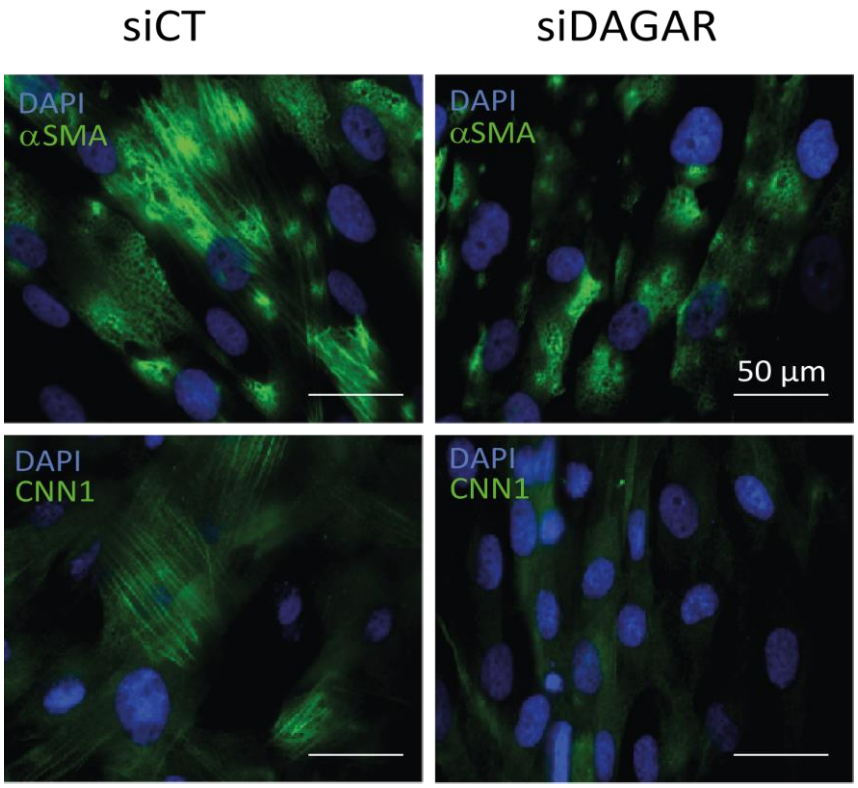

Figure 14. Immunofluorescence under control conditions (siCT) and after silencing of DAGAR (siDAGAR) in human pulmonary artery smooth muscle cells (hPASMC). Formation of alpha smooth muscle actin (αSMA – upper panel) and calponin1 (CNN1 – lower panel) fibers is observed only in siCT condition. DAPI was used for nuclear localization.

In addition, the silencing of *DAGAR* induced an increase in proliferation, represented by a greater expression of the proliferation marker Ki67 at the nuclear level (Figure 15 A and B) and an increase in the percentage of cells in the S phase of the cell cycle (Figure 15 C) observed by flow cytometry after the incorporation of Propidium Iodide, also known as Bromodeoxyuridine (BrU +).

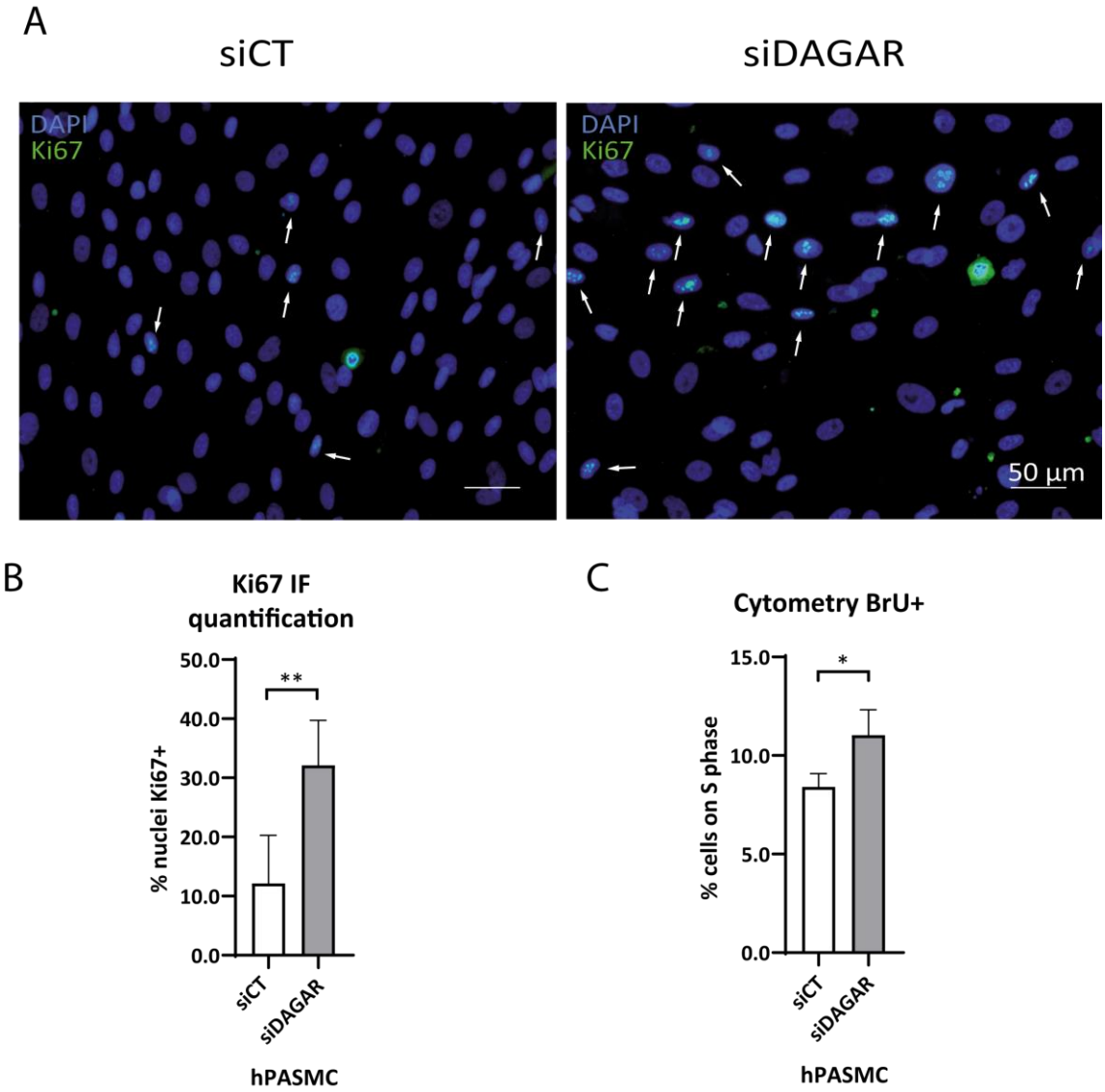

*Figure 15. Changes in cell proliferation evaluated in control condition (siCT) and after silencing of DAGAR (siDAGAR) in human pulmonary artery smooth muscle cells (hPASMC). A) Immunofluorescence staining Ki67 and DAPI. Nuclear colocalization of the proliferation marker Ki67 is indicated with white arrows. B) Quantification of the percentage of positive nuclei for Ki67 (n = 6). Analyzed by Student's T test. C) Percentage of cells positive for the incorporation of bromodeoxyuridine observed by flow cytometry (n = 4). Data analyzed by Student's t test. p <0.05 *; p <0.01 **.*

3.1.4 Analysis of proteins associated with DAGAR

In order to investigate the function of *DAGAR*, a *pull-down* of endogenous *DAGAR* was performed using a set of small biotinylated DNA probes (called raPOOLs),

complementary to various sectors of the mature transcript, capable of recognize both mentioned variants (Section 3.1.2.2), followed by mass spectrophotometric analysis of the proteins co-precipitated with *DAGAR*. Data analysis after removing proteins obtained by non-specific binding, using as a reference those found in the control conditions (for more information see section 2.10), retrieved a list of 240 specifically bound proteins (Section 6.4, Table 6.4.1).

An interesting finding was the Ki67 protein, whose expression increased significantly at the nuclear level after the silencing of *DAGAR* (Figure 15 A and B). This suggests that there could be a direct regulation of Ki67 by *DAGAR*. However, more experiments are needed to confirm this.

To obtain an overview of the pathways and functions related to the proteins found, enrichment analyzes were performed using the R Studio software (Boston, USA) In the first instance, the UniprotR package [275], was used, which works with information available on the Uniprot server. Within the analysis of molecular function (Figure 16), it was possible to recognize as the main enriched terms "*RNA binding*" and "*nucleic acid binding*", which reflects that the proteins that were precipitated with *DAGAR* have the ability to bind to RNA, advocating for binding specificity with the proteins found. In third and fourth place are the terms "*cadherin binding* " and " *cell adhesion molecule binding* ", suggesting that the function of *DAGAR* may be directly linked to cell-to-cell contact, being not only induced by it, but also forming part of the subsequent events.

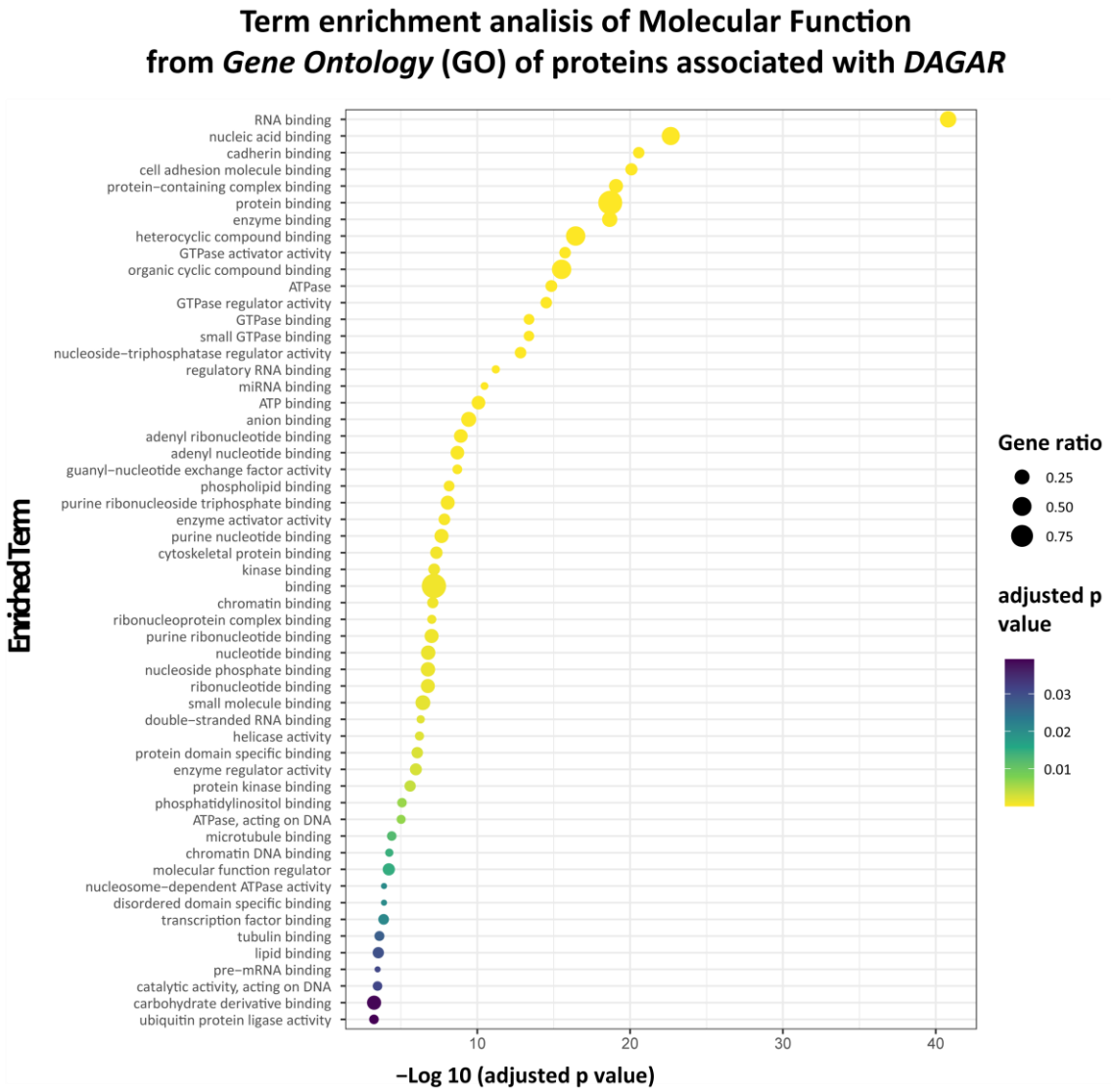

Figure 16. Enrichment analysis of terms associated with molecular function from the Gene Ontology (GO) database. The main enriched terms are observed for the set of proteins co-precipitated with DAGAR. The size of the dot represents the gene ratio (number of genes associated with that particular term/total number of genes). The color scale represents the adjusted p value. The negative logarithm base 10 of the adjusted p value is observed on the X axis. On the Y axis, the enriched terms ordered inversely to their adjusted p value are illustrated.

Interestingly, the term "*GTPase regulator activity*" is enriched in this analysis, in accordance with the Reactome signaling pathways analysis (Figure 17), carried out with the ReactomePA package [269], where it reports that the main pathway represented is "*Rho GTPase cycle*". It should be noted the presence of important pathways for the differentiation of SMC, such as "*Transcriptional regulation by TP53*", which represents an important pathway of tumor suppression, which modulates the proliferation and differentiation of various cell types, as well as "*Pre-NOTCH transcription and translation*" or "*Pre-NOTCH expression and processing*" being the NOTCH pathway of given importance for cell contact-dependent SMC differentiation. Another interesting finding

was the enrichment of terms related to the organization and remodeling of chromatin, in particular "*Chromatin modifying enzymes*" and "*Chromatin organization*", suggesting the possibility that *DAGAR* fulfills a regulatory role on the structure of chromatin through interacting proteins.

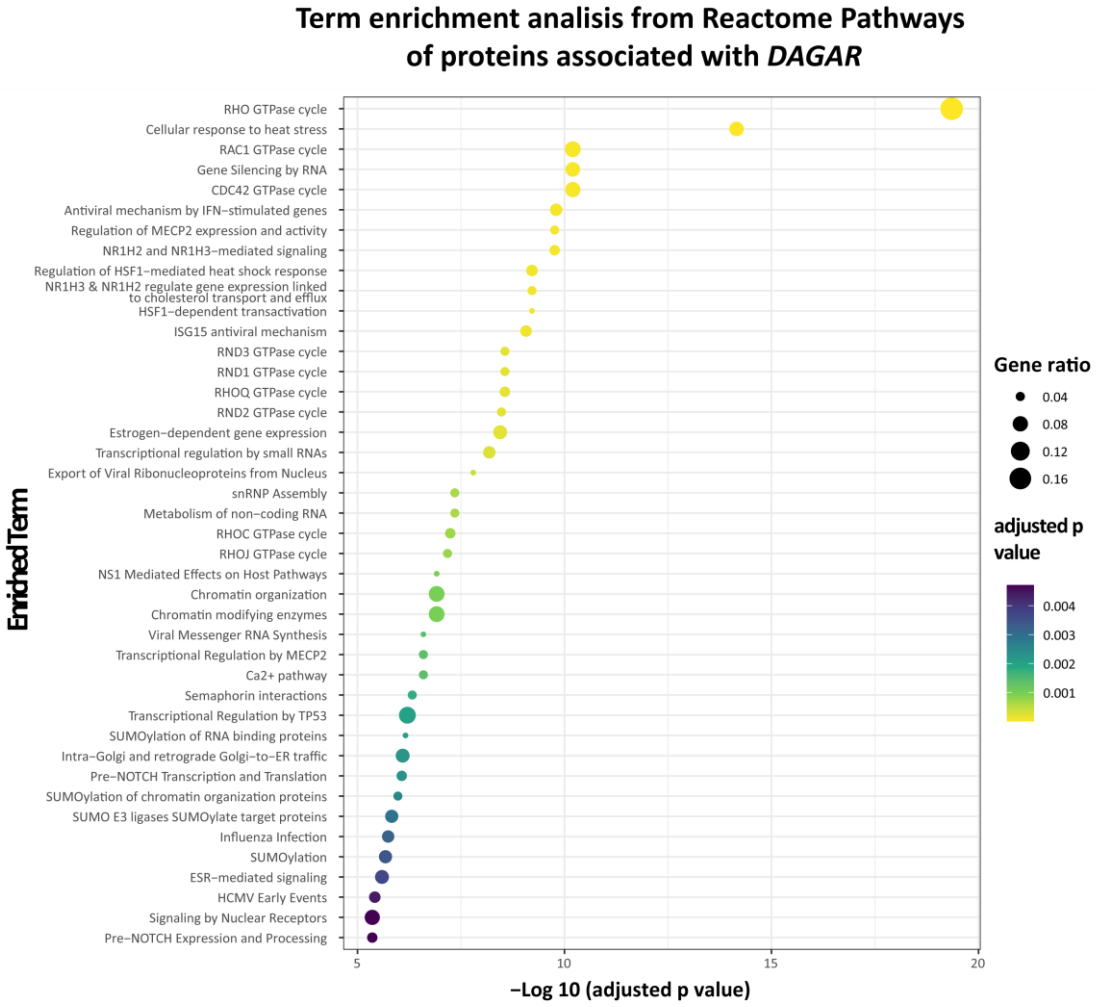

Figure 17. Enrichment analysis of terms associated with signaling pathways from the Reactome Pathways database. The main enriched terms are observed for the set of proteins co-precipitated with DAGAR. The size of the dot represents the gene ratio (number of genes associated with that particular term / total number of genes). The color scale represents the adjusted p value. The negative logarithm base 10 of the adjusted p value is observed on the X axis. On the Y axis, the enriched terms ordered inversely to their adjusted p value are observed.

Finally, the term "*Metabolism of non-coding RNA*" suggests that part of the precipitated proteins would be related to the metabolism of this candidate lncRNA, or that this lncRNA could regulate aspects related to the processing of non-coding RNAs. In this sense, the association with VIRMA, a structural protein of the methyltransferase complex involved in the deposition of m^6A; and CNOT1, which is part of the CCR4-NOT deadenylation complex, paved the way for the study of its regulation, which will be explored later.

3.1.5 Analysis of DAGAR expression in remodeled arteries from patients

At last, and in order to investigate a potential role of *DAGAR in vivo,* its expression in total RNA derived from human pulmonary arteries was characterized by RT-qPCR. The expression of *DAGAR was* retrospectively analyzed in patients with chronic obstructive pulmonary disease (COPD) in relation to non-smoking control patients (NS) [121]. A significant decrease in this lncRNA was observed in COPD patients compared to control patients (Figure 18). This result is consistent with what was observed during *in vitro* SMC dedifferentiation induced by TNFα treatment, since COPD is a pathology that involves the dedifferentiation and excessive proliferation of SMC from pulmonary arteries [276].

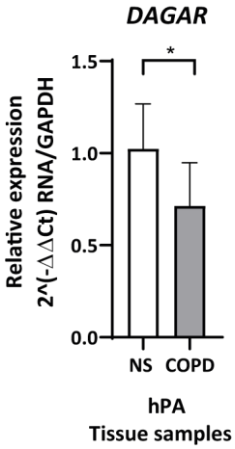

*Figure 18. DAGAR expression in patients with chronic obstructive pulmonary disease (COPD). The normalized relative expression of DAGAR is observed in COPD patients (n = 8) compared to non-smoking control patients (NF, n = 5). Data analyzed by Student's t test. p <0.05 *.*

3.2 Part II

3.2.1 Characterization of the proteins involved in N6-methyladenosine RNA modification biology during human SMC differentiation

As a first step in the characterization of this regulatory mechanism throughout SMC differentiation, the expression of the main proteins involved in the metabolism of m^6A was analyzed (Figure 19 A). The presence of the main catalytic unit of the methyltransferase complex (METTL3), as well as the demethylase FTO, was verified at different times of the differentiation model in SMC. In addition, a clear decrease in the YTHDF1/2/3 reader proteins was observed, being almost undetectable at D6 of differentiation. Relative optical density was quantified with GAPDH as a loading control

and the change in YTHDF1/2/3 expression was analyzed (Figure 19 B). A significant effect of the "differentiation" factor (with levels D0, D2 and D6) on the mean relative optical density of YTHDF family readers (1/2/3) was observed. In particular, significant changes were identified between D0 and D2, as well as between D0 and D6. This suggests a role for these proteins in the maintenance of a dedifferentiated/proliferative state. A more in-depth characterization was performed for the reader of interest, YTHDF2, involved in the m^{6}A-dependent RNA degradation pathway. Statistical analysis of the relative optical density YTHDF2/GAPDH showed that this decrease is progressive and significantly different in each stage analyzed for this reader.

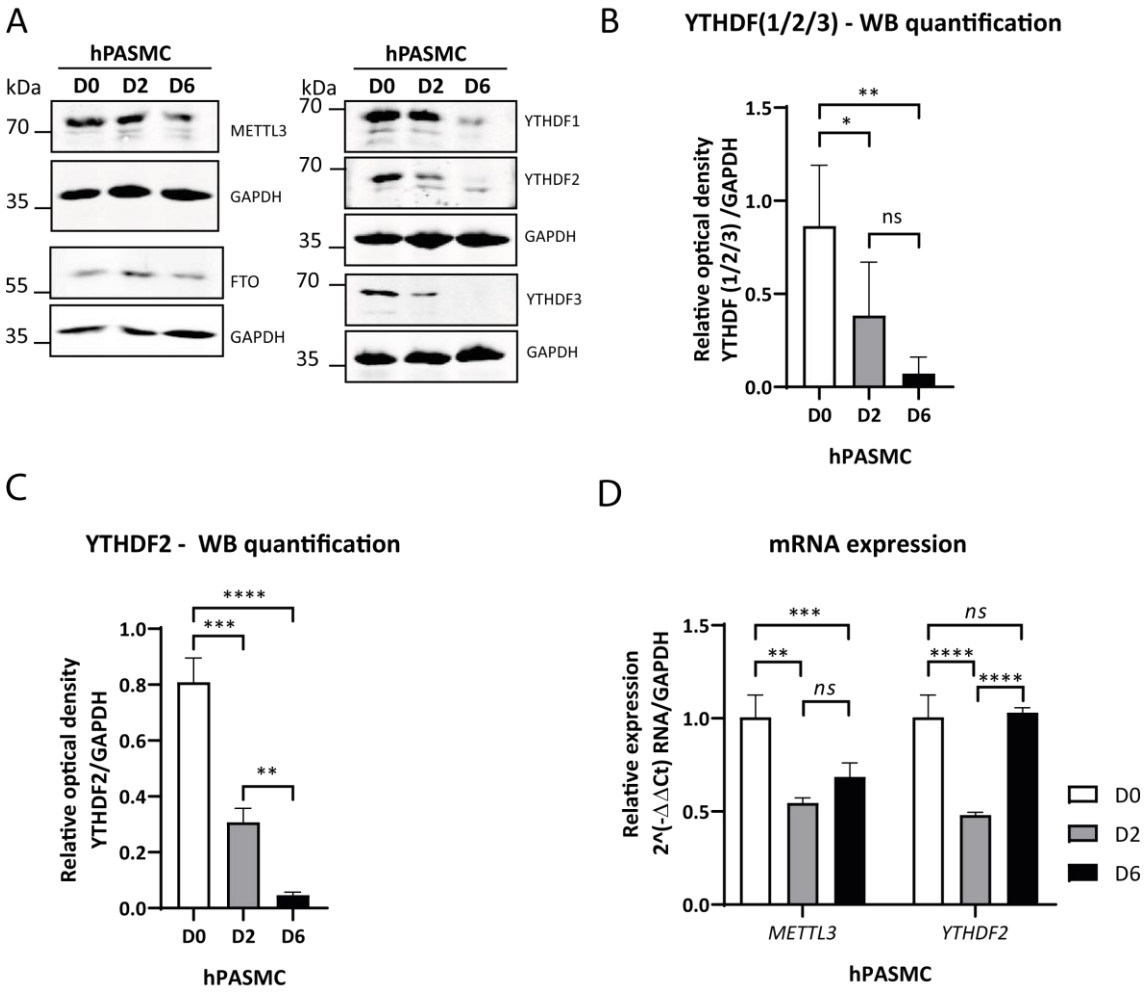

Figure 19. Expression of the m6A methylation machinery in human pulmonary artery smooth muscle cells (hPASMC) in proliferative/dedifferentiated (D0, cells at 70% confluence), at the beginning of differentiation (D2, cells 100% confluent) and differentiated (D6, 4 days after reaching confluence) states. A) Representative Western blot for METTL3, FTO, YTHDF1, YTHDF2 and YTHDF3, with GAPDH as loading control. B) Analysis of the relative optical density for the WBs of YTHDF1/2/3 in conjunction with GAPDH as loading control (n = 3). Data analyzed by one-way ANOVA (factor differentiation, with levels D0, D2 and D6) with blocks for the "readers" factor (levels YTHDF1, YTHDF2 and YTHDF3). The significance plotted corresponds to post-hoc tests of multiple comparisons (Tukey). C) Analysis of the relative optical density for YTHDF2 with GAPDH as loading control (n = 3). Data analyzed by one-way ANOVA (differentiation factor with levels D0, D2 and D6). The significance plotted corresponds to post-hoc tests of multiple comparisons (Tukey). D) Normalized relative expression of METTL3 and YTHDF2 observed by RT-qPCR with GAPDH as loading control (n = 3). Analyzed by one-way Anova (differentiation factor, with levels D0, D2 and D6) and multiple

*post-hoc comparisons using Tukey's test. The significance plotted corresponds to post-hoc tests of multiple comparisons (Tukey). p <0.05 *; p <0.01 **; p <0.001 ***; p <0.0001 ****.*

At the mRNA level, the changes in *METTL3* expression were similar to that observed for its protein, with a decrease of approximately 50% from the beginning of differentiation (D2) and maintained in D6. On the other hand, the expression of *YTHDF2* decreased significantly in D2, but recovered its expression in D6 at levels without statistically significant differences with respect to D0, denoting a transient mRNA regulation at the beginning of differentiation (D2). In addition, the discrepancy observed between the expression of the mRNA (Figure 19 D) and the protein (Figure 19 C) of YTHDF2 in D6 suggests a second regulatory mechanism, in this case post-translational, dominating its modulation in differentiated SMC.

The analysis of these proteins during the induction of quiescence by cellular contact in MRC5 fibroblasts, showed a decrease in METTL3, as well as in the YTHDF1/2/3 readers; and an increase in FTO (Figure 20 A). Interestingly, a discrepancy was observed between the expression at the protein and mRNA levels for *METTL3*, *YTHDF*2 and *YTHDF3*, which were regulated inversely, significantly increasing their expression. This data suggests a post-translational regulatory mechanism for the modulation of these proteins similar to the regulation of YTHDF2 in differentiated SMC (D2 - D6).

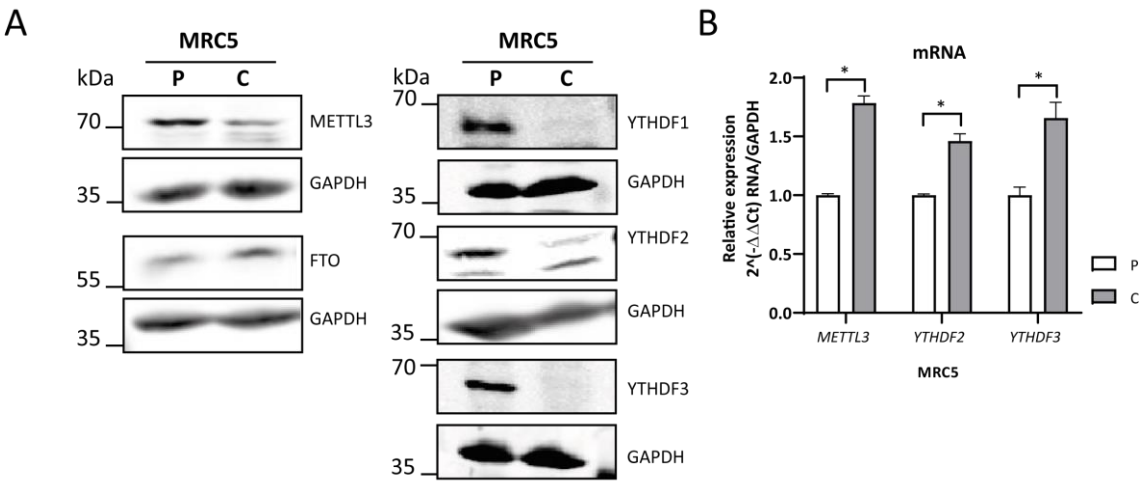

*Figure 20. Expression of the methylation machinery in proliferative MRC5 fibroblasts (MRC5 P, at 70% confluence) and confluent (MRC5 C, 48h after reaching 100% confluence). A) Western Blot of METTL3, FTO, YTHDF1, YTHDF2 and YTHDF3 with GAPDH as loading control. B) Normalized relative expression of METTL3, YTHDF2 and YTHDF3 mRNA obtained by RT-qPCR with GAPDH as loading control (n = 2). Data analyzed by Student's t test with Welch correction on the base 2 logarithmic transformation of the normalized relative expression. p <0.05 *.*

Interestingly the regulation in protein expression observed after the arrest of the cell cycle in G2/M induced by treatment for 24 h with 10 µM of Ro3306 was similar to that observed after the exit of the cell cycle in G0 in confluent MRC5 cells (MRC5 C), with a marked decrease in the expression of YTHDF2/3 readers and an increase in FTO demethylase. In contrast, METTL3 and YTHDF1 maintained their expression without major changes compared to the control treatment (Figure 21A). At the mRNA level, *METTL3* showed an increasing trend, while *YTHDF2* and *YTHDF3* did not show differences with respect to the control. However, the changes at the mRNA level were not statistically significant (Figure 21 B).

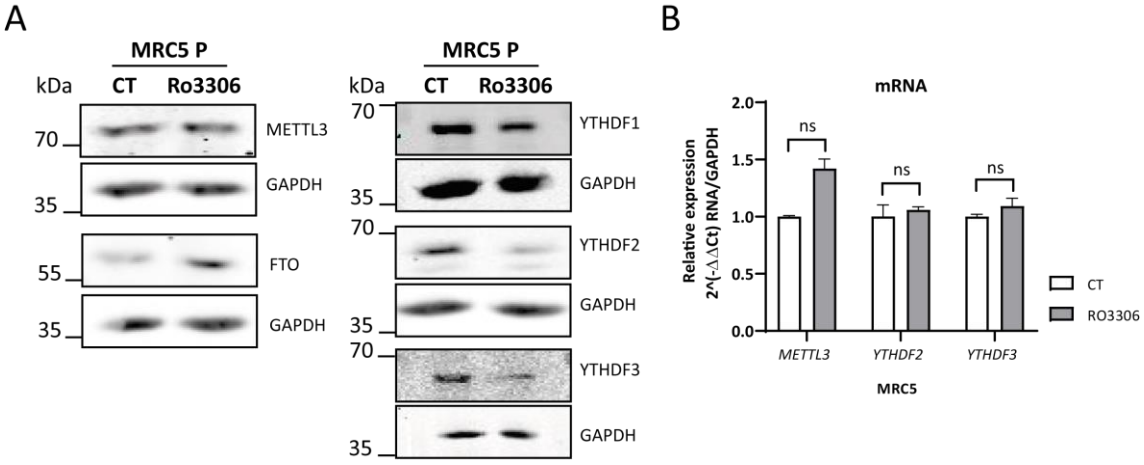

*Figure 21. Expression of the methylation machinery in proliferative MRC5 fibroblasts (MRC5 P, 70% confluence) treated with 10 µM of Ro3306 or the equivalent volume of vehicle (CT) for 24h. A) Western Blot of METTL3, FTO, YTHDF1, YTHDF2 and YTHDF3 with GAPDH as loading control. B) Normalized relative expression of METTL3, YTHDF2 and YTHDF3 mRNA obtained by RT-qPCR with GAPDH as loading control (n = 2). Data analyzed by Student's t test with Welch correction on the base 2 logarithmic transformation of the normalized relative expression. p <0.05 *.*

The same analysis in the cell cycle arrest induced though the inhibition of CDK1 by treatment with Ro3306 showed, again, a discrepancy between the regulation at the protein and mRNA level mainly of YTHDF2 and YTHDF3. Despite the differences observed for METTL3 and YTHDF1, it is evident that the regulation occurs in a similar way to that observed with the exit of the cell cycle in G0, supporting the hypothesis that YTHDF reader family of proteins are regulated post-translationally as a consequence of cell cycle arrest. To test this hypothesis, the expression of the methylation machinery was analyzed in confluent MRC5 treated for 4 h with 20 µM of the proteasome inhibitor MG132 or vehicle. In addition, its expression was analyzed after treatment for 4 h with 10 µg/µl of Brefeldin A to evaluate the contribution of non-canonical autophagy [254] in this process (Figure 22).

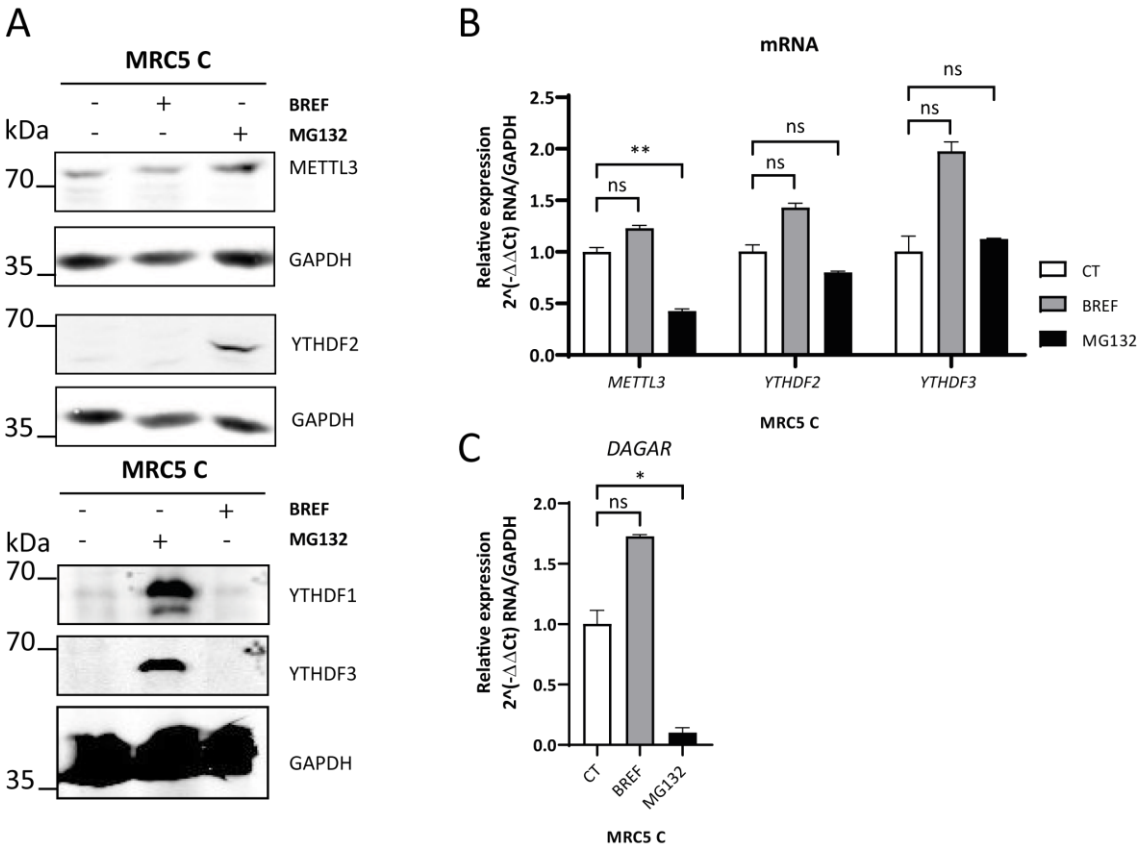

*Figure 22. Expression of the methylation machinery and DAGAR after treatment with either MG132, Brefeldin A or vehicle in confluent MRC5 fibroblasts (MRC5 C, 48h after reaching 100% confluence). A) Western blot of METTL3, YTHDF1, YTHDF2 and YTHDF3, with GAPDH as loading control after treatment for 4 h with 20 µM MG132 or 10 µg/µl Brefeldin A (BREF). B) Normalized relative expression of METTL3, YTHDF2 and YTHDF3 mRNA measured by RT-qPCR with GAPDH as loading control in vehicle (CT) treated MRC5 C, Brefeldin A (BREF) or MG132 (n = 2). Data analyzed using Brown-Forsythe and Welch one-way ANOVA for the treatment factor (with CT, BREF and MG132 levels) and Dunnett's post-hoc test for multiple comparisons referred to the control. The base 2 logarithm of the normalized relative expression was used as the response variable. The significance plotted corresponds to post-hoc tests of multiple comparisons (Dunnett). C) Normalized relative expression of DAGAR measured by RT-qPCR with GAPDH as loading control in MRC5 C treated with vehicle (CT), Brefeldin A (BREF) or MG132 (n = 2). Data analyzed using Brown-Forsythe and Welch one-way ANOVA for the treatment factor (with CT, BREF and MG132 levels) and Dunnett's post-hoc test for multiple comparisons referred to the control. The base 2 logarithm of the normalized relative expression was used as the response variable. The significance plotted corresponds to post-hoc tests of multiple comparisons (Dunnett). p> 0.05 ns; p <0.05 *; p <0.01 **.*

Consistently, a marked recovery of the expression of the YTHDF 1/2/3 readers and an increase in METTL3 was observed only after treatment with MG-132 (Figure 22 A). Treatment with Brefeldin A did not induce changes in the expression of the evaluated proteins. Interestingly, *METTL3* decreased its expression after inhibition of the proteasome at the mRNA level, while no changes were detected for the *YTHDF2/ 3* mRNAs (Figure 22 B). This observation demonstrates that the regulation of these reader proteins in contact-induced quiescence occurs by proteasome-dependent post-

translational pathways. This is probably a common regulatory mechanism for YTHDF1/2/3 in MRC5, SMC, and other cell types.

Taking into account the pronounced change observed in the expression of the reader proteins after the inhibition of the proteasome, the expression of *DAGAR* was analyzed after the treatment with MG-132. A significant decrease in its expression was observed at levels comparable to proliferative MRC5 cells, (Figure 22 C) pointing out that the expression of *DAGAR* is regulated by proteins that are actively degraded by the proteasomal pathway during cell cycle exit (quiescent condition). Taking this data in conjunction with the association of *DAGAR* with proteins of the methyltransferase complex and the CCR4-NOT deadenylation complex, it is logical to reason that *DAGAR* might be regulated by YTHDF2. Interestingly, the expression of *DAGAR*, as well as the mRNA of *YTHDF2* and *YTHDF3* showed an increasing trend after treatment with Brefeldin A, although these changes were not statistically significant. Nevertheless, to rule out that there is a regulation at the mRNA level in this regard it would be necessary to perform additional experiments and increase the statistical sample size (n). However, this point exceeds the aims of the present work.

3.2.2 Effects of the inhibition of the YTHDF2 reader protein on the differentiation of human SMC

In order to investigate the role of m^6A-dependent RNA degradation in the differentiation of SMC, loss of function experiments were carried out for YTHDF2, the main reader involved in the degradation pathway for RNAs with this modification. siPOOLs directed against YTHDF2 were transfected into SMC at the beginning of differentiation (D2). The silencing efficiency was analyzed by WB and RT-qPCR (Figure 23 A and B). Normalized relative expression was calculated (see section 2.6) and changes in SMC specific marker expression were analyzed. The relative expression of all evaluated SMC markers was significantly higher after silencing, demonstrating that the decrease in YTHDF2 significantly increases the transcriptional profile associated with differentiated SMC (Figure 23A).

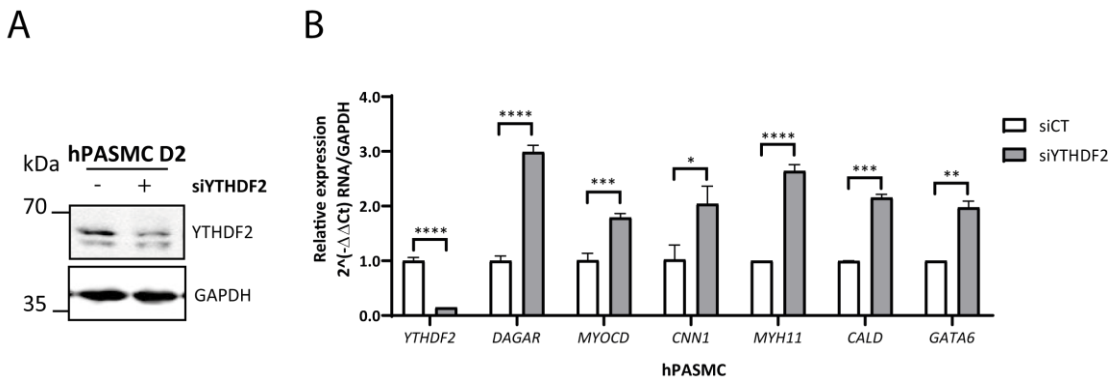

*Figure 23. Expression of YTHDF2 and smooth muscle cell markers after silencing of YTHDF2 (siYTHDF2) compared to control siPOOL (siCT) in human pulmonary artery smooth muscle cells at the beginning of differentiation (hPASMC D2). A) Representative Western Blot control of YTHDF2 with GAPDH as loading control after silencing of YTHDF2 with the use of siPOOLs. B) Normalized relative expression of YTHDF2, DAGAR, MYOCD, CNN1, MYH11, CALD and GATA6 after YTHDF2 silencing, with GAPDH as loading control, measured by RT-qPCR (n = 3). Data analyzed by Student's T test (YTHDF2, DAGAR, MYOCD, CNN1, MYH11) or Student's T test with Welch correction (CALD, GATA6) on the base 2 logarithm of the normalized relative expression. p <0.05 *; p <0.01 **; p <0.001 ***; p <0.0001 ****.*

Interestingly, a significant increase in the expression of *DAGAR* was also observed, suggesting that the regulation of this lncRNA is mediated by the m^{6}A/YTHDF2 axis. In this sense, subsequent experiments were carried out to discriminate whether the change in the expression of *DAGAR* after the silencing of YTHDF2 was a consequence of a direct or secondary regulation. Taking into account the association of *DAGAR* with proteins of the methyltransferase complex, the sequence of *DAGAR* was analyzed using the SerialCloner program (http://serialbasics.free.fr/Serial_Cloner.html) and 66 sites with the consensus DRACH motif were found. To confirm the presence of this modification in *DAGAR*, an immunoprecipitation of m^{6}A modified RNA was carried out using an anti-m^{6}A antibody in total RNA derived from SMC (Figure 24 A) and MRC5 (Figure 24 B), both in proliferating (SMC D0, proliferative MRC5), and quiescent cells (SMC D2, confluent MRC5).

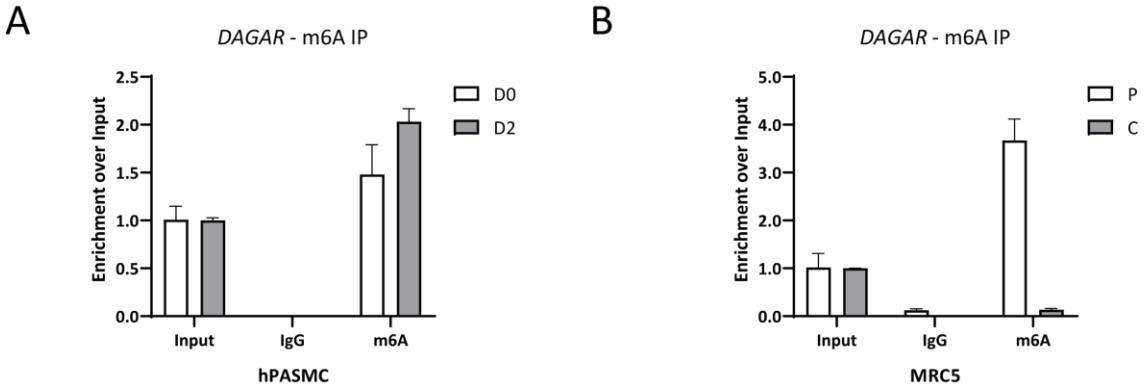

Figure 24. Analysis of DAGAR expression after immunoprecipitation of modified m^{6}A RNA from total RNA. The relative enrichment is observed using an anti-m^{6}A (m^{6}A) or anti-IgG (IgG) antibody on the initial fraction (Input) in: A) Human

pulmonary artery smooth muscle cells (hPASMC) in proliferative state (D0, 70% confluence) or at the beginning of differentiation (D2, 100% confluence) (n = 3). B) MRC5 fibroblasts proliferating (P, 70% confluence) or quiescent (C, 48h after reaching 100% confluence) (n = 2).

An enrichment of *DAGAR* was observed by RT-qPCR in the fractions immunoprecipitated with the anti-m^{6}A antibody, while no expression was observed in the control immunoprecipitation with the anti-IgG antibody (Figure 24 A), indicating a possible mechanism of regulation mediated by m^{6}A modification. No differences were observed in the m^{6}A modification enrichment levels between D0 and D2 in SMC. Interestingly, a marked decrease in the enrichment of *DAGAR* in the m^{6}A fraction was observed in quiescent MRC5 cells (Figure 24 B), denoting that there are differences in the regulation of this modification in *DAGAR* between both cell types. This could be due to increased demethylation and/or diminished m^{6}A deposition in quiescent MRC5 cells. However, it was observed that the silencing of YTHDF2 in MRC5 (Figure 25 A and B) promoted a significant increase in the expression of *DAGAR* (Figure 25 B), in a similar way to that observed in SMC after the silencing of YTHDF2 (Figure 23 B). These results support that the regulatory mechanism of *DAGAR* through YTHDF2 is comparable in both cell types.

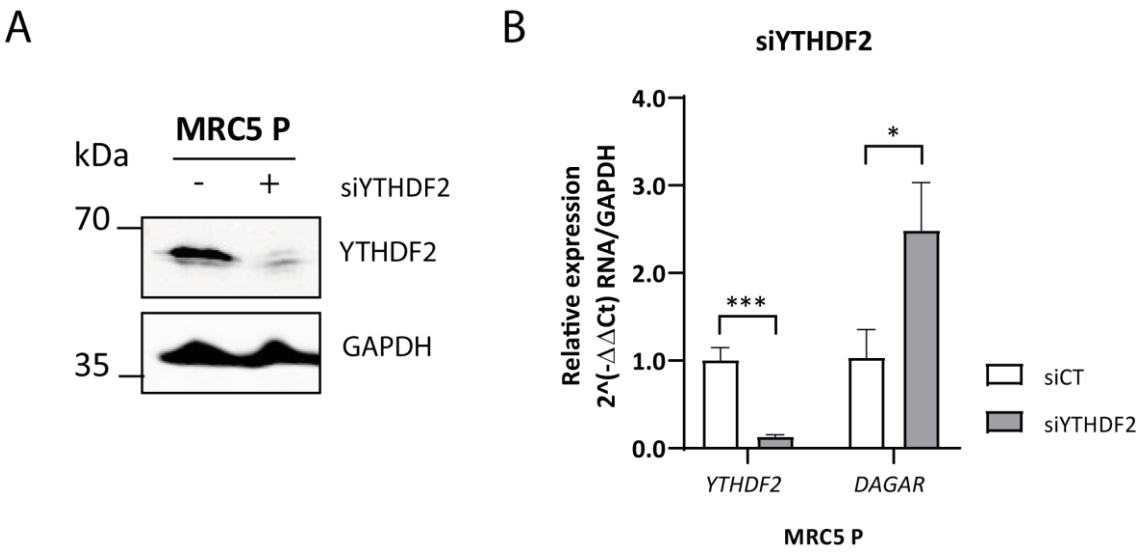

*Figure 25. Expression of YTHDF2 and DAGAR after silencing of YTHDF2 (siYTHDF2) compared to the control siPOOL (siCT) in proliferative MRC5 fibroblasts (MRC5 P, at 70% confluence). A) Representative Western Blot control of YTHDF2 with GAPDH as loading control after silencing of YTHDF2 with the use of siPOOLs. B) Normalized relative expression of YTHDF2 and DAGAR after YTHDF2 silencing, with GAPDH as loading control, measured by RT-qPCR (n = 3). Data analyzed by Student's t test on the base 2 logarithmic transformation of the normalized relative expression. p <0.05 *; p <0.001 ***.*

This observation suggests that *DAGAR* stabilization is not dependent on SMC differentiation itself, but rather on the induction of quiescence (cell cycle exit).

In this sense, it was evaluated whether the regulation of YTHDF2 after CDK1 inhibition was linked to the observed increase in the expression of *DAGAR*. To this end, wild type (WT) and CRISPR/CAS9 mutated C643 cells were used (Figure 26). One METTL3 Knockout clone and three different YTHDF2 Knockout clones were used (Figure 26A). The expression of *DAGAR* increased in C643 WT cells after treatment with the CDK1 inhibitor (Ro3306) as observed previously in MRC5 fibroblasts. However, neither the knockout mutants for METTL3 nor YTHDF2 increased *DAGAR* expression in response to CDK1 inhibition, suggesting that the regulation of *DAGAR* induced by Ro3306 is dependent on m^6deposition and YTHDF2 mediated degradation in this cell type (Figure 26 B). Furthermore, C643 Knockout lines showed an increasing trend in *DAGAR* basal expression compared to C643 WT (Dotted line in Figure 26 B). Taken together, the evidence suggests a direct regulatory mechanism of m^6A mediated degradation of *DAGAR* by YTHDF2 common to C643 cells, MRC5 fibroblasts, and SMC.

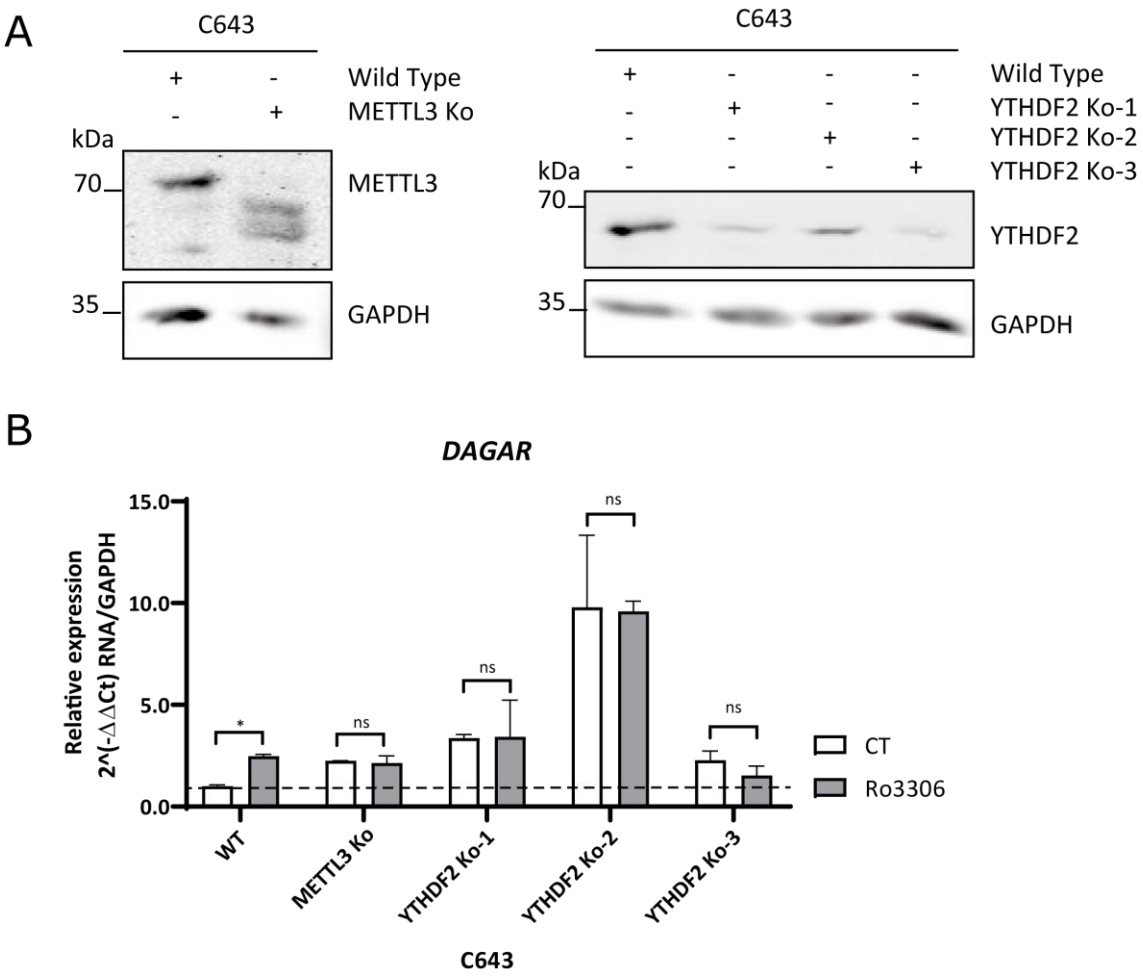

*Figure 26. Expression of DAGAR after Ro3306 treatment in C643 knockout cells for METTL3 and YTHDF2. A) Representative Western Blot of METTL3 (METTL3 Ko, left) or YTHDF2 (YTHDF2 Ko-1/2/3 right) in the C643 knockout lines compared to the wild type (WT) phenotype, with GAPDH as loading control. B) Relative normalized expression of DAGAR after treatment with 10 µM Ro3306 for 24h compared to vehicle (CT) in C643 WT, METTL3 Ko and YTHDF2 Ko-1/2/3 cells measured by RT-qPCR (n = 2). Data analyzed by Student's t test with Welch correction on the base 2 logarithmic transformation of the normalized relative expression. The dotted line refers to the vehicle-treated WT condition. p> 0.05 ns; p <0.05 *.*

3.2.3 RNAs regulated by YTHDF2 during SMC differentiation

Taking into account that the decrease in YTHDF2 caused an increase in the expression of key genes for the differentiation of SMC (Figure 23), the next objective was to identify the main target transcripts regulated by YTHDF2. To this purpose, YTHDF2 immunoprecipitation followed by deep sequencing of RNAs bound to this protein (RIP-Seq) in Proliferative SMC (D0) and at the beginning of differentiation (D2) was performed (Figure 27A). For this analysis, three conditions were used in triplicate: An initial condition (Input), the fraction enriched for YTHDF2 using an antibody against this protein (RIP-YTHDF2) and a negative control with an antibody directed to the gamma heavy chain of the antibody (RIP-IgG). In this way, the RIP-IgG control was used

as a filter for nonspecific binding (to see exclusion criteria see section 2.15) and then a subgroup composed of those target transcripts that were significantly enriched in RIP-YTHDF2 compared to Input was obtained.

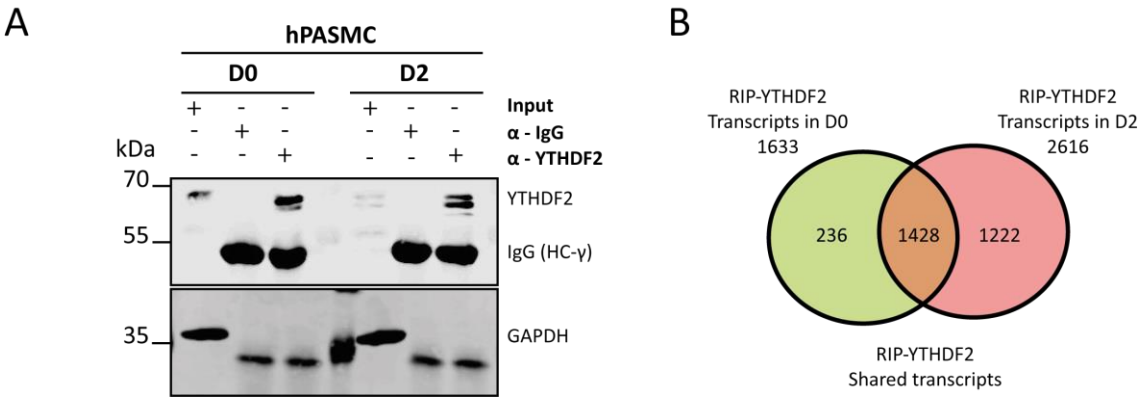

Figure 27. Immunoprecipitation and deep sequencing of RNA co-precipitated with YTHDF2 (RIP-YTHDF2) in human pulmonary artery smooth muscle cells (hPASMC) in a proliferative state (D0, 70% confluence) or at the beginning of differentiation (D2 , 100% confluence) (n = 3). A) Representative Western Blot where the initial fraction (Input), the fraction enriched with an anti-IgG antibody and the fraction enriched using an anti-YTHDF2 antibody are observed both in D0 and in D2 with GAPDH as loading control. B) Number of enriched transcripts (adjusted p value < 0.05) in RIP-YTHDF2 compared to Input in hPASMC D0 and D2.

After filtering the data, a list of significantly enriched RNAs in RIP-YTHDF2 compared to Input was obtained with 1633 genes in D0 condition and 2616 in D2. Of these transcripts, 1428 were represented in both conditions (Figure 27 B). Surprisingly, the genes detected in the RIP-YTHDF2 condition both in proliferating cells (D0) and at the beginning of differentiation (D2) showed a massive enrichment corresponding to the type "smooth muscle cell" in the Human Gene Atlas database, which indicates that YTHDF2 could regulate a large number of characteristic genes of this cell type (Figure 28).

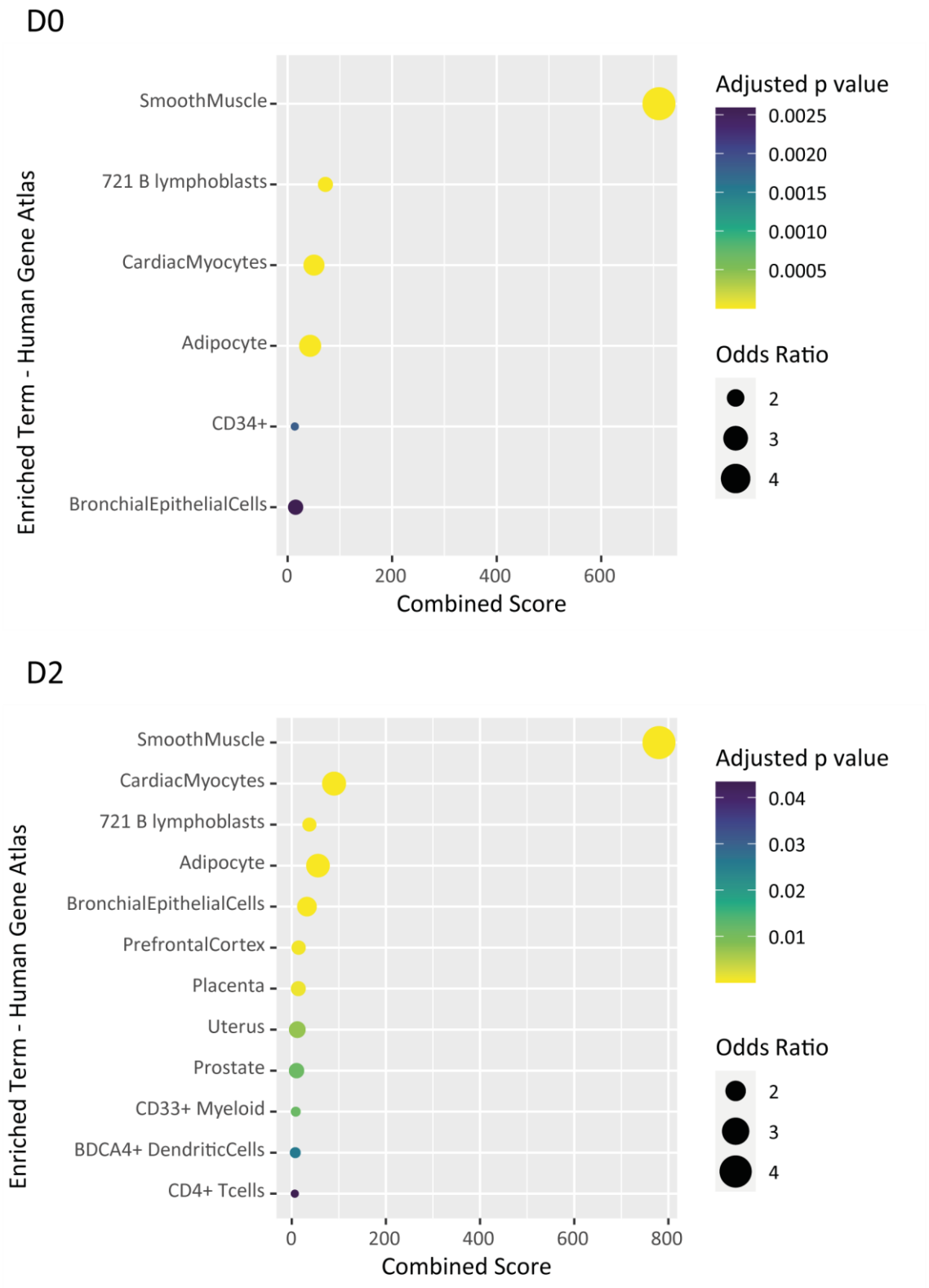

Figure 28. Enrichment analysis of terms associated with cell types for a set of genes from the Human Gene Atlas database. The main enriched terms are observed for the set of transcripts co-precipitated with YTHDF2 in human pulmonary artery smooth muscle cells (hPASMC) in a proliferative state (D0, 70% confluence. Upper panel) and at the beginning of differentiation (D2, 100% confluence. Lower panel). The size of the point represents the Odds ratio (probability index of the appearance of a set of the observed size compared to that expected by chance). The color scale represents the adjusted p value. The X-axis shows the Combined Score (significance index that is useful for ordering in enrichment analysis). On the Y axis, the enriched terms ordered inversely to their adjusted p value are observed.

The enrichment analysis for terms associated with signaling pathways from *Reactome Pathways* showed a general profile of mRNAs that encode proteins related to the organization of the extracellular matrix, proliferation and cell adhesion in the D0 condition of RIP-YTHDF2. At the beginning of differentiation (D2), an additional enrichment of RNAs that are translated into proteins related to SMC differentiation and contraction was observed (Figure 29 C and Section 6.5, Figures 6.5.1 and 6.5.2). This indicates that the target genes of YTHDF2 vary according to the state of differentiation, probably coupling to the transcriptional program that is going to be established sequentially.

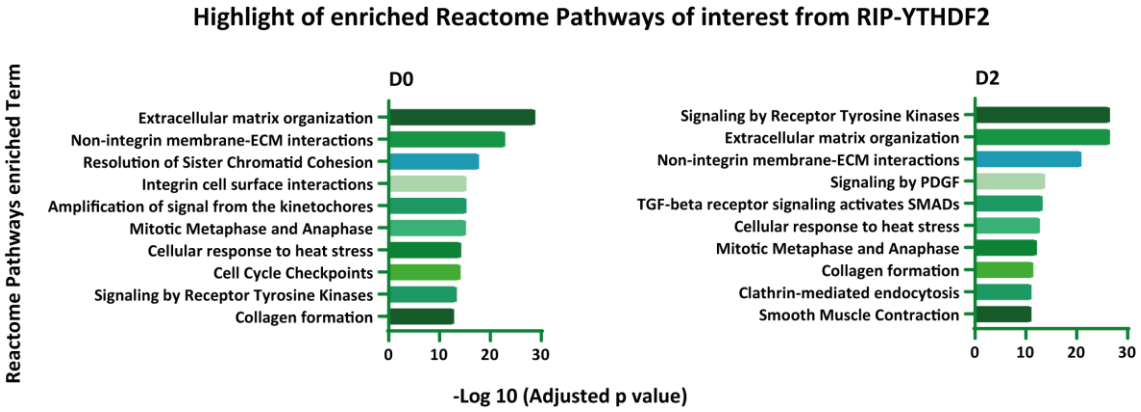

Figure 29. Enrichment analysis of terms associated with signaling pathways for a set of genes from the Reactome Pathways database. The main terms of interest enriched are observed for the set of transcripts co-precipitated with YTHDF2 in human pulmonary artery smooth muscle cells (hPASMC) in a proliferative state (D0, 70% confluence. Left panel) or at the beginning of differentiation (D2, 100% confluence. Right panel). The negative logarithm base 10 of the adjusted p value is observed on the X axis. On the Y axis, the enriched terms ordered inversely to their adjusted p value are observed. The full list is available in (Section 6.5).

A data of particular interest is that a significant enrichment of MYH11 mRNA was obtained in the RIP-YTHDF2 condition in both D0 and D2 (Figure 30). MYH11 is currently recognized as the most specific smooth muscle cell marker to date. Therefore, it was then analyzed whether the MYH11 mRNA is modified with m^6A using an IP of m^6A from total RNA in D0 and D2. The presence of MYH11 was found at levels comparable to the Input in both conditions, while it was not detectable in the immunoprecipitation for IgG, used as a control for nonspecific binding (Figure 31). These results, together with its binding to YTHDF2, and the observed increase in its expression after the silencing of YTHDF2 in SMC indicate a direct regulation mechanism through the recognition of modified m^6A sites, followed by its degradation mediated by YTHDF2.

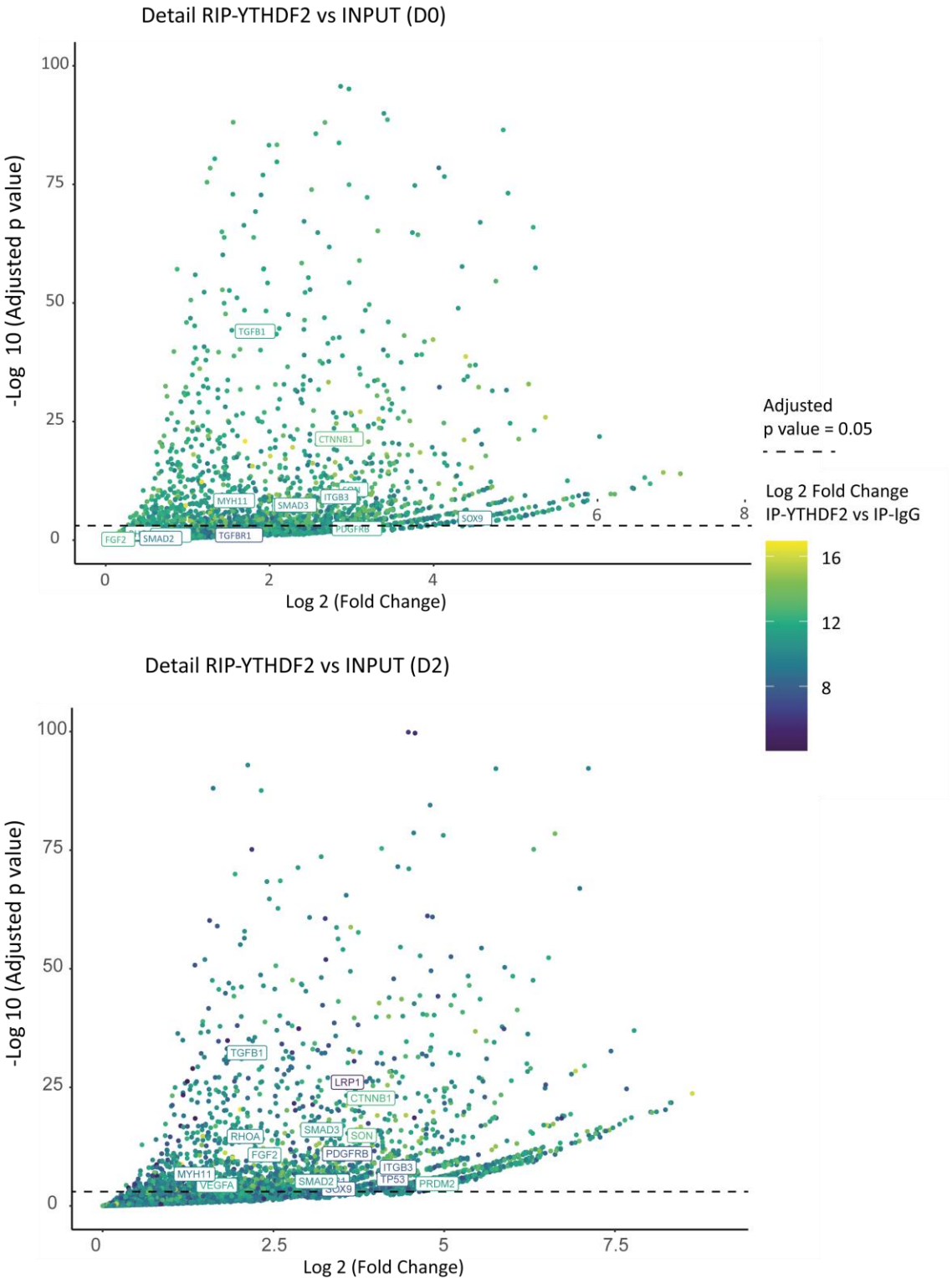

Figure 30. Scatter diagram of transcripts co-precipitated with YTHDF2 (RIP-YTHDF2) in human pulmonary artery smooth muscle cells (hPASMC) in a proliferative state (D0, 70% confluence. Upper panel) or at the beginning of differentiation (D2, 100% confluence. Lower panel) compared to the initial condition (Input). The X axis shows the logarithm base 2 of the relative change of expression (Log2 (Fold Change)). On the Y axis, the inverse logarithm base 10 of the adjusted p value is observed. The color scale represents the logarithm base 2 of the enrichment in the RIP-YTHDF2 condition with respect to the control condition (IP-IgG). The dotted line marks the limit of statistical significance for the adjusted p value (adjusted p <0.05). The labels correspond to transcripts validated by RT-qPCR. Graphical representation limited to -Log 10 (p adjusted value) <100, Log 2 (Fold change) <8.

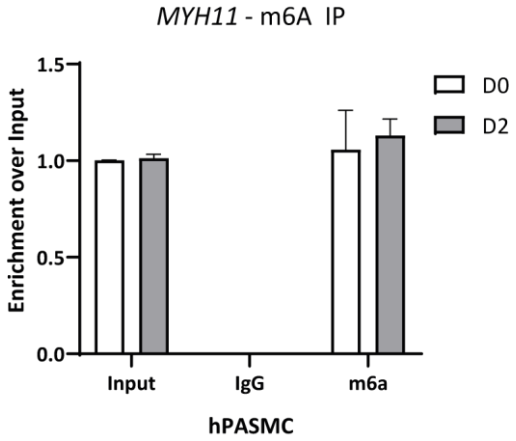

Figure 31. Analysis of MYH11 expression after immunoprecipitation of modified m6A RNA from total RNA. The relative enrichment is observed using an anti-m^{6}A (m^{6}A) or anti-IgG (IgG) antibody on the initial fraction (Input) in human pulmonary artery smooth muscle cells (hPASMC) in a proliferative state (D0, 70% confluence). (n = 2) or at the beginning of differentiation (D2, 100% confluence) (n = 3).

Important ligands and receptors associated with essential pathways in the proliferation, differentiation and homeostasis of SMC, such as the TGFβ family (the TGFβ1 ligand and both receptor subunits, TGFβRI and TGFβRII, as well as SMAD2/3), the platelet-derived growth factor pathway (PDGFA, PDGFB, and its receptor PDGFRβ) and vascular endothelial growth factor (VEGFA) were found, among others.

To validate the findings of the RNA deep sequencing, some of the most important genes related to SMC differentiation were selected and the presence of the transcripts was explored by RT-qPCR (Labels Figure 30 and Figure 32). Furthermore, SON enrichment was measured as a positive control, since this mRNA is known to be degraded by YTHDF2 in HeLa cells [203]. A lower general enrichment of the selected mRNAs can be observed with respect to the Input in the RIP-YTHDF2 condition in D2 with respect to D0 (Figure 32A). However, a marked enrichment in RIP-YTHDF2 was observed in comparison to the control immunoprecipitation (RIP-IgG) (Figure 32 B) showing the specificity of the found binding. The selected genes include: TGFβ signaling, represented by ligand mRNA (*TGFB1*), TGFβ receptor subunit 1 (*TGFBR1*), and two pathway effectors (*SMAD2* and *SMAD3*) [68, 277, 278]; *RhoA*, whose protein is involved in the polymerization of the cytoskeleton and is capable of affecting the localization of MRTFs and consequently the transcription of SMC-specific genes [55, 279]; *TP53* , which codes for an important tumor suppressor involved in SMC differentiation [280]; *LRP1*, which is translated into a leptin receptor, involved in phenotypic modulation during pulmonary hypertension and arteriosclerosis [281-283]; PDGF-BB receptor (*PDGFRB)*

mRNA, fundamental in the SMC response to promitogenic and promigratory events triggered by endothelial cells [34, 50, 87, 103, 284]; *VEGFA*, which produces the VEGF pathway ligand involved in angiogenic responses, particularly stimulating endothelial cell proliferation and survival in response to hypoxia [95, 96]; *FGF2*, capable of inducing proliferation in SMC [285]; The mRNA encoding *SOX9*, capable of inhibiting MYOCD SRF-dependent gene transcription [286, 287]; and *MYH11* mRNA , the most specific SMC marker known to date [19].

A

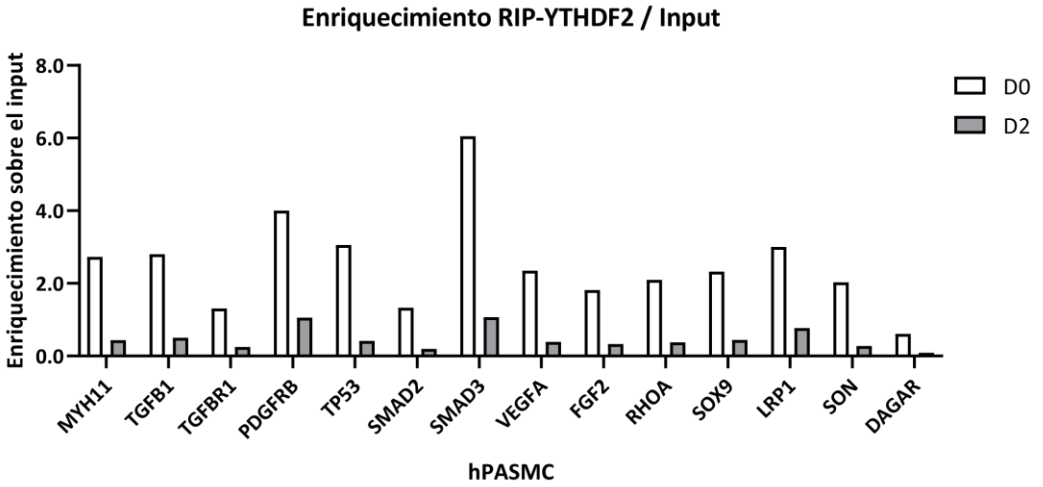

B

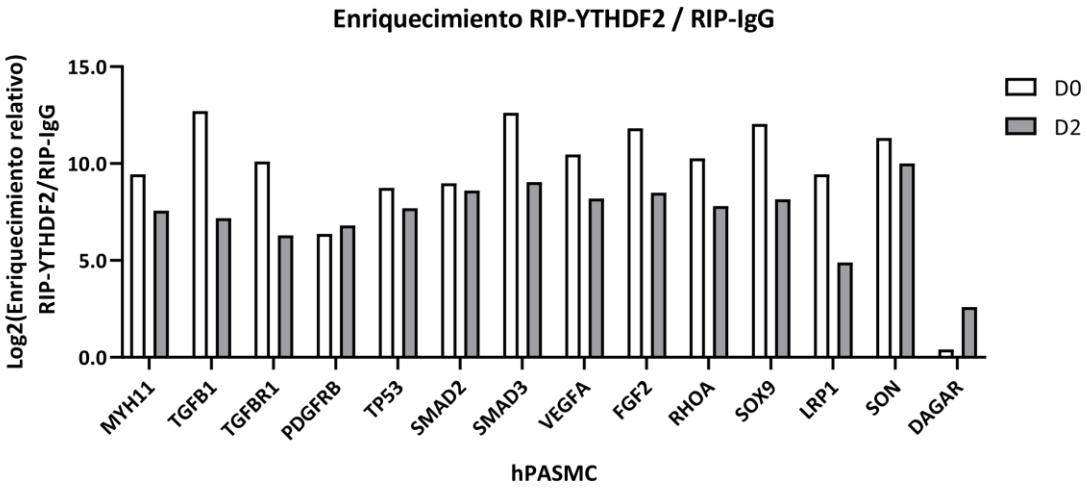

Figure 32. Validation of transcripts co-immunoprecipitated with YTHDF2 (RIP-YTHDF2) in human pulmonary artery smooth muscle cells (hPASMC) in a proliferative state (D0, 70% confluence) or at the beginning of differentiation (D2, 100% of confluence). A) Relative enrichment on the initial fraction (Input) after immunoprecipitation with anti-YTHDF2 (RIP-YTHDF2) for each gene analyzed by RT-qPCR. B) Logarithm base 2 of the relative enrichment in RIP-YTHDF2 on immunoprecipitation with anti-IgG (RIP-IgG) for each gene analyzed by RT-qPCR.

It should be noted that although the general consensus is that YTHDF2 degrades those mRNAs to which it binds, it was found that *FGF2* does not change its expression after the silencing of YTHDF2 (Figure 33).

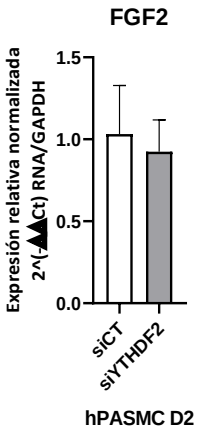

Figure 33. Normalized relative expression of FGF2 after silencing of YTHDF2 (siYTHDF2) in human pulmonary artery smooth muscle cells (hPASMC) at the beginning of differentiation (D2), with GAPDH as loading control, measured by RT-qPCR (n = 3). Data analyzed by Student's t test on the base 2 logarithmic transformation of the normalized relative expression. No significant differences were found between the control silencing (siCT) and that specific for YTHDF2 (siYTHDF2).

This adds complexity to the interpretation of the results obtained, which is why a detailed analysis of all the enriched pathways is not performed in the RIP-YTHDF2 condition, and the interpretation of the results is limited to the effect of YTHDF2 on SMC differentiation, based on the expression changes observed after YTHDF2 silencing. However, the description of the transcripts linked to this reading protein in SMC is a valuable contribution to future research by this and other research groups.

Chapter 4

DISCUSSION

4 Discussion

4.1 Selection and characterization of candidates

The RNA deep sequencing carried out in proliferative SMC (D0) and at the beginning of differentiation (D2) showed the existence of numerous lncRNAs that are expressed differentially between both conditions (Figure 6). An equivalent number of lncRNAs that increased and decreased their expression were selected and further validated in the complete model of differentiation, as well as in endothelial cells (Figure 7). Although three candidates showed specificity for SMC and a progressive pattern of change of their expression in the differentiation process, only lncRNA4 (*DAGAR* hereinafter) was selected for further characterization. The reason was based on the fact that *DAGAR* showed the greatest relative change in its expression with respect to proliferative SMC, and was completely undetectable in endothelial cells.

The transcript obtained by RNA deep sequencing was mapped to the TCONS_00006193 region of the Genome Browser database [288]. TCONS_00006193 is a conserved sequence, annotated in experiments performed on normal human lung fibroblasts (*NLF*). However, subsequent experiments performed on SMC and MRC5 fibroblasts demonstrated a discrepancy in the structure of the annotated transcript and the experimentally obtained. The FANTOM CAT database [273, 289, 290], which has an extensive collection of transcription start sites for lncRNAs, describes several alternative transcripts in the region corresponding to TCONS_00006193 (Figure 8). By designing specific primers capable of amplifying different areas of the transcript, its characterization was carried out. The results obtained confirmed the presence of two of the variants described in FANTOM CAT for the *DAGAR* locus in SMC. Although it is not possible to completely rule out the existence of additional variants in these or other cell types, fragments corresponding to the other variants presented in the scheme were not obtained in SMC (Figure 8). From this information, specific primers were designed to measure by RT-qPCR the expression of the detected variants and it was observed that both *DAGAR-1* and *DAGAR-2* increased their expression in a similar fashion during differentiation. In the same way, after silencing by siPOOLs, a significant decrease in both variants was observed (Figure 10). Because of this; and taking into account the

technical difficulties associated with variant-specific silencing, it was decided to study *DAGAR* by the use of primers capable of recognize both variants.

Furthermore, as part of the characterization, it was determined that *DAGAR* is polyadenylated (Figure 9).

4.2 *DAGAR* and the cell cycle

The results of this study show that *DAGAR* is related to states of quiescence or cell cycle exit. Its expression increased in MRC5 fibroblasts after cell cycle arrest, due to nutrient starvation, inhibition of CDK1 or cell-to cell contact inhibition of growth (Figure 12). The arrest induced by these three conditions are not identical, since the exit occurs at different *cell cycle checkpoints*, namely, in the G0/G1 phase after nutrient deprivation or by cell-cell contact [27] and in G2/M phase after CDK1 inhibition [251]. In addition, the recovery during 24 h in basal medium after 24 h of treatment with the CDK1 inhibitor, did not show significant differences with respect to the control, directly linking the inhibition of CDK1 with the change in the expression of *DAGAR*. Taking this result in conjunction with the aforementioned data, allows the conclusion that *DAGAR* expression is directly related to cell cycle exit. It should be noted that the analysis of the proteins identified by mass spectrometry that precipitated together with *DAGAR* (Section 6.4, Table 6.4.1) showed that this lncRNA interacts with the proliferation marker Ki67, possibly fulfilling a functional role associated with cell cycle exit in response to cell-to-cell contact. The increase in the percentage of positive nuclei for Ki67 and the percentage of cells in S phase after the silencing of *DAGAR* (Figure 15 A and B), supports this hypothesis. Taken together, the evidence allows to rationalize a strong correlation between cell cycle arrest and *DAGAR* induction, which at the same time would be playing an important role in this process.

4.3 *DAGAR* and the differentiation of SMC

DAGAR was found significantly increased during the differentiation of human pulmonary artery SMC, with almost undetectable expression in these cells in a proliferative state (Figure 11 A and B). Conversely, a significant decrease in *DAGAR* expression was observed after SMC dedifferentiation induced by TNFα treatment (Figure *11 C*), as well as in total RNA derived from pulmonary arteries of COPD patients

when compared to non-smoking patients (Figure 18), being both the treatment with TNFα and the COPD condition scenarios where SMC proliferation is enhanced [276, 291].

Although the loss of function of *DAGAR* indicates an important role for the acquisition of a differentiated phenotype, observed by a decrease in the expression of *MYOCD*, *TAGLN* and *CNN1* mRNA (Figure 13A), as well as in the formation of ACTA2 and CNN1 fibers (Figure 14), the mechanism of action is still unknown. The precipitation of proteins by RNA-protein affinity purification (raPOOL) followed by mass spectrophotometry, showed a large number of proteins that interact with *DAGAR* (Section 6.4, Table 6.4.1), pointing out some of the possible pathways involved. in its metabolism and function. The enrichment analysis of terms associated with molecular function of *Gene Ontology* (Figure 16) ranked first (ordered according to their adjusted p value) the regulation of Rho GTPase activity. This could explain the phenotype observed after the silencing of *DAGAR*, with a decrease in the formation of ACTA2 and CNN1 fibers since it has been described that RhoA mediates the polymerization of glomerular actin to fibrillar actin in the cytoskeleton [55]. This event itself can trigger differentiation events in response to various signals from the environment, depleting G-actin from the cytoplasm and allowing the translocation of myocardin-related factors (MRTF) to the nucleus [56]. This mechanism of induction of differentiation through the modulation of Rho GTPases has been suggested for the *lncRNA MYOSLID*, which amplifies the transcriptional plan associated with differentiation in SMC [136].

On the other hand, in the Reactome pathways term enrichment analysis, (Figure 17), several terms associated with the regulation of transcription through chromatin restructuring were observed, a mechanism of action known for other lncRNAs (reviewed in [128]), as is the case of *SWINGN* [292]. *SWINGN* is capable of influencing the activity of the SWI/SNF chromatin remodeling complex called SMARCB1 through its interaction with it. The action of SWI/SNF complexes has been described as an important epigenetic mechanism for the differentiation of SMC [293, 294]. In particular, the action of ATPases BRG1 (SMARCA4) and BRM is necessary for the expression of specific smooth muscle genes dependent on MYOCD [294] and SRF/MRTF-A [293]. In this sense, a direct association of *DAGAR* with BRG1 (SMARCA4) was found, suggesting the possibility that *DAGAR* interacts with this complex and regulates its activity.

In addition to terms associated with the modification of the chromatin structure, others related to specific transcriptional regulation were observed, such as "*Transcriptional regulation by TP53"* and "*Pre-NOTCH transcription and translation"*. In relation to this, it has been observed that the *lncRNA GAS5* mediates the stabilization of the TP53-EP300 complex, suppressing proliferation and inducing apoptosis of SMC of the neointima layer in a model of balloon injury-induced vascular remodeling in rat carotid artery [295], hinting at another possible SMC regulatory mechanism associated with co-precipitated proteins. In this case, binding of DAGAR to EP300, but not TP53, was observed. For its part, EP300 has a complex role in the differentiation of SMC. Its silencing has been reported to accelerate SMC differentiation, while the inhibition of its histone acetyltransferase (*HAT*) activity blocks the differentiation process [296]. On the other hand, EP300 is required, together with MAML, for gene transcription after activation of Notch pathways [297]. Signaling through Jag-1/Notch is necessary for the establishment and maintenance of a contractile/differentiated phenotype in arterial smooth muscle cells [298]. Taking into account the enrichment of the terms "*Pre-NOTCH transcription and translation"* and " *Pre-NOTCH expression and processing "* , it is possible that *DAGAR* fulfills functions related to the NOTCH signaling pathway both upstream, regulating the transcription and translation of NOTCH receptors, and downstream, regulating the activity of EP300. The induction of *DAGAR* expression observed after cell-to-cell contact in both SMC and MRC5 suggests that this lncRNA may be involved in NOTCH pathways-mediated differentiation. It should be noted that although the results of the enrichment analysis of proteins co-precipitated with *DAGAR* constitute clues about its function, a large number of additional experiments are required to verify that *DAGAR* regulates proliferation and/or differentiation by any of them.

4.4 Regulation of *DAGAR* and SMC markers by YTHDF2

The Reactome pathways gene set enrichment analysis of the proteins co-precipitated with *DAGAR* (Figure 17) depicted the enrichment of pathways associated with lncRNA metabolism ("*Metabolism of non-coding RNAs"*). In relation to this, the presence of components of the m^6A methyltransferase complex and of the CCR4-NOT

deadenylation complex (VIRMA and CNOT1 respectively) among the co-precipitated proteins (Section 6.4, Table 6.4.1), was particularly suggestive.

In line with these results, the presence of m^{6}A was determined in *DAGAR* (Figure 24) and it was identified that its expression is regulated by YTHDF2 (Figure 23 B and 25 B). The silencing of this protein (siYTHDF2) elicited an increase in *DAGAR* expression in pulmonary artery SMC (Figure 23B) and MRC5 fibroblasts (Figure 25B) when compared to control silencing (siCT), similarly to that observed in C643 YTHDF2 knockout cells compared to C643 wild type (Figure 26). Furthermore, the increase in *DAGAR* expression induced by CDK1 inhibition was suppressed in all three C643 clones knockout for YTHDF2 as well as in the METTL3 knockout cell line (Figure 26). Together, these results allow the interpretation that this regulatory mechanism is dependent on the m^{6}A pathway.

Strikingly, the silencing of YTHDF2 in SMC significantly induced mRNA expression of SMC-specific markers (Figure 25B). Among the most important findings, a direct regulation of *MYH11* was observed by the m^{6}A/YTHDF2 degradation pathway since, in addition to harboring this modification, *MYH11* was found enriched in the immunoprecipitation of YTHDF2 in both D0 and D2 (Figure 30), and its expression increased during the silencing of this protein (Figure 23 B). This fact itself evidences a direct regulation of SMC differentiation by YTHDF2, since *MYH11* is considered as the most specific marker for this cell type [19]. In this sense, it has been described that it is possible to detect smooth muscle cells that have modulated their phenotype and lost the expression of all their markers, including MYH11, through the analysis of histone modifications present in its promoter [299]. The di-methylation of histone H3 lysine 4 (H3K4me2) in the MYH11 promoter is specific for smooth muscle cells [300], and allows the re-expression of MYH11 when the cell returns to a contractile state [299]. On the other hand, those cells that do not belong to the smooth muscle lineage have a tri-methylation at lysine 27 of histone H3 (H3K27me3) in the MYH11 promoter, which represses its expression [299]. In addition to this, it has been described that MYH11 mRNA is also regulated at the posttranscriptional level in SMC by the action of miR-330-5p and that this regulation is modulated by *Sox2ot lncRNA* [191]. However, this is the first work to report the regulation of *MYH11* mRNA by the m^{6}A/YTHDF2 pathway. It should be noted that in addition to *MYH11*, the mRNAs of the transcriptional factors *GATA6* and *MYOCD*, and of proteins associated with contractility (TAGLN, CNN1 and

CALD1) also increased their expression after the silencing of YTHDF2 (Figure 23 B), demonstrating a general regulation of the transcriptional plan associated with differentiated SMC.

The decrease in the expression at the protein level of YTHDF2 during differentiation (Figure 19 A and C) supports this hypothesis. In concert with YTHDF2, the expression of YTHDF1 and YTHDF3 also showed a similar regulation during this process (Figure 19 A and B), framing a transitional role of the m^6A YTHDF1/2/3 readers between proliferative and differentiated phenotypes. The stabilization of mRNAs that encode for contractile smooth muscle proteins such as MYH11 or CALD1, as well as the expression of transcription factors and co-factors (eg GATA6 and MYOCD respectively) are fundamental for the establishment of a contractile phenotype. Although a direct association of *GATA6* or *MYOCD* with YTHDF2 was not found, a significant increase in their mRNA was observed after the silencing of this protein, suggesting that the regulation of the transcriptional plan mediated by YTHDF2 during the differentiation of SMC occurs both directly by degradation of modified mRNAs, as well as indirectly through the regulation of the expression of transcription factors and/or signaling pathways that regulate specific smooth muscle genes. Furthermore, it is known that for the establishment of the differentiated phenotype in SMC it is necessary for the cells to exit the cell cycle and to enter a quiescent state (G0/G1) [17, 301]. Since YTHDF2 is a positive regulator of the cell cycle [302, 303], its expression and/or activity must decrease for cells to acquire a quiescent state. In this sense, a marked decrease in YTHDF reader proteins was also observed during cell cycle arrest in MRC5 (Figure 20 A and Figure 21 A), a phenomenon that has also been reported in other cell types [302, 304]. Interestingly, the mRNA levels of YTHDF2 and YTHDF3 did not follow the same pattern of decrease as their respective proteins under the same conditions (Figure 20 B and Figure 21 B), and they maintained their expression or even perceived an increase during either SMC differentiation (Figure 19 D) or cell cycle arrest in MRC respectively. In quiescent MRC5 fibroblasts (MRC5 C), the expression of the three reader proteins was rescued at levels similar to those observed in proliferating cells (MRC5 P) after inhibition of the proteasome by treatment with MG-132, directly involving proteasomal degradation in the regulation of YTHDF1/2/3 (Figure 22 A). These results are in agreement with previous studies in HeLa cells, in which they show that after the exit of

the cell cycle, YTHDF2 is ubiquitinated and degraded by the proteasomal pathway [302]. On the other hand, the expression of *DAGAR* decreased significantly in quiescent MRC5 cells after the inhibition of the proteasome (Figure 22 C), at levels comparable with proliferative cells, demonstrating that *DAGAR* is regulated by proteins that are actively degraded by this pathway. The presence of the m^{6}A modification in *DAGAR* (Figure 24); the increase in its expression after the silencing of YTHDF2 in both MRC5 and SMC (Figure 25 B and Figure 23 B); and the blocking of its induction after CDK1 inhibition in C643 METTL3 and YTHDF2 knockout clones (Figure 26 B), it is likely that there is a direct link between the rescue of YTHDF2 and the decrease in *DAGAR* after inhibition of the proteasome.

This post-translational regulation of gene expression could provide a rapid response mechanism to changes in cell state. From the findings presented in this work, derives the hypothesis that YTHDF readers increase their expression in SMC in response to dedifferentiation and proliferation signals. In accordance with this hypothesis, the *Disease Gene Network* gene set enrichment analysis yielded a large number of diseases associated with dysregulated proliferation, such as different types of cancer and fibrosis (Section 6.6: *Disease Gene Network* enrichment for RIP-YTHDF2, Figures 6.6.1 and 6.6.2). Of particular interest to the subject of this thesis, a specific enrichment of the term "vascular diseases" (*Vascular Diseases*) was found together with aortic and intracranial aneurysms.

In correlation with the data presented here, an association of the m^{6}A methylation machinery with the maintenance of cardiac homeostasis [305, 306], as well as with the development of aneurysms [307] has been documented. Furthermore, it has been observed that the expression of YTHDF1 increases in SMC, concomitantly with proliferation, during the development of pulmonary hypertension [308]. In addition to this, YTHDF1 and YTHDF3 decrease their protein expression during the differentiation of embryonic stem cells into cardiomyocytes, and it has been described that they regulate this process [309]. Beyond the differences in the cellular models, the importance of the regulation of the differentiation mediated by m ^{6} A has been investigated in a recent work that demonstrates its involvement in the differentiation process of stem cells derived from adipose tissue (*Adipose Derived Stem Cells*) towards SMC [310].

It should not go unnoticed that YTHDF2 also interacts with other RNA modifications. On the one hand, YTHDF2 has been implicated in the maturation of ribosomal RNA through the recognition of 5-methylcytosine (m^5C) [311]. In relation to this point, the precision measurements carried out during the quality control of the RNA derived from the immunoprecipitation of YTHDF2 showed an enrichment in the areas corresponding to rRNA (data not shown). However, the samples were depleted of rRNA prior to the generation of libraries for RNA deep sequencing. Furthermore, YTHDF2 has recently been documented to mediate the degradation of RNAs modified with N1-methyladenosine (m^1A) [312]. Due to this, the target genes described here may arise from the association of YTHDF2 both through the recognition of m^6A and m^1A.

The Reactome enrichment analysis of terms associated with signaling pathways performed on the genes identified in the YTHDF2 immunoprecipitation experiment (RIP-YTHDF2) followed by RNA deep sequencing showed the interaction of YTHDF2 with mRNA from key genes that regulate SMC homeostasis (Figure 29 and Section 6.5, Figure 6.5.1 and 6.5.2). In particular, the presence of transcripts associated with the TGFβ, PDGF and VEGF pathways was identified, as well as specific SMC markers. The difference between transcripts enriched in YTHDF2-RIP in proliferative SMC (D0) and at the beginning of differentiation (D2) supports the hypothesis that YTHDF2 is a key regulator of the phenotypic change in SMC, since an increase of the differentiated SMC-related pathways was found in D2, and a general predominance of pathways related to both cell-to-cell contact and cell cycle progression was observed in D0. The enrichment of genes related to the cell cycle probably ensures the degradation of cell cycle intermediates at the appropriate times, as previously described in other cell types [302, 303, 313].

Strikingly, a lower gene enrichment was observed in the RIP-YTHDF2 fraction over the initial fraction (Input), as well as a higher background expression for the genes analyzed in RIP-YTHDF2 at D2 compared to D0 by RT-qPCR (Figure 32 A). This may be due to the differences in the expression of YTHDF2 in D0 and D2, making it difficult to recover the protein and therefore its associated transcripts, although a greater amount of total protein was used for immunoprecipitation at D2. At the same time, this decreases the signal-to-noise ratio, the specific binding being understood as “signal” and the binding associated with nonspecific immunoprecipitation as “noise” (RIP-IgG). This

phenomenon was only observed by RT-qPCR, since the enrichments obtained after RNA deep sequencing were similar in RIP-YTHDF2 at D0 and D2. However, the high enrichment of the validated genes in RIP-YTHDF2 with respect to RIP-IgG by RT-qPCR is indicative that the associations found are specific (Figure 32B). For most of the genes analyzed, no signal was observed at all in the RIP-IgG condition, as is the case with *DAGAR.* However, because the expression of this lncRNA is very low, the signal detected both by deep sequencing and by RT-qPCR in RIP-YTHDF2 condition, was not strong enough to confirm direct recognition by YTHDF2. One possible explanation for this point is that the expression of *DAGAR* is regulated by both YTHDF2 and YTHDF3 cooperatively. In this regard, YTHDF3 can negatively regulate the expression of lncRNAs [314]. Furthermore, it has been observed that YTHDF1 and YTHDF2 compete for binding to YTHDF3 [315] to regulate YAP mRNA, and that the interaction of YTHDF1 or YTHDF2 with YTHDF3 increases translation or degradation of the target mRNA respectively [204]. This mechanism could explain the quantitative difference observed in the induction of *DAGAR* after the silencing of YTHDF2 (Figure 23 B and Figure 25 B), compared to the respective experiment after cell cycle arrest (Figure 12). In the latter, a joint decrease of YTHDF2 and YTHDF3 is observed (Figure 20 and Figure 21). In the same sense, inhibition of the proteasome in quiescent MRC5 cells induced a decrease in *DAGAR* to levels comparable to proliferating cells (Figure 22 C), at the same time that it recovered the expression of YTHDF1/2/3 (Figure 22 A). Although all the evidence presented indicates a regulation of *DAGAR* by YTHDF2, further experiments are needed to show that YTHDF2 does indeed bind to *DAGAR*.

Other important target genes for SMC that are documented in this work have been previously reported in other cell types, such as TGFβ1, both subunits of its receptor (TGFβRI and TGFβRII), SMAD3 and SMAD5, PDGFRβ and VEGFA [302, 304, 316, 317]. PDGFRβ has also been reported to increase its expression after YTHDF2 silencing in a model of neuronal differentiation from induced Pluripotent Stem Cells (iPSC) [246], providing strength to the findings presented herein. It is likely that this regulation allows a fine-tuning of SMC-specific gene expression through post-translational control of the YTHDF2 reader protein and thus also enables rapid establishment of the dedifferentiation/proliferation program once YTHDF2 stabilization occurs. Taking into account that the binding of YTHDF2 to transcripts in the cell nucleus can occur,

promoting its translation by cap-independent mechanisms, more experiments are required to corroborate which target genes are destabilized by YTHDF2, and if there are transcripts that are stabilized for their translation in this cell type. In relation to this point, it was observed that although *FGF2* is enriched in RIP-YTHDF2 (Figure 30 and Figure 32), the silencing of this m^{6}A reader does not affect its expression at the mRNA level (Figure 33). Since FGF2 is related to a proliferative phenotype in SMC [285], this finding suggests that its recognition by YTHDF2 could stabilize the m^{6}A modification in this transcript and promote its cap-independent translation. However, more experiments are necessary to validate this hypothesis.

Similarly, it has been recently reported that TGFβ1 can be cap-independently translated through m^{6}A modifications in its 5' *UTR* region, a mechanism that, as mentioned above, can be facilitated by the binding of YTHDF2 [247], however this has not yet been proven to be the case in this cell line. Furthermore, it has been described that TGFβ signaling induces SMAD2/3-dependent co-transcriptional deposition of m^{6}A in downstream genes during development, fulfilling a fundamental role for the timely release of pluripotency and the commitment to neuroectoderm [278]. Taking into consideration the role of TGFβ signaling in SMC differentiation, it is likely that the binding of YTHDF2 to the *TGFβ1* ligand mRNA in this cell type stabilizes modifications in the 5'UTR region, promoting its translation. As mentioned in the introduction, TGFβ signaling induces SMC differentiation through SMAD2/3/4 (reviewed in [318]). Taking into account the role of SMAD 2/3 in the co-transcriptional deposition of m^{6}A in target genes during the compromise towards neuroectoderm during development [278], it is possible to hypothesize that this cascade could trigger the modification of specific SMC genes that begin to express themselves, making them susceptible to being recognized and degraded by YTHDF2. After reaching confluence, the decrease in the expression of the YTHDF readers due to the induction of quiescence would allow the stabilization of these transcripts and therefore the establishment of the transcriptional program of differentiation. In view of the fact that the main catalytic protein of the methyltransferase complex (METTL3) maintains its expression in differentiated SMC (Figure 19 A), it is expected that the methylation of target genes will continue to occur. Therefore, in the face of the stabilization of the YTHDF reader proteins in response to reentry to the cell cycle, a rapid removal of the transcripts that code for contractile and

specific smooth muscle proteins would occur. Although a large amount of additional evidence is necessary to test this hypothesis, YTHDF2 seems to constitute a transition factor between the contractile and proliferative phenotype, functioning as a negative regulator of the SMC differentiation program, a role that has been demonstrated in other differentiation models [246, 304]. Below a graphical summary is presented, with highlights of the main pathways proposed in this thesis for the regulation of SMC differentiation (Figure 34).

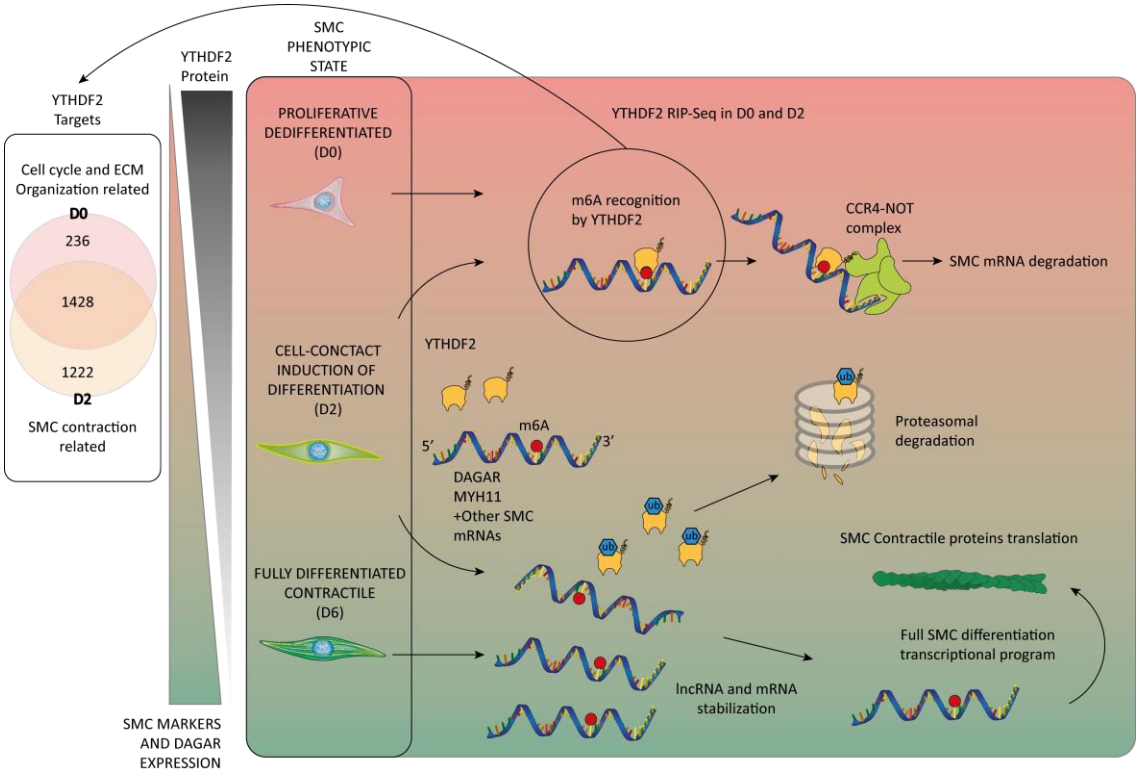

Figure 34. Graphic summary of the proposed mechanism for the phenotypic regulation of human pulmonary artery smooth muscle cells (SMC) mediated by epigenetic mechanisms (expression of DAGAR and regulation of YTHDF2). The differentiation of SMC with three differentiated stages is observed in a color gradient from pink to green (D0, corresponding to proliferative SMC, D2 cells at the beginning of differentiation, and D6 representing differentiated SMC). Proliferative cells express YTHDF2, which recognizes m^{6}A-modified RNAs and mediates their degradation, which inhibits SMC differentiation. After contact inhibition, YTHDF2 is ubiquitinated and degraded by proteasomal pathway, allowing the increase in the expression and stabilization of DAGAR and other mRNAs important for the differentiation of SMC. These events would allow the replacement of the transcriptional plan and promote a differentiated SMC phenotype. The findings derived from immunoprecipitation and deep sequencing of RNAs bound to YTHDF2 are highlighted on the left.

4.4 Conclusion

In summary, this study documents a novel long non-coding RNA, which we have named *DAGAR* due to its close relationship with SMC differentiation and cell cycle arrest

(*Differentiation And Growth Arrest-related lncRNA*). Although its molecular mechanism of action could not be deciphered, its regulation through the m^6A methylation machinery is described. Specifically, YTHDF2 is highly expressed in proliferative cells and induces degradation of *DAGAR.* During SMC differentiation, the decrease in the YTHDF2 reading protein allows stabilization of *DAGAR* and adequate differentiation of SMC. In this sense, a fundamental role of the m^6A methylation machinery in the differentiation of SMC was also discovered. This is the first work to evaluate the expression of the m^6A methylation machinery, including METTL3, YTHDF1/2/3 and FTO, during the differentiation of SMC derived from human pulmonary artery, with special focus on the function, regulation and characterization of YTHDF2 target genes. The data generated in the development of this doctoral thesis adds a new long non-coding RNA with an important role in the regulation of SMC homeostasis and probably in cell cycle exit in other cell types. Furthermore, this work sheds light on the role of m^6A during the phenotypic modulation of SMC, a field still merely explored but highly promising.

5 Bibliography

1. Roth, G.A., et al., *Global Burden of Cardiovascular Diseases and Risk Factors, 1990-2019: Update From the GBD 2019 Study.* J Am Coll Cardiol, 2020. **76**(25): p. 2982-3021.
2. WorldHealthOrganization, *World health statistics 2016: monitoring health for the SDGs, sustainable development goals.* World Health Organization, 2016.
3. Weir-McCall, J.R., et al., *The role of pulmonary arterial stiffness in COPD.* Respir Med, 2015. **109**(11): p. 1381-90.
4. Heusch, G., et al., *Cardiovascular remodelling in coronary artery disease and heart failure.* Lancet, 2014. **383**(9932): p. 1933-43.
5. Aird, W.C., *Spatial and temporal dynamics of the endothelium.* J Thromb Haemost, 2005. **3**(7): p. 1392-406.
6. Hughes, S. and T. Chan-Ling, *Characterization of smooth muscle cell and pericyte differentiation in the rat retina in vivo.* Invest Ophthalmol Vis Sci, 2004. **45**(8): p. 2795-806.
7. Wang, G., et al., *Origin and differentiation of vascular smooth muscle cells.* J Physiol, 2015. **593**(14): p. 3013-30.
8. Leopold, J.A. and B.A. Maron, *Molecular Mechanisms of Pulmonary Vascular Remodeling in Pulmonary Arterial Hypertension.* Int J Mol Sci, 2016. **17**(5).
9. Munoz-Esquerre, M., et al., *Systemic and Pulmonary Vascular Remodelling in Chronic Obstructive Pulmonary Disease.* PLoS One, 2016. **11**(4): p. e0152987.
10. Hopkins, N. and P. McLoughlin, *The structural basis of pulmonary hypertension in chronic lung disease: remodelling, rarefaction or angiogenesis?* J Anat, 2002. **201**(4): p. 335-48.
11. Eddahibi, S., et al., *Pathobiology of pulmonary arterial hypertension.* Eur Respir J, 2002. **20**(6): p. 1559-72.
12. Stenmark, K.R., K.A. Fagan, and M.G. Frid, *Hypoxia-induced pulmonary vascular remodeling: cellular and molecular mechanisms.* Circ Res, 2006. **99**(7): p. 675-91.
13. Lynch, M.D. and F.M. Watt, *Fibroblast heterogeneity: implications for human disease.* J Clin Invest, 2018. **128**(1): p. 26-35.
14. Wang, X. and R.A. Khalil, *Matrix Metalloproteinases, Vascular Remodeling, and Vascular Disease.* Adv Pharmacol, 2018. **81**: p. 241-330.
15. Owens, G.K., M.S. Kumar, and B.R. Wamhoff, *Molecular regulation of vascular smooth muscle cell differentiation in development and disease.* Physiol Rev, 2004. **84**(3): p. 767-801.
16. Tang, H., et al., *Endothelial HIF-2alpha contributes to severe pulmonary hypertension due to endothelial-to-mesenchymal transition.* Am J Physiol Lung Cell Mol Physiol, 2018. **314**(2): p. L256-L275.
17. Coll-Bonfill, N., et al., *Slug is increased in vascular remodeling and induces a smooth muscle cell proliferative phenotype.* PLoS ONE, 2016. **11**.
18. Owens, G.K., *Molecular control of vascular smooth muscle cell differentiation and phenotypic plasticity.* Novartis Found Symp, 2007. **283**: p. 173-174,238-241.
19. Gomez, D. and G.K. Owens, *Smooth muscle cell phenotypic switching in atherosclerosis.* Cardiovasc Res, 2012. **95**(2): p. 156-64.
20. Shankman, L.S., et al., *KLF4-dependent phenotypic modulation of smooth muscle cells has a key role in atherosclerotic plaque pathogenesis.* Nat Med, 2015. **21**(6): p. 628-37.
21. Singh, S. and M. Torzewski, *Fibroblasts and Their Pathological Functions in the Fibrosis of Aortic Valve Sclerosis and Atherosclerosis.* Biomolecules, 2019. **9**(9).
22. Coen, M., G. Gabbiani, and M.L. Bochaton-Piallat, *Myofibroblast-mediated adventitial remodeling: an underestimated player in arterial pathology.* Arterioscler Thromb Vasc Biol, 2011. **31**(11): p. 2391-6.

23. Fang, C.L., et al., *Resistin-like molecule-beta (RELM-beta) targets airways fibroblasts to effect remodelling in asthma: from mouse to man.* Clin Exp Allergy, 2015. **45**(5): p. 940-952.
24. Hinz, B. and G. Gabbiani, *Fibrosis: recent advances in myofibroblast biology and new therapeutic perspectives.* F1000 Biol Rep, 2010. **2**: p. 78.
25. Li, G., et al., *Direct in vivo evidence demonstrating neointimal migration of adventitial fibroblasts after balloon injury of rat carotid arteries.* Circulation, 2000. **101**(12): p. 1362-5.
26. Siow, R.C., C.M. Mallawaarachchi, and P.L. Weissberg, *Migration of adventitial myofibroblasts following vascular balloon injury: insights from in vivo gene transfer to rat carotid arteries.* Cardiovasc Res, 2003. **59**(1): p. 212-21.
27. Hayes, O., et al., *Cell confluency is as efficient as serum starvation for inducing arrest in the G0/G1 phase of the cell cycle in granulosa and fibroblast cells of cattle.* Anim Reprod Sci, 2005. **87**(3-4): p. 181-92.
28. Diez, M., et al., *Endothelial progenitor cells undergo an endothelial-to-mesenchymal transition-like process mediated by TGFbetaRI.* Cardiovasc Res, 2010. **88**(3): p. 502-11.
29. Davis-Dusenbery, B.N., C. Wu, and A. Hata, *Micromanaging vascular smooth muscle cell differentiation and phenotypic modulation.* Arteriosclerosis, Thrombosis, and Vascular Biology, 2011. **31**: p. 2370-2377.
30. Coll-Bonfill, N., et al., *Noncoding RNAs in smooth muscle cell homeostasis: implications in phenotypic switch and vascular disorders.* Pflugers Arch, 2016. **468**(6): p. 1071-87.
31. Gao, P.J., et al., *Differentiation of vascular myofibroblasts induced by transforming growth factor-beta1 requires the involvement of protein kinase Calpha.* J Mol Cell Cardiol, 2003. **35**(9): p. 1105-12.
32. Davis, J. and J.D. Molkentin, *Myofibroblasts: trust your heart and let fate decide.* J Mol Cell Cardiol, 2014. **70**: p. 9-18.
33. Rajkumar, V.S., et al., *Platelet-derived growth factor-beta receptor activation is essential for fibroblast and pericyte recruitment during cutaneous wound healing.* Am J Pathol, 2006. **169**(6): p. 2254-65.
34. Millette, E., et al., *Platelet-derived growth factor-BB transactivates the fibroblast growth factor receptor to induce proliferation in human smooth muscle cells.* Trends Cardiovasc Med, 2006. **16**(1): p. 25-8.
35. Kumar, M.S. and G.K. Owens, *Combinatorial control of smooth muscle-specific gene expression.* Arterioscler Thromb Vasc Biol, 2003. **23**(5): p. 737-47.
36. Wang, D., et al., *Activation of cardiac gene expression by myocardin, a transcriptional cofactor for serum response factor.* Cell, 2001. **105**(7): p. 851-62.
37. Wang, D.Z., et al., *Potentiation of serum response factor activity by a family of myocardin-related transcription factors.* Proc Natl Acad Sci U S A, 2002. **99**(23): p. 14855-60.
38. Sun, Q., et al., *Defining the mammalian CArGome.* Genome Res, 2006. **16**(2): p. 197-207.
39. Miano, J.M., X. Long, and K. Fujiwara, *Serum response factor: master regulator of the actin cytoskeleton and contractile apparatus.* Am J Physiol Cell Physiol, 2007. **292**(1): p. C70-81.
40. Durocher, D. and M. Nemer, *Combinatorial interactions regulating cardiac transcription.* Dev Genet, 1998. **22**(3): p. 250-62.
41. Morrisey, E.E., et al., *GATA-6: a zinc finger transcription factor that is expressed in multiple cell lineages derived from lateral mesoderm.* Dev Biol, 1996. **177**(1): p. 309-22.
42. Mano, T., et al., *Reversal of GATA-6 downregulation promotes smooth muscle differentiation and inhibits intimal hyperplasia in balloon-injured rat carotid artery.* Circ Res, 1999. **84**(6): p. 647-54.
43. Perlman, H., et al., *GATA-6 induces p21(Cip1) expression and G1 cell cycle arrest.* J Biol Chem, 1998. **273**(22): p. 13713-8.

44. Long, X., et al., *Myocardin is sufficient for a smooth muscle-like contractile phenotype.* Arterioscler Thromb Vasc Biol, 2008. **28**(8): p. 1505-10.
45. Li, S., et al., *The serum response factor coactivator myocardin is required for vascular smooth muscle development.* Proc Natl Acad Sci U S A, 2003. **100**(16): p. 9366-70.
46. Yoshida, T., K. Kawai-Kowase, and G.K. Owens, *Forced expression of myocardin is not sufficient for induction of smooth muscle differentiation in multipotential embryonic cells.* Arterioscler Thromb Vasc Biol, 2004. **24**(9): p. 1596-601.
47. Qiu, P., et al., *Myocardin enhances Smad3-mediated transforming growth factor-beta1 signaling in a CArG box-independent manner: Smad-binding element is an important cis element for SM22alpha transcription in vivo.* Circ Res, 2005. **97**(10): p. 983-91.
48. Wamhoff, B.R., et al., *L-type voltage-gated Ca2+ channels modulate expression of smooth muscle differentiation marker genes via a rho kinase/myocardin/SRF-dependent mechanism.* Circ Res, 2004. **95**(4): p. 406-14.
49. Yoshida, T., M.H. Hoofnagle, and G.K. Owens, *Myocardin and Prx1 contribute to angiotensin II-induced expression of smooth muscle alpha-actin.* Circ Res, 2004. **94**(8): p. 1075-82.
50. Deaton, R.A., Q. Gan, and G.K. Owens, *Sp1-dependent activation of KLF4 is required for PDGF-BB-induced phenotypic modulation of smooth muscle.* American Journal of Physiology-Heart and Circulatory Physiology, 2009. **296**: p. H1027-H1037.
51. Tang, R.H., et al., *Myocardin inhibits cellular proliferation by inhibiting NF-kappaB(p65)-dependent cell cycle progression.* Proc Natl Acad Sci U S A, 2008. **105**(9): p. 3362-7.
52. Imamura, M., et al., *Expression and functional activity of four myocardin isoforms.* Gene, 2010. **464**(1-2): p. 1-10.
53. Nakagaki-Silva, E.E., et al., *Identification of RBPMS as a mammalian smooth muscle master splicing regulator via proximity of its gene with super-enhancers.* Elife, 2019. **8**.
54. Mouilleron, S., et al., *Molecular basis for G-actin binding to RPEL motifs from the serum response factor coactivator MAL.* EMBO J, 2008. **27**(23): p. 3198-208.
55. Hill, C.S., J. Wynne, and R. Treisman, *The Rho family GTPases RhoA, Rac1, and CDC42Hs regulate transcriptional activation by SRF.* Cell, 1995. **81**(7): p. 1159-70.
56. Guettler, S., et al., *RPEL motifs link the serum response factor cofactor MAL but not myocardin to Rho signaling via actin binding.* Mol Cell Biol, 2008. **28**(2): p. 732-42.
57. Velasquez, L.S., et al., *Activation of MRTF-A-dependent gene expression with a small molecule promotes myofibroblast differentiation and wound healing.* Proc Natl Acad Sci U S A, 2013. **110**(42): p. 16850-5.
58. Yoshida, T., et al., *Myocardin is a key regulator of CArG-dependent transcription of multiple smooth muscle marker genes.* Circ Res, 2003. **92**(8): p. 856-64.
59. Morita, T. and K. Hayashi, *Arp5 is a key regulator of myocardin in smooth muscle cells.* J Cell Biol, 2014. **204**(5): p. 683-96.
60. Taurin, S., et al., *Phosphorylation of myocardin by extracellular signal-regulated kinase.* J Biol Chem, 2009. **284**(49): p. 33789-94.
61. Badorff, C., et al., *Glycogen synthase kinase 3beta inhibits myocardin-dependent transcription and hypertrophy induction through site-specific phosphorylation.* Circ Res, 2005. **97**(7): p. 645-54.
62. Ackers-Johnson, M., et al., *Myocardin regulates vascular smooth muscle cell inflammatory activation and disease.* Arterioscler Thromb Vasc Biol, 2015. **35**(4): p. 817-28.
63. Talasila, A., et al., *Myocardin regulates vascular response to injury through miR-24/-29a and platelet-derived growth factor receptor-beta.* Arterioscler Thromb Vasc Biol, 2013. **33**(10): p. 2355-65.
64. Dubois, C.M., et al., *Processing of transforming growth factor beta 1 precursor by human furin convertase.* J Biol Chem, 1995. **270**(18): p. 10618-24.

65. Lopez-Casillas, F., J.L. Wrana, and J. Massague, *Betaglycan presents ligand to the TGF beta signaling receptor.* Cell, 1993. **73**(7): p. 1435-44.
66. Rozes-Salvador, V., et al., *New Player in Endosomal Trafficking: Differential Roles of Smad Anchor for Receptor Activation (SARA) Protein.* Mol Cell Biol, 2018. **38**(24).
67. Shi, Y. and J. Massague, *Mechanisms of TGF-beta signaling from cell membrane to the nucleus.* Cell, 2003. **113**(6): p. 685-700.
68. Hautmann, M.B., C.S. Madsen, and G.K. Owens, *A transforming growth factor beta (TGFbeta) control element drives TGFbeta-induced stimulation of smooth muscle alpha-actin gene expression in concert with two CArG elements.* J Biol Chem, 1997. **272**(16): p. 10948-56.
69. Hirschi, K.K., et al., *Transforming growth factor-beta induction of smooth muscle cell phenotpye requires transcriptional and post-transcriptional control of serum response factor.* J Biol Chem, 2002. **277**(8): p. 6287-95.
70. Gridley, T., *Notch signaling in the vasculature.* Curr Top Dev Biol, 2010. **92**: p. 277-309.
71. Castel, D., et al., *Dynamic binding of RBPJ is determined by Notch signaling status.* Genes Dev, 2013. **27**(9): p. 1059-71.
72. Noseda, M., et al., *Smooth Muscle alpha-actin is a direct target of Notch/CSL.* Circ Res, 2006. **98**(12): p. 1468-70.
73. Doi, H., et al., *Jagged1-selective notch signaling induces smooth muscle differentiation via a RBP-Jkappa-dependent pathway.* J Biol Chem, 2006. **281**(39): p. 28555-64.
74. Boucher, J.M., et al., *The miR-143/145 cluster is a novel transcriptional target of Jagged-1/Notch signaling in vascular smooth muscle cells.* J Biol Chem, 2011. **286**(32): p. 28312-21.
75. Morrow, D., et al., *Notch-mediated CBF-1/RBP-J{kappa}-dependent regulation of human vascular smooth muscle cell phenotype in vitro.* Am J Physiol Cell Physiol, 2005. **289**(5): p. C1188-96.
76. Kemp, P.R., et al., *Cloning and analysis of the promoter region of the rat SM22 alpha gene.* Biochem J, 1995. **310 (Pt 3)**: p. 1037-43.
77. White, S.L. and R.B. Low, *Identification of promoter elements involved in cell-specific regulation of rat smooth muscle myosin heavy chain gene transcription.* J Biol Chem, 1996. **271**(25): p. 15008-17.
78. Gan, Q., et al., *Smooth muscle cells and myofibroblasts use distinct transcriptional mechanisms for smooth muscle alpha-actin expression.* Circ Res, 2007. **101**(9): p. 883-92.
79. Shimizu, R.T., et al., *The smooth muscle alpha-actin gene promoter is differentially regulated in smooth muscle versus non-smooth muscle cells.* J Biol Chem, 1995. **270**(13): p. 7631-43.
80. Massari, M.E. and C. Murre, *Helix-loop-helix proteins: regulators of transcription in eucaryotic organisms.* Mol Cell Biol, 2000. **20**(2): p. 429-40.
81. Johnson, A.D. and G.K. Owens, *Differential activation of the SMalphaA promoter in smooth vs. skeletal muscle cells by bHLH factors.* Am J Physiol, 1999. **276**(6): p. C1420-31.
82. Qiu, P. and L. Li, *Histone acetylation and recruitment of serum responsive factor and CREB-binding protein onto SM22 promoter during SM22 gene expression.* Circ Res, 2002. **90**(8): p. 858-65.
83. Yang, J., X. Li, and N.W. Morrell, *Id proteins in the vasculature: from molecular biology to cardiopulmonary medicine.* Cardiovasc Res, 2014. **104**(3): p. 388-98.
84. Hayashi, K., et al., *Bone morphogenetic protein-induced MSX1 and MSX2 inhibit myocardin-dependent smooth muscle gene transcription.* Mol Cell Biol, 2006. **26**(24): p. 9456-70.
85. Coll, N., et al., *Slug can contribute to the phenotypic modulation of smooth muscle cells.* European Respiratory Journal, 2012. **40**(Suppl 56).

86. Fredriksson, L., H. Li, and U. Eriksson, *The PDGF family: four gene products form five dimeric isoforms.* Cytokine Growth Factor Rev, 2004. **15**(4): p. 197-204.
87. Kemp, S.S., et al., *Defining Endothelial Cell-Derived Factors That Promote Pericyte Recruitment and Capillary Network Assembly.* Arterioscler Thromb Vasc Biol, 2020. **40**(11): p. 2632-2648.
88. Liu, Y., et al., *Kruppel-like factor 4 abrogates myocardin-induced activation of smooth muscle gene expression.* J Biol Chem, 2005. **280**(10): p. 9719-27.
89. Sundberg-Smith, L.J., et al., *Adhesion stimulates direct PAK1/ERK2 association and leads to ERK-dependent PAK1 Thr212 phosphorylation.* J Biol Chem, 2005. **280**(3): p. 2055-64.
90. Czibik, G., *Complex role of the HIF system in cardiovascular biology.* J Mol Med (Berl), 2010. **88**(11): p. 1101-11.
91. Gupta, N., et al., *Activation of NLRP3 inflammasome complex potentiates venous thrombosis in response to hypoxia.* Proc Natl Acad Sci U S A, 2017. **114**(18): p. 4763-4768.
92. Chung, H.Y., et al., *Expression Patterns of HIF-1alpha Under Hypoxia in Vascular Smooth Muscle Cells of Venous Malformations.* Ann Plast Surg, 2015. **75**(3): p. 332-7.
93. Luo, Y., et al., *CD146-HIF-1alpha hypoxic reprogramming drives vascular remodeling and pulmonary arterial hypertension.* Nat Commun, 2019. **10**(1): p. 3551.
94. Tirpe, A.A., et al., *Hypoxia: Overview on Hypoxia-Mediated Mechanisms with a Focus on the Role of HIF Genes.* Int J Mol Sci, 2019. **20**(24).
95. Zhang, D., F.L. Lv, and G.H. Wang, *Effects of HIF-1alpha on diabetic retinopathy angiogenesis and VEGF expression.* Eur Rev Med Pharmacol Sci, 2018. **22**(16): p. 5071-5076.
96. Eichmann, A. and M. Simons, *VEGF signaling inside vascular endothelial cells and beyond.* Curr Opin Cell Biol, 2012. **24**(2): p. 188-93.
97. Dai, J., et al., *Smooth muscle cell-specific FoxM1 controls hypoxia-induced pulmonary hypertension.* Cell Signal, 2018. **51**: p. 119-129.
98. Dai, Z., et al., *Endothelial and Smooth Muscle Cell Interaction via FoxM1 Signaling Mediates Vascular Remodeling and Pulmonary Hypertension.* Am J Respir Crit Care Med, 2018. **198**(6): p. 788-802.
99. Scuteri, A., et al., *The relationship between the metabolic syndrome and arterial wall thickness: A mosaic still to be interpreted.* Atherosclerosis, 2016. **255**: p. 11-16.
100. Yoshimatsu, Y., et al., *TNF-alpha enhances TGF-beta-induced endothelial-to-mesenchymal transition via TGF-beta signal augmentation.* Cancer Sci, 2020. **111**(7): p. 2385-2399.
101. Coll-Bonfill, N., et al., *Transdifferentiation of endothelial cells to smooth muscle cells play an important role in vascular remodelling.* Am J Stem Cells, 2015. **4**(1): p. 13-21.
102. Ali, M.S., et al., *TNF-alpha induces phenotypic modulation in cerebral vascular smooth muscle cells: implications for cerebral aneurysm pathology.* J Cereb Blood Flow Metab, 2013. **33**(10): p. 1564-73.
103. Peppel, K., et al., *Activation of vascular smooth muscle cells by TNF and PDGF: overlapping and complementary signal transduction mechanisms.* Cardiovasc Res, 2005. **65**(3): p. 674-82.
104. Mittal, B., et al., *Matrix metalloproteinases in coronary artery disease.* Adv Clin Chem, 2014. **64**: p. 1-72.
105. Warner, S.J. and P. Libby, *Human vascular smooth muscle cells. Target for and source of tumor necrosis factor.* J Immunol, 1989. **142**(1): p. 100-9.
106. Starke, R.M., et al., *Cigarette smoke modulates vascular smooth muscle phenotype: implications for carotid and cerebrovascular disease.* PLoS One, 2013. **8**(8): p. e71954.
107. Tanaka, H., et al., *Proliferating arterial smooth muscle cells after balloon injury express TNF-alpha but not interleukin-1 or basic fibroblast growth factor.* Arterioscler Thromb Vasc Biol, 1996. **16**(1): p. 12-8.

108. Bonasio, R., S. Tu, and D. Reinberg, *Molecular signals of epigenetic states*, in *Science*. 2010. p. 612-616.
109. Zhang, Y., et al., *Overview of Histone Modification.* Adv Exp Med Biol, 2021. **1283**: p. 1-16.
110. Moore, L.D., T. Le, and G. Fan, *DNA methylation and its basic function.* Neuropsychopharmacology, 2013. **38**(1): p. 23-38.
111. Klemm, S.L., Z. Shipony, and W.J. Greenleaf, *Chromatin accessibility and the regulatory epigenome.* Nat Rev Genet, 2019. **20**(4): p. 207-220.
112. Fu, Y., et al., *Gene expression regulation mediated through reversible m(6)A RNA methylation.* Nat Rev Genet, 2014. **15**(5): p. 293-306.
113. Mattick, J.S., *Non-coding RNAs: the architects of eukaryotic complexity.* EMBO Rep, 2001. **2**(11): p. 986-91.
114. McClain, W.H., *Rules that govern tRNA identity in protein synthesis.* J Mol Biol, 1993. **234**(2): p. 257-80.
115. Moore, P.B. and T.A. Steitz, *The roles of RNA in the synthesis of protein.* Cold Spring Harb Perspect Biol, 2011. **3**(11): p. a003780.
116. Wilkinson, M.E., C. Charenton, and K. Nagai, *RNA Splicing by the Spliceosome.* Annu Rev Biochem, 2020. **89**: p. 359-388.
117. Hombach, S. and M. Kretz, *Non-coding RNAs: Classification, Biology and Functioning.* Adv Exp Med Biol, 2016. **937**: p. 3-17.
118. Smekalova, E.M., et al., *Telomerase RNA biosynthesis and processing.* Biochemistry (Mosc), 2012. **77**(10): p. 1120-8.
119. Zhang, P., et al., *Non-Coding RNAs and their Integrated Networks.* J Integr Bioinform, 2019. **16**(3).
120. Bartel, D.P., *MicroRNAs: genomics, biogenesis, mechanism, and function.* Cell, 2004. **116**(2): p. 281-97.
121. Musri, M.M., et al., *MicroRNA Dysregulation in Pulmonary Arteries from Chronic Obstructive Pulmonary Disease. Relationships with Vascular Remodeling.* Am J Respir Cell Mol Biol, 2018. **59**(4): p. 490-499.
122. Hata, A., *Functions of microRNAs in cardiovascular biology and disease.* Annu Rev Physiol, 2013. **75**: p. 69-93.
123. Wong, L.L., et al., *MicroRNA and Heart Failure.* Int J Mol Sci, 2016. **17**(4): p. 502.
124. Lu, Y., et al., *Impact of miRNA in Atherosclerosis.* Arterioscler Thromb Vasc Biol, 2018. **38**(9): p. e159-e170.
125. Zhang, C., *MicroRNA-145 in vascular smooth muscle cell biology: a new therapeutic target for vascular disease.* Cell Cycle, 2009. **8**(21): p. 3469-73.
126. Simion, V., S. Haemmig, and M.W. Feinberg, *LncRNAs in vascular biology and disease.* Vascul Pharmacol, 2018.
127. Kugel, J.F. and J.A. Goodrich, *The regulation of mammalian mRNA transcription by lncRNAs: recent discoveries and current concepts.* Epigenomics, 2013. **5**(1): p. 95-102.
128. Han, P. and C.P. Chang, *Long non-coding RNA and chromatin remodeling.* RNA Biol, 2015. **12**(10): p. 1094-8.
129. Huang, T.S., et al., *LINC00341 exerts an anti-inflammatory effect on endothelial cells by repressing VCAM1.* Physiol Genomics, 2017. **49**(7): p. 339-345.
130. Willingham, A.T., et al., *A strategy for probing the function of noncoding RNAs finds a repressor of NFAT.* Science, 2005. **309**(5740): p. 1570-3.
131. Gonzalez, I., et al., *A lncRNA regulates alternative splicing via establishment of a splicing-specific chromatin signature.* Nat Struct Mol Biol, 2015. **22**(5): p. 370-6.
132. Wang, G.Q., et al., *Sirt1 AS lncRNA interacts with its mRNA to inhibit muscle formation by attenuating function of miR-34a.* Sci Rep, 2016. **6**: p. 21865.

133. Zhang, B.Y., Z. Jin, and Z. Zhao, *Long intergenic noncoding RNA 00305 sponges miR-136 to regulate the hypoxia induced apoptosis of vascular endothelial cells.* Biomed Pharmacother, 2017. **94**: p. 238-243.
134. Kotake, Y., et al., *Long non-coding RNA ANRIL is required for the PRC2 recruitment to and silencing of p15(INK4B) tumor suppressor gene.* Oncogene, 2011. **30**(16): p. 1956-62.
135. Gumireddy, K., et al., *Identification of a long non-coding RNA-associated RNP complex regulating metastasis at the translational step.* EMBO J, 2013. **32**(20): p. 2672-84.
136. Zhao, J., et al., *MYOSLID Is a Novel Serum Response Factor-Dependent Long Noncoding RNA That Amplifies the Vascular Smooth Muscle Differentiation Program.* Arterioscler Thromb Vasc Biol, 2016. **36**(10): p. 2088-99.
137. Hansen, T.B., et al., *Natural RNA circles function as efficient microRNA sponges.* Nature, 2013. **495**(7441): p. 384-8.
138. Holdt, L.M., et al., *Circular non-coding RNA ANRIL modulates ribosomal RNA maturation and atherosclerosis in humans.* Nat Commun, 2016. **7**: p. 12429.
139. Rinn, J.L. and H.Y. Chang, *Genome regulation by long noncoding RNAs.* Annu Rev Biochem, 2012. **81**: p. 145-66.
140. Ahadi, A., et al., *Long non-coding RNAs harboring miRNA seed regions are enriched in prostate cancer exosomes.* Sci Rep, 2016. **6**: p. 24922.
141. Wang, S., C. Zhang, and X. Zhang, *Downregulation of long noncoding RNA ANRIL promotes proliferation and migration in hypoxic human pulmonary artery smooth muscle cells.* Mol Med Rep, 2020. **21**(2): p. 589-596.
142. Hu, D.J., et al., *Overexpression of long noncoding RNA ANRIL inhibits phenotypic switching of vascular smooth muscle cells to prevent atherosclerotic plaque development in vivo.* Aging (Albany NY), 2020. **13**(3): p. 4299-4316.
143. Zou, Z.Q., et al., *Down-regulation of SENCR promotes smooth muscle cells proliferation and migration in db/db mice through up-regulation of FoxO1 and TRPC6.* Biomed Pharmacother, 2015. **74**: p. 35-41.
144. Ballantyne, M.D., et al., *Smooth Muscle Enriched Long Noncoding RNA (SMILR) Regulates Cell Proliferation.* Circulation, 2016. **133**(21): p. 2050-65.
145. Mahmoud, A.D., et al., *The Human-Specific and Smooth Muscle Cell-Enriched LncRNA SMILR Promotes Proliferation by Regulating Mitotic CENPF mRNA and Drives Cell-Cycle Progression Which Can Be Targeted to Limit Vascular Remodeling.* Circ Res, 2019. **125**(5): p. 535-551.
146. Lim, Y.H., et al., *Identification of Long Noncoding RNAs Involved in Differentiation and Survival of Vascular Smooth Muscle Cells.* Mol Ther Nucleic Acids, 2020. **22**: p. 209-221.
147. Bennett, M., et al., *Novel Transcript Discovery Expands the Repertoire of Pathologically-Associated, Long Non-Coding RNAs in Vascular Smooth Muscle Cells.* Int J Mol Sci, 2021. **22**(3).
148. Tang, R., et al., *The long non-coding RNA GAS5 regulates transforming growth factor beta (TGF-beta)-induced smooth muscle cell differentiation via RNA Smad-binding elements.* J Biol Chem, 2017. **292**(34): p. 14270-14278.
149. Zhang, R.Y., et al., *LncRNA AC105942.1 Downregulates hnRNPA2/B1 to Attenuate Vascular Smooth Muscle Cells Proliferation.* DNA Cell Biol, 2021. **40**(5): p. 652-661.
150. Mangum, K.D., et al., *Transcriptional and posttranscriptional regulation of the SMC-selective blood pressure-associated gene, ARHGAP42.* Am J Physiol Heart Circ Physiol, 2020. **318**(2): p. H413-H424.
151. Kang, C.M., et al., *Long noncoding RNA AL355711 promotes smooth muscle cell migration through the ABCG1/MMP3 pathway.* Int J Mol Med, 2021. **48**(6).
152. Tan, P., et al., *LncRNA-ANRIL inhibits cell senescence of vascular smooth muscle cells by regulating miR-181a/Sirt1.* Biochem Cell Biol, 2019. **97**(5): p. 571-580.

153. Hu, Y., et al., *LncRNA ANRIL Facilitates Vascular Smooth Muscle Cell Proliferation and Suppresses Apoptosis via Modulation of miR-7/FGF2 Pathway in Intracranial Aneurysms.* Neurocrit Care, 2021.
154. Zhang, C., et al., *LncRNA ANRIL acts as a modular scaffold of WDR5 and HDAC3 complexes and promotes alteration of the vascular smooth muscle cell phenotype.* Cell Death Dis, 2020. **11**(6): p. 435.
155. Li, H., et al., *LncRNA BANCR facilitates vascular smooth muscle cell proliferation and migration through JNK pathway.* Oncotarget, 2017. **8**(70): p. 114568-114575.
156. Gong, J., et al., *Long non-coding RNA CASC2 suppresses pulmonary artery smooth muscle cell proliferation and phenotypic switch in hypoxia-induced pulmonary hypertension.* Respir Res, 2019. **20**(1): p. 53.
157. Li, J., et al., *LncRNA CDKN2B-AS1 hinders the proliferation and facilitates apoptosis of ox-LDL-induced vascular smooth muscle cells via the ceRNA network of CDKN2B-AS1/miR-126-5p/PTPN7.* Int J Cardiol, 2021. **340**: p. 79-87.
158. Zhou, Y., et al., *LncRNA CRNDE regulates the proliferation and migration of vascular smooth muscle cells.* J Cell Physiol, 2019.
159. He, X., et al., *Long noncoding RNA GAS5 induces abdominal aortic aneurysm formation by promoting smooth muscle apoptosis.* Theranostics, 2019. **9**(19): p. 5558-5576.
160. Le, T., et al., *Knockdown of long noncoding RNA GAS5 reduces vascular smooth muscle cell apoptosis by inactivating EZH2-mediated RIG-I signaling pathway in abdominal aortic aneurysm.* J Transl Med, 2021. **19**(1): p. 466.
161. Das, S., et al., *A Novel Angiotensin II-Induced Long Noncoding RNA Giver Regulates Oxidative Stress, Inflammation, and Proliferation in Vascular Smooth Muscle Cells.* Circ Res, 2018. **123**(12): p. 1298-1312.
162. Li, D.Y., et al., *H19 Induces Abdominal Aortic Aneurysm Development and Progression.* Circulation, 2018. **138**(15): p. 1551-1568.
163. Zhang, L., et al., *H19 knockdown suppresses proliferation and induces apoptosis by regulating miR-148b/WNT/beta-catenin in ox-LDL -stimulated vascular smooth muscle cells.* J Biomed Sci, 2018. **25**(1): p. 11.
164. Su, H., et al., *LncRNA H19 promotes the proliferation of pulmonary artery smooth muscle cells through AT1R via sponging let-7b in monocrotaline-induced pulmonary arterial hypertension.* Respir Res, 2018. **19**(1): p. 254.
165. Yung, Y., et al., *HAS2-AS1 is a novel LH/hCG target gene regulating HAS2 expression and enhancing cumulus cells migration.* J Ovarian Res, 2019. **12**(1): p. 21.
166. Caon, I., et al., *Sirtuin 1 reduces hyaluronan synthase 2 expression by inhibiting nuclear translocation of NF-kappaB and expression of the long-noncoding RNA HAS2-AS1.* J Biol Chem, 2020. **295**(11): p. 3485-3496.
167. Lu, Y., et al., *LncRNA HCG18 is critical for vascular smooth muscle cell proliferation and phenotypic switching.* Hum Cell, 2020. **33**(3): p. 537-544.
168. Xu, J., et al., *Long non-coding RNA HIF1A-AS1 is upregulated in intracranial aneurysms and participates in the regulation of proliferation of vascular smooth muscle cells by upregulating TGF-beta1.* Exp Ther Med, 2019. **17**(3): p. 1797-1801.
169. Guo, X., et al., *Long Non-coding RNA-mRNA Correlation Analysis Reveals the Potential Role of HOTAIR in Pathogenesis of Sporadic Thoracic Aortic Aneurysm.* Eur J Vasc Endovasc Surg, 2017. **54**(3): p. 303-314.
170. Liu, X., et al., *Long noncoding RNA LINC00341 promotes the vascular smooth muscle cells proliferation and migration via miR-214/FOXO4 feedback loop.* Am J Transl Res, 2019. **11**(3): p. 1835-1842.
171. Wang, W., et al., *LINC01278 Sponges miR-500b-5p to Regulate the Expression of ACTG2 to Control Phenotypic Switching in Human Vascular Smooth Muscle Cells During Aortic Dissection.* J Am Heart Assoc, 2021. **10**(9): p. e018062.

172. Wu, G., et al., *LincRNA-p21 regulates neointima formation, vascular smooth muscle cell proliferation, apoptosis, and atherosclerosis by enhancing p53 activity.* Circulation, 2014. **130**(17): p. 1452-1465.
173. Wang, X., et al., *Expression of Long Noncoding RNA LIPCAR Promotes Cell Proliferation, Cell Migration, and Change in Phenotype of Vascular Smooth Muscle Cells.* Med Sci Monit, 2019. **25**: p. 7645-7651.
174. Cui, C., et al., *lncRNA 430945 promotes the proliferation and migration of vascular smooth muscle cells via the ROR2/RhoA signaling pathway in atherosclerosis.* Mol Med Rep, 2019. **19**(6): p. 4663-4672.
175. Lin, X., et al., *lncRNA-ES3/miR-34c-5p/BMF axis is involved in regulating high-glucose-induced calcification/senescence of VSMCs.* Aging (Albany NY), 2019. **11**(2): p. 523-535.
176. Cheng, Q., et al., *Long non-coding RNA LOC285194 regulates vascular smooth muscle cell apoptosis in atherosclerosis.* Bioengineered, 2020. **11**(1): p. 53-60.
177. Huang, B., et al., *LncRNA LOXL1-AS is up-regulated in thoracic aortic aneurysm and regulated proliferation and apoptosis of aortic smooth muscle cells.* Biosci Rep, 2019. **39**(9).
178. Ou, M., et al., *Long noncoding RNA MALAT1 contributes to pregnancy-induced hypertension development by enhancing oxidative stress and inflammation through the regulation of the miR-150-5p/ET-1 axis.* FASEB J, 2020. **34**(5): p. 6070-6085.
179. Wang, M., et al., *LncRNA MEG3-derived miR-361-5p regulate vascular smooth muscle cells proliferation and apoptosis by targeting ABCA1.* Am J Transl Res, 2019. **11**(6): p. 3600-3609.
180. Fasolo, F., et al., *Long Noncoding RNA MIAT Controls Advanced Atherosclerotic Lesion Formation and Plaque Destabilization.* Circulation, 2021. **144**(19): p. 1567-1583.
181. Vacante, F., et al., *The function of miR-143, miR-145 and the MiR-143 host gene in cardiovascular development and disease.* Vascul Pharmacol, 2019. **112**: p. 24-30.
182. Fang, G., et al., *LncRNA MRAK048635_P1 is critical for vascular smooth muscle cell function and phenotypic switching in essential hypertension.* Biosci Rep, 2019. **39**(3).
183. Choi, M., et al., *Transcriptional control of a novel long noncoding RNA Mymsl in smooth muscle cells by a single Cis-element and its initial functional characterization in vessels.* J Mol Cell Cardiol, 2020. **138**: p. 147-157.
184. Zhou, F., et al., *Nuclear Paraspeckle Assembly Transcript 1 Enhances Hydrogen Peroxide-Induced Human Vascular Smooth Muscle Cell Injury by Regulating miR-30d-5p/A Disintegrin and Metalloprotease 10.* Circ J, 2021.
185. Zhang, Z., et al., *Knockdown of lncRNA PVT1 Inhibits Vascular Smooth Muscle Cell Apoptosis and Extracellular Matrix Disruption in a Murine Abdominal Aortic Aneurysm Model.* Mol Cells, 2019. **42**(3): p. 218-227.
186. Pan, W., et al., *LncRNA SAMMSON Overexpression Suppresses Vascular Smooth Muscle Cell Proliferation via Inhibiting miR-130a Maturation to Participate in Intracranial Aneurysm.* Neuropsychiatr Dis Treat, 2021. **17**: p. 1793-1799.
187. Cai, Z., et al., *LncRNA SENCR suppresses abdominal aortic aneurysm formation by inhibiting smooth muscle cells apoptosis and extracellular matrix degradation.* Bosn J Basic Med Sci, 2021. **21**(3): p. 323-330.
188. Ye, F., et al., *Preliminary study on the mechanism of long noncoding RNA SENCR regulating the proliferation and migration of vascular smooth muscle cells.* J Cell Physiol, 2020. **235**(12): p. 9635-9643.
189. Bell, R.D., et al., *Identification and initial functional characterization of a human vascular cell-enriched long noncoding RNA.* Arterioscler Thromb Vasc Biol, 2014. **34**(6): p. 1249-59.
190. Lin, Y., et al., *Long non-coding RNA SNHG16 regulates human aortic smooth muscle cell proliferation and migration via sponging miR-205 and modulating Smad2.* J Cell Mol Med, 2019. **23**(10): p. 6919-6929.

191. Xiao, W., et al., *LncRNA Sox2ot modulates the progression of thoracic aortic aneurysm by regulating miR-330-5p/Myh11.* Biosci Rep, 2020. **40**(7).
192. Wang, X. and J. Chen, *Long non-coding RNA TUG1 promotes proliferation and migration in PDGF-BB-stimulated HASMCs by regulating miR-216a-3p/SMURF2 axis.* BMC Mol Cell Biol, 2021. **22**(1): p. 56.
193. Shi, Z., Q. Zhu, and J. Fan, *lncRNA TUG1 promotes atherosclerosis progression by targeting miR-382-5p.* Int J Clin Exp Pathol, 2021. **14**(9): p. 972-979.
194. Zehendner, C.M., et al., *Long Noncoding RNA TYKRIL Plays a Role in Pulmonary Hypertension via the p53-mediated Regulation of PDGFRbeta.* Am J Respir Crit Care Med, 2020. **202**(10): p. 1445-1457.
195. Zou, L., et al., *XIST knockdown suppresses vascular smooth muscle cell proliferation and induces apoptosis by regulating miR-1264/WNT5A/beta-catenin signaling in aneurysm.* Biosci Rep, 2021. **41**(3).
196. Yao, Q.P., et al., *Profiles of long noncoding RNAs in hypertensive rats: long noncoding RNA XR007793 regulates cyclic strain-induced proliferation and migration of vascular smooth muscle cells.* J Hypertens, 2017. **35**(6): p. 1195-1203.
197. Wu, Y.X., et al., *Long Noncoding RNA XR007793 Regulates Proliferation and Migration of Vascular Smooth Muscle Cell via Suppressing miR-23b.* Med Sci Monit, 2018. **24**: p. 5895-5903.
198. Boccaletto, P., et al., *MODOMICS: a database of RNA modification pathways. 2017 update.* Nucleic Acids Res, 2018. **46**(D1): p. D303-D307.
199. Jonkhout, N., et al., *The RNA modification landscape in human disease.* RNA, 2017. **23**(12): p. 1754-1769.
200. Jank, P. and H.J. Gross, *Methyl-deficient mammalian transfer RNA: II. Homologous methylation in vitro of liver tRNA from normal and ethionine-fed rats: ethionine effect on 5-methyl-cytidine synthesis in vivo.* Nucleic Acids Res, 1974. **1**(10): p. 1259-67.
201. Wei, C.M., A. Gershowitz, and B. Moss, *5'-Terminal and internal methylated nucleotide sequences in HeLa cell mRNA.* Biochemistry, 1976. **15**(2): p. 397-401.
202. Wei, C.M. and B. Moss, *Nucleotide sequences at the N6-methyladenosine sites of HeLa cell messenger ribonucleic acid.* Biochemistry, 1977. **16**(8): p. 1672-6.
203. Wang, X., et al., *N6-methyladenosine-dependent regulation of messenger RNA stability.* Nature, 2014. **505**(7481): p. 117-20.
204. Shi, H., et al., *YTHDF3 facilitates translation and decay of N(6)-methyladenosine-modified RNA.* Cell Res, 2017. **27**(3): p. 315-328.
205. Xu, H., et al., *m(6)A mRNA Methylation Is Essential for Oligodendrocyte Maturation and CNS Myelination.* Neuron, 2019.
206. Wang, H., et al., *N6-methyladenosine induced miR-143-3p promotes the brain metastasis of lung cancer via regulation of VASH1.* Mol Cancer, 2019. **18**(1): p. 181.
207. Yu, J., et al., *The m6A methyltransferase METTL3 cooperates with demethylase ALKBH5 to regulate osteogenic differentiation through NF-kappaB signaling.* Mol Cell Biochem, 2020. **463**(1-2): p. 203-210.
208. Yan, G., et al., *m(6)A Methylation of Precursor-miR-320/RUNX2 Controls Osteogenic Potential of Bone Marrow-Derived Mesenchymal Stem Cells.* Mol Ther Nucleic Acids, 2019. **19**: p. 421-436.
209. Yu, R., et al., *m6A Reader YTHDF2 Regulates LPS-Induced Inflammatory Response.* Int J Mol Sci, 2019. **20**(6).
210. Lee, Y., et al., *Molecular Mechanisms Driving mRNA Degradation by m(6)A Modification.* Trends Genet, 2020. **36**(3): p. 177-188.
211. Ke, S., et al., *m(6)A mRNA modifications are deposited in nascent pre-mRNA and are not required for splicing but do specify cytoplasmic turnover.* Genes Dev, 2017. **31**(10): p. 990-1006.

212. Horiuchi, K., T. Kawamura, and T. Hamakubo, *Wilms' Tumor 1-Associating Protein complex regulates alternative splicing and polyadenylation at potential G-quadruplex-forming splice site sequences.* J Biol Chem, 2021: p. 101248.
213. Liu, J., et al., *A METTL3-METTL14 complex mediates mammalian nuclear RNA N6-adenosine methylation.* Nat Chem Biol, 2014. **10**(2): p. 93-5.
214. Wang, P., K.A. Doxtader, and Y. Nam, *Structural Basis for Cooperative Function of Mettl3 and Mettl14 Methyltransferases.* Mol Cell, 2016. **63**(2): p. 306-317.
215. Ping, X.L., et al., *Mammalian WTAP is a regulatory subunit of the RNA N6-methyladenosine methyltransferase.* Cell Res, 2014. **24**(2): p. 177-89.
216. Schwartz, S., et al., *Perturbation of m6A writers reveals two distinct classes of mRNA methylation at internal and 5' sites.* Cell Rep, 2014. **8**(1): p. 284-96.
217. Lence, T., et al., *m(6)A modulates neuronal functions and sex determination in Drosophila.* Nature, 2016. **540**(7632): p. 242-247.
218. Horiuchi, K., et al., *Identification of Wilms' tumor 1-associating protein complex and its role in alternative splicing and the cell cycle.* J Biol Chem, 2013. **288**(46): p. 33292-302.
219. Patil, D.P., et al., *m(6)A RNA methylation promotes XIST-mediated transcriptional repression.* Nature, 2016. **537**(7620): p. 369-373.
220. Knuckles, P., et al., *Zc3h13/Flacc is required for adenosine methylation by bridging the mRNA-binding factor Rbm15/Spenito to the m(6)A machinery component Wtap/Fl(2)d.* Genes Dev, 2018. **32**(5-6): p. 415-429.
221. Wen, J., et al., *Zc3h13 Regulates Nuclear RNA m(6)A Methylation and Mouse Embryonic Stem Cell Self-Renewal.* Mol Cell, 2018. **69**(6): p. 1028-1038 e6.
222. Ruzicka, K., et al., *Identification of factors required for m(6) A mRNA methylation in Arabidopsis reveals a role for the conserved E3 ubiquitin ligase HAKAI.* New Phytol, 2017. **215**(1): p. 157-172.
223. Jia, G., et al., *N6-methyladenosine in nuclear RNA is a major substrate of the obesity-associated FTO.* Nat Chem Biol, 2011. **7**(12): p. 885-7.
224. Ensfelder, T.T., et al., *ALKBH5-induced demethylation of mono- and dimethylated adenosine.* Chem Commun (Camb), 2018. **54**(62): p. 8591-8593.
225. Zheng, G., et al., *ALKBH5 is a mammalian RNA demethylase that impacts RNA metabolism and mouse fertility.* Mol Cell, 2013. **49**(1): p. 18-29.
226. Wu, R., et al., *m6A methylation promotes white-to-beige fat transition by facilitating Hif1a translation.* EMBO Rep, 2021: p. e52348.
227. Tang, C., et al., *ALKBH5-dependent m6A demethylation controls splicing and stability of long 3'-UTR mRNAs in male germ cells.* Proc Natl Acad Sci U S A, 2018. **115**(2): p. E325-E333.
228. Darnell, R.B., S. Ke, and J.E. Darnell, Jr., *Pre-mRNA processing includes N(6) methylation of adenosine residues that are retained in mRNA exons and the fallacy of "RNA epigenetics".* RNA, 2018. **24**(3): p. 262-267.
229. Zhao, B.S., et al., *Our views of dynamic N(6)-methyladenosine RNA methylation.* RNA, 2018. **24**(3): p. 268-272.
230. Edupuganti, R.R., et al., *N(6)-methyladenosine (m(6)A) recruits and repels proteins to regulate mRNA homeostasis.* Nat Struct Mol Biol, 2017. **24**(10): p. 870-878.
231. Xu, C., et al., *Structural Basis for the Discriminative Recognition of N6-Methyladenosine RNA by the Human YT521-B Homology Domain Family of Proteins.* J Biol Chem, 2015. **290**(41): p. 24902-13.
232. Imai, Y., et al., *Cloning of a gene, YT521, for a novel RNA splicing-related protein induced by hypoxia/reoxygenation.* Brain Res Mol Brain Res, 1998. **53**(1-2): p. 33-40.
233. Hartmann, A.M., et al., *The interaction and colocalization of Sam68 with the splicing-associated factor YT521-B in nuclear dots is regulated by the Src family kinase p59(fyn).* Mol Biol Cell, 1999. **10**(11): p. 3909-26.

234. Stoilov, P., I. Rafalska, and S. Stamm, *YTH: a new domain in nuclear proteins.* Trends Biochem Sci, 2002. **27**(10): p. 495-7.
235. Zhang, Z., et al., *The YTH domain is a novel RNA binding domain.* J Biol Chem, 2010. **285**(19): p. 14701-10.
236. Xiao, W., et al., *Nuclear m(6)A Reader YTHDC1 Regulates mRNA Splicing.* Mol Cell, 2016. **61**(4): p. 507-519.
237. Roundtree, I.A., et al., *YTHDC1 mediates nuclear export of N(6)-methyladenosine methylated mRNAs.* Elife, 2017. **6**.
238. Hsu, P.J., et al., *Ythdc2 is an N(6)-methyladenosine binding protein that regulates mammalian spermatogenesis.* Cell Res, 2017. **27**(9): p. 1115-1127.
239. Bailey, A.S., et al., *The conserved RNA helicase YTHDC2 regulates the transition from proliferation to differentiation in the germline.* Elife, 2017. **6**.
240. Wojtas, M.N., et al., *Regulation of m(6)A Transcripts by the 3'-->5' RNA Helicase YTHDC2 Is Essential for a Successful Meiotic Program in the Mammalian Germline.* Mol Cell, 2017. **68**(2): p. 374-387 e12.
241. Patil, D.P., B.F. Pickering, and S.R. Jaffrey, *Reading m(6)A in the Transcriptome: m(6)A-Binding Proteins.* Trends Cell Biol, 2018. **28**(2): p. 113-127.
242. Wang, X., et al., *N(6)-methyladenosine Modulates Messenger RNA Translation Efficiency.* Cell, 2015. **161**(6): p. 1388-99.
243. Meyer, K.D., et al., *5' UTR m(6)A Promotes Cap-Independent Translation.* Cell, 2015. **163**(4): p. 999-1010.
244. Du, H., et al., *YTHDF2 destabilizes m(6)A-containing RNA through direct recruitment of the CCR4-NOT deadenylase complex.* Nat Commun, 2016. **7**: p. 12626.
245. Frye, M., et al., *RNA modifications modulate gene expression during development.* Science, 2018. **361**(6409): p. 1346-1349.
246. Heck, A.M., et al., *YTHDF2 destabilizes m(6)A-modified neural-specific RNAs to restrain differentiation in induced pluripotent stem cells.* RNA, 2020. **26**(6): p. 739-755.
247. Zhou, J., et al., *Dynamic m(6)A mRNA methylation directs translational control of heat shock response.* Nature, 2015. **526**(7574): p. 591-4.
248. Li, A., et al., *Cytoplasmic m(6)A reader YTHDF3 promotes mRNA translation.* Cell Res, 2017. **27**(3): p. 444-447.
249. Huang, H., et al., *Recognition of RNA N(6)-methyladenosine by IGF2BP proteins enhances mRNA stability and translation.* Nat Cell Biol, 2018. **20**(3): p. 285-295.
250. Vassilev, L.T., et al., *Selective small-molecule inhibitor reveals critical mitotic functions of human CDK1.* Proc Natl Acad Sci U S A, 2006. **103**(28): p. 10660-5.
251. Vassilev, L.T., *Cell cycle synchronization at the G2/M phase border by reversible inhibition of CDK1.* Cell Cycle, 2006. **5**(22): p. 2555-6.
252. Guo, N. and Z. Peng, *MG132, a proteasome inhibitor, induces apoptosis in tumor cells.* Asia Pac J Clin Oncol, 2013. **9**(1): p. 6-11.
253. Sun, F., et al., *Proteasome Inhibitor MG132 Enhances Cisplatin-Induced Apoptosis in Osteosarcoma Cells and Inhibits Tumor Growth.* Oncol Res, 2018. **26**(4): p. 655-664.
254. Grose, C. and D.J. Klionsky, *Alternative autophagy, brefeldin A and viral trafficking pathways.* Autophagy, 2016. **12**(9): p. 1429-30.
255. Chardin, P. and F. McCormick, *Brefeldin A: the advantage of being uncompetitive.* Cell, 1999. **97**(2): p. 153-5.
256. Ueda, R., *Rnai: a new technology in the post-genomic sequencing era.* J Neurogenet, 2001. **15**(3-4): p. 193-204.
257. Hannus, M., et al., *siPools: highly complex but accurately defined siRNA pools eliminate off-target effects.* Nucleic Acids Res, 2014. **42**(12): p. 8049-61.
258. Ma, Y., L. Zhang, and X. Huang, *Genome modification by CRISPR/Cas9.* FEBS J, 2014. **281**(23): p. 5186-93.

259. Ho-Xuan, H., et al., *Comprehensive analysis of translation from overexpressed circular RNAs reveals pervasive translation from linear transcripts.* Nucleic Acids Res, 2020. **48**(18): p. 10368-10382.
260. Schmittgen, T.D. and K.J. Livak, *Analyzing real-time PCR data by the comparative C(T) method.* Nat Protoc, 2008. **3**(6): p. 1101-8.
261. Taylor, S.C., et al., *The Ultimate qPCR Experiment: Producing Publication Quality, Reproducible Data the First Time.* Trends Biotechnol, 2019. **37**(7): p. 761-774.
262. R Core Team, *R: A language and environment for statistical computing*. 2020, R Foundation for Statistical Computing.
263. Weichmann, F., et al., *Validation strategies for antibodies targeting modified ribonucleotides.* RNA, 2020. **26**(10): p. 1489-1506.
264. Hadley Wickham, R.F., Lionel Henry and Kirill Müller., *dplyr: A Grammar of Data Manipulation.* 2020.
265. Wickham., H., *ggplot2: Elegant Graphics for Data Analysis.* Springer-Verlag New York, 2016.
266. Johannes Rainer, *EnsDb.Hsapiens.v86: Ensembl based annotation package.* 2017.
267. Guangchuang Yu, L.-G.W., Guang-Rong Yan, Qing-Yu He., *DOSE: an R/Bioconductor package for Disease Ontology Semantic and Enrichment analysis.* Bioinformatics 2015(31): p. 4.
268. Guangchuang Yu, L.-G.W., Yanyan Han and Qing-Yu He., *clusterProfiler: an R package for comparing biological themes among gene clusters.* OMICS: A Journal of Integrative Biology, 2012. **16**: p. 5.
269. Guangchuang Yu, Q.-Y.H., *ReactomePA: an R/Bioconductor package for reactome pathway analysis and visualization.* Molecular BioSystems 2016, 2016(12): p. 2.
270. Love, M.I., Huber, W., Anders, S., *Moderated estimation of fold change and dispersion for RNA-seq data with DESeq2.* Genome Biology, 2014(15): p. 12.
271. Chen, E.Y., et al., *Enrichr: interactive and collaborative HTML5 gene list enrichment analysis tool.* BMC Bioinformatics, 2013. **14**: p. 128.
272. Kuleshov, M.V., et al., *Enrichr: a comprehensive gene set enrichment analysis web server 2016 update.* Nucleic Acids Res, 2016. **44**(W1): p. W90-7.
273. Hon, C.C., et al., *An atlas of human long non-coding RNAs with accurate 5' ends.* Nature, 2017. **543**(7644): p. 199-204.
274. Slomovic, S., et al., *Polyadenylation of ribosomal RNA in human cells.* Nucleic Acids Res, 2006. **34**(10): p. 2966-75.
275. Mohamed Soudy, A.M.A., Eman Ali Ahmed, Aya Osama, Shahd Ezzeldin, Sebaey Mahgou and Sameh Magdeldin, *UniprotR: Retrieving and visualizing protein sequence and functional information from Universal Protein Resource (UniProt knowledgebase).* Journal of Proteomics, 2020. **213**: p. 103613.
276. Santos, S., et al., *Characterization of pulmonary vascular remodelling in smokers and patients with mild COPD.* Eur Respir J, 2002. **19**(4): p. 632-8.
277. Tsukazaki, T., et al., *SARA, a FYVE domain protein that recruits Smad2 to the TGFbeta receptor.* Cell, 1998. **95**(6): p. 779-91.
278. Bertero, A., et al., *The SMAD2/3 interactome reveals that TGFbeta controls m(6)A mRNA methylation in pluripotency.* Nature, 2018. **555**(7695): p. 256-259.
279. Edlund, S., et al., *Transforming growth factor-beta-induced mobilization of actin cytoskeleton requires signaling by small GTPases Cdc42 and RhoA.* Mol Biol Cell, 2002. **13**(3): p. 902-14.
280. Wang, X.F., et al., *[Involvement of p53-dependent pathway in the antiproliferative activity of emodin in human smooth muscle cell].* Zhonghua Xin Xue Guan Bing Za Zhi, 2006. **34**(1): p. 44-9.

281. Calvier, L., et al., *LRP1 Deficiency in Vascular SMC Leads to Pulmonary Arterial Hypertension That Is Reversed by PPARgamma Activation.* Circ Res, 2019. **124**(12): p. 1778-1785.
282. Zucker, M.M., et al., *LRP1 promotes synthetic phenotype of pulmonary artery smooth muscle cells in pulmonary hypertension.* Biochim Biophys Acta Mol Basis Dis, 2019. **1865**(6): p. 1604-1616.
283. Zhou, L., et al., *LRP1 regulates architecture of the vascular wall by controlling PDGFRbeta-dependent phosphatidylinositol 3-kinase activation.* PLoS One, 2009. **4**(9): p. e6922.
284. Grainger, D.J., et al., *Mitogens for adult rat aortic vascular smooth muscle cells in serum-free primary culture.* Cardiovasc Res, 1994. **28**(8): p. 1238-42.
285. Ucuzian, A.A., et al., *Characterization of the chemotactic and mitogenic response of SMCs to PDGF-BB and FGF-2 in fibrin hydrogels.* J Biomed Mater Res A, 2010. **94**(3): p. 988-96.
286. Xu, Z., et al., *SOX9 and myocardin counteract each other in regulating vascular smooth muscle cell differentiation.* Biochem Biophys Res Commun, 2012. **422**(2): p. 285-90.
287. Martin, E., et al., *TSHZ3 and SOX9 regulate the timing of smooth muscle cell differentiation in the ureter by reducing myocardin activity.* PLoS One, 2013. **8**(5): p. e63721.
288. Kent, W.J., et al., *The human genome browser at UCSC.* Genome Res, 2002. **12**(6): p. 996-1006.
289. Lizio, M., et al., *Gateways to the FANTOM5 promoter level mammalian expression atlas.* Genome Biol, 2015. **16**: p. 22.
290. Lizio, M., et al., *Update of the FANTOM web resource: expansion to provide additional transcriptome atlases.* Nucleic Acids Res, 2019. **47**(D1): p. D752-D758.
291. Yan, F., et al., *Roles of airway smooth muscle dysfunction in chronic obstructive pulmonary disease.* J Transl Med, 2018. **16**(1): p. 262.
292. Grossi, E., et al., *A lncRNA-SWI/SNF complex crosstalk controls transcriptional activation at specific promoter regions.* Nat Commun, 2020. **11**(1): p. 936.
293. Zhang, M., et al., *A novel role of Brg1 in the regulation of SRF/MRTFA-dependent smooth muscle-specific gene expression.* J Biol Chem, 2007. **282**(35): p. 25708-16.
294. Zhou, J., et al., *The SWI/SNF chromatin remodeling complex regulates myocardin-induced smooth muscle-specific gene expression.* Arterioscler Thromb Vasc Biol, 2009. **29**(6): p. 921-8.
295. Tang, R., et al., *LncRNA GAS5 regulates vascular smooth muscle cell cycle arrest and apoptosis via p53 pathway.* Biochim Biophys Acta Mol Basis Dis, 2019. **1865**(9): p. 2516-2525.
296. Spin, J.M., T. Quertermous, and P.S. Tsao, *Chromatin remodeling pathways in smooth muscle cell differentiation, and evidence for an integral role for p300.* PLoS One, 2010. **5**(12): p. e14301.
297. Wallberg, A.E., et al., *p300 and PCAF act cooperatively to mediate transcriptional activation from chromatin templates by notch intracellular domains in vitro.* Mol Cell Biol, 2002. **22**(22): p. 7812-9.
298. Boucher, J., T. Gridley, and L. Liaw, *Molecular pathways of notch signaling in vascular smooth muscle cells.* Front Physiol, 2012. **3**: p. 81.
299. Gomez, D., et al., *Detection of histone modifications at specific gene loci in single cells in histological sections.* Nat Methods, 2013. **10**(2): p. 171-7.
300. Liu, M., et al., *H3K4 di-methylation governs smooth muscle lineage identity and promotes vascular homeostasis by restraining plasticity.* Dev Cell, 2021. **56**(19): p. 2765-2782 e10.

301. Camejo, G., et al., *Binding of low density lipoproteins by proteoglycans synthesized by proliferating and quiescent human arterial smooth muscle cells.* J Biol Chem, 1993. **268**(19): p. 14131-7.
302. Fei, Q., et al., *YTHDF2 promotes mitotic entry and is regulated by cell cycle mediators.* PLoS Biol, 2020. **18**(4): p. e3000664.
303. Wu, R., et al., *FTO regulates adipogenesis by controlling cell cycle progression via m(6)A-YTHDF2 dependent mechanism.* Biochim Biophys Acta Mol Cell Biol Lipids, 2018. **1863**(10): p. 1323-1330.
304. Li, M., et al., *Ythdf2-mediated m(6)A mRNA clearance modulates neural development in mice.* Genome Biol, 2018. **19**(1): p. 69.
305. Mathiyalagan, P., et al., *FTO-Dependent N(6)-Methyladenosine Regulates Cardiac Function During Remodeling and Repair.* Circulation, 2019. **139**(4): p. 518-532.
306. Dorn, L.E., et al., *The N(6)-Methyladenosine mRNA Methylase METTL3 Controls Cardiac Homeostasis and Hypertrophy.* Circulation, 2019. **139**(4): p. 533-545.
307. Ma, D., et al., *Vascular Smooth Muscle FTO Promotes Aortic Dissecting Aneurysms via m6A Modification of Klf5.* Front Cardiovasc Med, 2020. **7**: p. 592550.
308. Hu, L., et al., *YTHDF1 Regulates Pulmonary Hypertension Through Translational Control of MAGED1.* Am J Respir Crit Care Med, 2021.
309. Wang, S., et al., *Differential roles of YTHDF1 and YTHDF3 in embryonic stem cell-derived cardiomyocyte differentiation.* RNA Biol, 2020: p. 1-10.
310. Lin, J., et al., *Hypoxia Promotes Vascular Smooth Muscle Cell (VSMC) Differentiation of Adipose-Derived Stem Cell (ADSC) by Regulating Mettl3 and Paracrine Factors.* Stem Cells Int, 2020. **2020**: p. 2830565.
311. Dai, X., et al., *YTHDF2 Binds to 5-Methylcytosine in RNA and Modulates the Maturation of Ribosomal RNA.* Anal Chem, 2020. **92**(1): p. 1346-1354.
312. Seo, K.W. and R.E. Kleiner, *YTHDF2 Recognition of N(1)-Methyladenosine (m(1)A)-Modified RNA Is Associated with Transcript Destabilization.* ACS Chem Biol, 2020. **15**(1): p. 132-139.
313. Huang, T., et al., *YTHDF2 promotes spermagonial adhesion through modulating MMPs decay via m(6)A/mRNA pathway.* Cell Death Dis, 2020. **11**(1): p. 37.
314. Ni, W., et al., *Long noncoding RNA GAS5 inhibits progression of colorectal cancer by interacting with and triggering YAP phosphorylation and degradation and is negatively regulated by the m(6)A reader YTHDF3.* Mol Cancer, 2019. **18**(1): p. 143.
315. Jin, D., et al., *m(6)A demethylase ALKBH5 inhibits tumor growth and metastasis by reducing YTHDFs-mediated YAP expression and inhibiting miR-107/LATS2-mediated YAP activity in NSCLC.* Mol Cancer, 2020. **19**(1): p. 40.
316. Shao, X.Y., et al., *Systematic Analyses of the Role of the Reader Protein of N (6)-Methyladenosine RNA Methylation, YTH Domain Family 2, in Liver Hepatocellular Carcinoma.* Front Mol Biosci, 2020. **7**: p. 577460.
317. Zheng, Z., et al., *Control of Early B Cell Development by the RNA N(6)-Methyladenosine Methylation.* Cell Rep, 2020. **31**(13): p. 107819.
318. Guo, X. and S.Y. Chen, *Transforming growth factor-beta and smooth muscle differentiation.* World J Biol Chem, 2012. **3**(3): p. 41-52.

6 Appendix

6.1 Primers used

Table 6.1.1. Primers table. The sequences of each primer used in this work are presented. In the column GENE (Observation) the gene name is detailed and observations about the amplicon are between parentheses. The Forward and Reverse sequences are detailed in the remaining columns.

GENE (Observation)	Primer Forward 5' - 3'	Primer Reverse 5' - 3'
CALD1	GGAGGTGAATGCCCAGAACA	AGGAATGCGGCCTCATCATC
CNN1	CACGACATTTTTGAGGCCAA	TTTCCTTTCGTCTTCGCCAT
CTNNB1	CACAAGCAGAGTGCTGAAGGTG	GATTCCTGAGAGTCCAAAGACAG
DAGAR	GGGAAATTCCTGGGATGCCA	TGGGAGCTCCACCTCTAGAC
DAGAR (END)	TCCATTTTCATCCTGCTGTG	CTGGAGTGCAGTTGCATGAT
DAGAR (START)	AGAATCCACATGGAGAACAGTG	AGGAGGTTCCAGCCAGTTTT
DAGAR (MIDDLE)	CACATGGGCTACATCTGCAC	CTTTGCCTTCTGCCATGAAT
DAGAR (NB 1)	GAGCTCCCATTGTGGGCAGAGGGAC	TATAGGCATCGTATTTTAATAAACAG
DAGAR (NB 2)	TCTGAAAACTGGCTGGAACC	CAATGGGAGCTCCACCTCTA
DAGAR1	ATGGAGAACAGTGGGAGGAG	ACCCAGTTTGTGGGACTTTG
DAGAR2	ATGGAGAACAGTGGGAGGAG	TCTGCAGCTCCTGTCTTCAA
FGF2	AGCGGCTGTACTGCAAAAACGG	CCTTTGATAGACACAACTCCTCTC
GAPDH	GTCTCCTCTGACTTCAACAGCG	ACCACCCTGTTGCTGTAGCCAA
GATA6	TTCCCATGACTCCAACTTCC	TGGGGGAAGTATTTTTGCTG
ITGB3	CATGGATTCCAGCAATGTCCTCC	TTGAGGCAGGTGGCATTGAAGG
Ki67	GCAGCCTTAACTGTGACACTTGC	GCCACCGTGCCCTGG
LRP1	CAACGGCATCTCAGTGGACTAC	TGTTGCTGGACAGAACCACCTC
METTL3	GCCAGGAGCTTGCTCTTACAC	GTGGGTCAGCCATCACAACTG
MYH11	GTCCAGGAGATGAGGCAGAAAC	GTCTGCGTTCTCTTTCTCCAGC
MYOCD	GCACCAAGCTCAGCTTAAGGA	TGGGAGTGGGCCTGGTTT
PDGFRB	TGCAGACATCGAGTCCTCCAAC	GCTTAGCACTGGAGACTCGTTG
PRDM2	TTGGGCTTGCTCAGGAGAAGAG	GCTGCTATCTCAGGGTTGTCTTC
RHOA	TCTGTCCCAACGTGCCCATCAT	CTGCCTTCTTCAGGTTTCACCG
SMAD2	GGGTTTTGAAGCCGTCTATCAGC	CCAACCACTGTAGAGGTCCATTC
SMAD3	TGAGGCTGTCTACCAGTTGACC	GTGAGGACCTTGTCAAGCCACT
SON	TTGGGCTTGCTCAGGAGAAGAG	GCTGCTATCTCAGGGTTGTCTTC
SOX9	AGGAAGCTCGCGGACCAGTAC	GGTGGTCCTTCTTGTGCTGCAC
TAGLN	GGAAGCCTTCTTTCCCCAGA	TCCAGCTCCTCGTCATACTTCTT
TGFB1	TACCTGAACCCGTGTTGCTCTC	GTTGCTGAGGTATCGCCAGGAA
TGFBRI	GACAACGTCAGGTTCTGGCTCA	CCGCCACTTTCCTCTCCAAACT
TP53	CCTCAGCATCTTATCCGAGTGG	TGGATGGTGGTACAGTCAGAGC
VEGFA	TTGCCTTGCTGCTCTACCTCCA	GATGGCAGTAGCTGCGCTGATA
YTHDF2	AGGGACAAAAGCCTCCGCC	CCTTGACCTTTTGGTCTCTGCT
YTHDF3	GCTACTTTCAAGCATACCACCTC	ACAGGACATCTTCATACGGTTATTG

6.2 Antibodies used

Table 6.2.1. Table of antibodies. All the antibodies used in this work are described. The first column (Antibody anti) reflects the target protein of the antibody, and the emission wavelength in nanometers in the case of secondary antibodies. The second and third columns correspond to the antibody manufacturer and reference number respectively. The specificity column describes whether the antibody corresponds to only one immunoglobulin subtype (monoclonal) or not (polyclonal). The origin column denotes the species in which the antibody was produced. The concentration at which the antibodies were used (dilution column), the clone from which it was derived, and particular observations corresponding to cross-reactions are also specified.

Antibody anti	**Fabricant**	**Reference**	**Specificity**	**Origin**	**Dilution**	**Clon**	**Observations**
αSMA (ACTA2)	DAKO Cytomation, Carpinteria, CA	M0851	Monoclonal	MOUSE	1:750	1A4	
CNN1	DAKO Cytomation, Carpinteria, CA	M3556	Monoclonal	MOUSE	1:75		
KI67	Novocastra, Newcastle, United Kingdom	ACK02	Monoclonal	MOUSE	1:50	K2	
YTHDF1	Proteintech Group Inc, Fisher scientific, USA.	17479-1-AP	Polyclonal	RABBIT	1:1000		
YTHDF2	Helmholtz Zentrum München and Meister Lab, Germany	Private	Monoclonal	RAT	1:50	9G11	
YTHDF2	Helmholtz Zentrum München and Meister Lab, Germany	Private	Monoclonal	MOUSE	1:50	32A11	
YTHDF2	Proteintech Group Inc, Fisher scientific, USA.	24744-1-AP	Polyclonal	RABBIT	1:1000		
YTHDF3	Helmholtz Zentrum München and Meister Lab, Germany	Private	Monoclonal	MOUSE	1:50	29C9	Cross reacts with YTHDF2
YTHDF3	Helmholtz Zentrum München and Meister Lab, Germany	Private	Monoclonal	MOUSE	1:50	30F11	Cross reacts with YTHDF2

YTHDF3	Santa Cruz Biotechnology, USA.	sc-377119	Monoclonal	MOUSE	1:500		
METTL3	Proteintech Group Inc, Fisher scientific, USA.	15073-1-AP	Polyclonal	RABBIT	1:1000	AG7110	
GAPDH	GeneTex, USA.	GTX627408P	Monoclonal	MOUSE	1:1000	GT239	
FTO	Abcam, United Kingdom	ab126605	Monoclonal	RABBIT	1:1000	EPR6894	
RAT IgG 680	Licor, USA.	925-68076	Monoclonal	GOAT	1:15000		
MOUSE IgG 680	Licor, USA.	926-32220	Monoclonal	GOAT	1:15000		
RABBIT IgG 680	Licor, USA.	926-32221	Monoclonal	GOAT	1:15000		
RAT IgG 800	Licor, USA.	926-32219	Monoclonal	GOAT	1:15000		
MOUSE IgG 800	Licor, USA.	926-32210	Monoclonal	GOAT	1:15000		
RABBIT IgG 800	Licor, USA.	926-32211	Monoclonal	GOAT	1:15000		
MOUSE IgG Alexa 488	Invitrogen/Life Technologies, Thermo Fisher, USA.	A28175	Monoclonal	GOAT	1:500		

6.3 RIP-YTHDF2 Mass Sequencing Data Quality Control

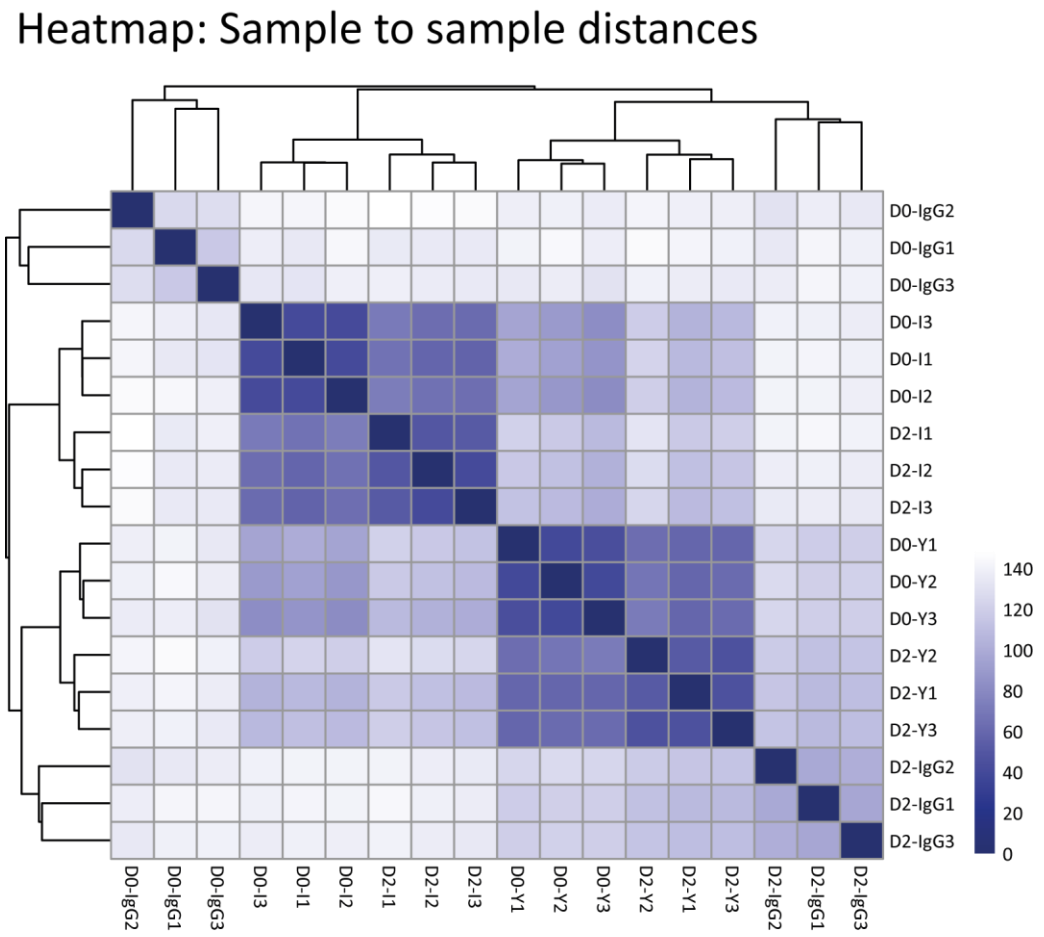

Figure 6.3.1. Heat map of sample-to-sample distances of data derived from RNA deep sequencing of human pulmonary artery smooth muscle cells (hPASMC) in D0 (Proliferative, at 70% confluence) and D2 (at the beginning of differentiation, at 100 % confluence) in the input condition (I), after immunoprecipitation with an anti-IgG antibody (IgG) and after immunoprecipitation with an anti-YTHDF2 antibody (Y). The lines represent the groupings as a function of distance. The grouping of the samples correlates with the experimental groups designed, showing a good quality of replicates.

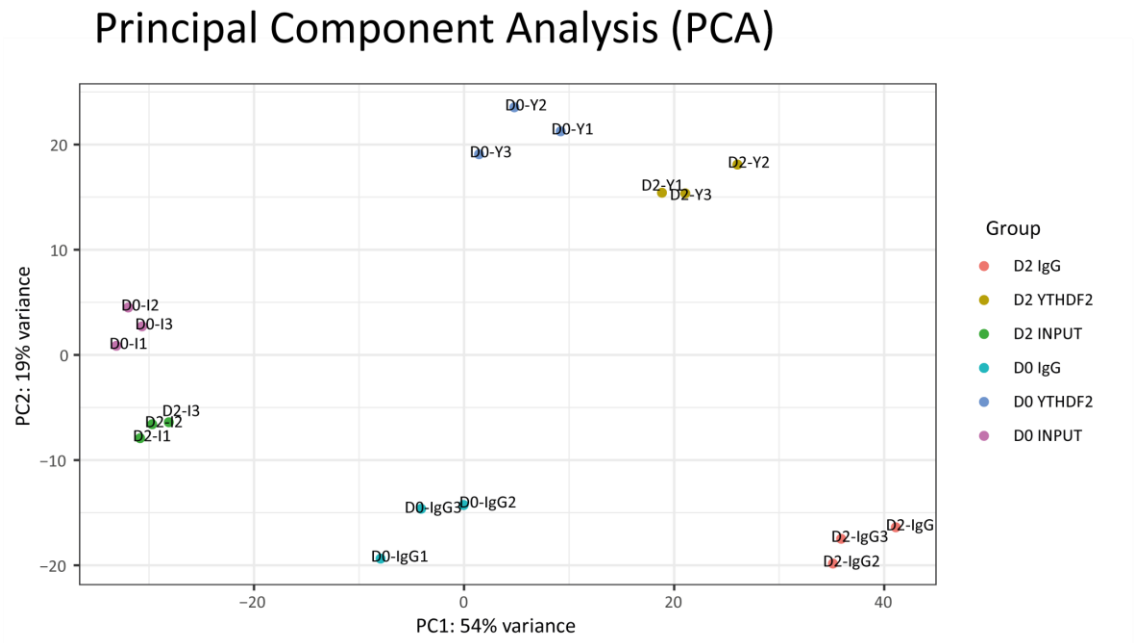

Figure 6.3.2. Principal Component Analysis (PCA) of Data Derived from Human Pulmonary Artery Smooth Muscle Cells (hPASMC) RNA deep sequencing at D0 (Proliferative, at 70% confluence) and D2 (at the beginning of differentiation, at 100% confluence) in input condition (I), after immunoprecipitation with an anti-IgG antibody (IgG) and after immunoprecipitation with an anti-YTHDF2 antibody (Y). The axes represent the two principal components after orthogonal dimensional reduction of the total variance of the data set. The main axis (PC1, in the X-axis) represents 54% of the variability of the data set, while the second main axis (PC2, in the y-axis) represents 19% of the total variability of the data set. It can be observed that the replicates group in the multivariate space, while experimental group separation is observed according to treatment and phenotype.

6.4 Specific proteins that co-precipitated with DAGAR

Table 6.4.1. Table of interacting proteins with DAGAR. Specific proteins that were co-precipitated with DAGAR are listed. The first column corresponds to the identification number on the Uniprot server. The second column (Name) represents the name of the gene associated with the protein. The third column (Score) represents the quality of the hit based on its abundance and coverage. The last column (% sequence coverage) shows the total percentage found of the amino acid sequence corresponding to the detected protein.

Uniprot accession	Symbol	Score	% Sequence coverage
P49327	FASN	7174,2	48,18797292
Q92616	GCN1	4948,7	37,81355298
P27708	CAD	4940,6	44,13483146
O75643	SNRNP200	4552,3	41,10486891
Q01082	SPTBN1	4152,2	39,34010152
Q13813	SPTAN1	3727,1	35,19417476
Q6P2Q9	PRPF8	3604,3	36,5738758
Q04637	EIF4G1	2963,4	38,21138211
P21333	FLNA	2802,5	27,65394787
Q9Y490	TLN1	2613,3	33,37268792
P12270	TPR	2451,4	25,05289886
A5YKK6	CNOT1	1976,9	22,22222222
Q92621	NUP205	1889,5	23,95626243
Q13085	ACACA	1878,7	20,67348679
P78527	PRKDC	1841,1	13,37209302
P46940	IQGAP1	1796,6	27,57996379
O75165	DNAJC13	1791,8	20,55283103
Q93008	USP9X	1775,1	16,38132296
Q96N67	DOCK7	1726,4	20,79439252
Q9H583	HEATR1	1671,8	21,26865672
P42345	MTOR	1537,5	19,30168694
O75369	FLNB	1450,7	17,37125288
Q5SW79	CEP170	1435,8	20,58080808
P27816	MAP4	1427,1	31,42361111
Q92538	GBF1	1395	20,81764389
Q8TEM1	NUP210	1216,6	16,37519873
Q15643	TRIP11	1210,5	20,01010611
P55196	AFDN	1195,9	17,43421053
Q641Q2	WASHC2A	1148,8	26,77106637
Q14160	SCRIB	1082,3	19,14110429

Q14008	CKAP5	1070,2	13,82874016
Q8N3C0	ASCC3	1065,9	11,94368756
Q9Y4E1	WASHC2C	1059,8	24,16666667
Q00610	CLTC	1025	17,91044776
P15924	DSP	1008,3	12,19087426
Q14C86	GAPVD1	997,3	16,37347767
P35658	NUP214	994,4	15,26315789
P50748	KNTC1	975,4	12,26799457
Q9UPU5	USP24	905	11,41221374
Q07864	POLE	885,3	10,19247594
Q12789	GTF3C1	881,9	12,70744429
Q9Y6D6	ARFGEF1	850,6	12,70957274
P42356	PI4KA	804,1	9,990485252
Q7LBC6	KDM3B	802,7	16,41113004
O60271	SPAG9	794,6	17,63815291
Q8TDY2	RB1CC1	791,3	13,86449184
O14981	BTAF1	789,9	12,49323959
O15020	SPTBN2	773,7	9,121338912
P51532	SMARCA4	730,8	11,47540984
Q9UPY3	DICER1	729,3	12,95525494
O75179	ANKRD17	639,9	8,182865924
Q6Y7W6	GIGYF2	635,3	15,39645881
Q9Y5S2	CDC42BPB	631,5	9,818819404
Q14980	NUMA1	629,3	11,30023641
Q9H1A4	ANAPC1	623,9	11,47119342
Q9UKV8	AGO2	601,3	16,99650757
Q7KZ85	SUPT6H	582,3	12,86210892
P49815	TSC2	559,1	12,56225789
P41091	EIF2S3	546,8	28,38983051
Q8NEY1	NAV1	535,5	10,76185402
P0DMV8	HSPA1A	502	17,94071763
A3KMH1	VWA8	501,6	7,979002625
Q8IWZ3	ANKHD1	477,2	6,254917388
Q9Y4G6	TLN2	468,6	5,664830842
Q9Y6D5	ARFGEF2	467,1	7,170868347
O14578	CIT	463,9	6,462752837
Q5VYK3	ECPAS	457,4	9,268292683
Q69YN4	VIRMA	449,9	7,947019868
Q5VT25	CDC42BPA	444,2	8,891454965

A6NHR9	SMCHD1	440,2	5,486284289
P42694	HELZ	439,7	7,98146241
O43432	EIF4G3	428,5	7,886435331
Q13439	GOLGA4	420,8	4,753363229
P48634	PRRC2A	418	7,974038016
Q8N201	INTS1	416,8	5,890410959
O60293	ZFC3H1	409,1	5,630970337
P11142	HSPA8	405,6	14,39628483
Q14669	TRIP12	405,2	5,722891566
P11047	LAMC1	404,5	6,463642014
P24928	POLR2A	401,2	7,208121827
Q5TAX3	TUT4	397,6	6,569343066
P35579	MYH9	390,4	7,091836735
Q3V6T2	CCDC88A	374,6	5,344735436
Q13535	ATR	370,3	4,65204236
Q96BY7	ATG2B	368,7	5,197305101
Q9Y2I1	NISCH	364,2	8,244680851
Q2KHR3	QSER1	354,2	6,167146974
Q8TEU7	RAPGEF6	351,7	7,620237352
Q9UPQ9	TNRC6B	351,6	6,437534097
Q8IWJ2	GCC2	346,7	6,294536817
Q12756	KIF1A	342,7	6,094674556
Q5T5U3	ARHGAP21	341,6	3,93258427
Q562E7	WDR81	338,2	6,543019062
A2RRP1	NBAS	338	4,301982286
Q86XA9	HEATR5A	337,7	5,931372549
Q14839	CHD4	335,7	6,171548117
Q6GYQ0	RALGAPA1	331,4	4,616895874
P07942	LAMB1	328,8	4,983202688
O60333	KIF1B	323,4	4,405286344
O14976	GAK	309,4	6,331045004
P41229	KDM5C	307,8	7,435897436
Q96AY4	TTC28	304,8	4,111245466
Q5VZL5	ZMYM4	304,5	8,010335917
P52292	KPNA2	300,1	15,31190926
Q14674	ESPL1	297,5	4,811320755
Q5VZ89	DENND4C	294,2	6,024096386
Q9H3S7	PTPN23	281,9	7,151589242
Q9H9G7	AGO3	268,5	7,093023256

Q12873	CHD3	257,3	4,9
Q08378	GOLGA3	257,2	6,141522029
Q92793	CREBBP	250,1	2,334152334
Q9P2D3	HEATR5B	248,2	3,814582327
Q9UL18	AGO1	241,8	8,401400233
Q9Y2I7	PIKFYVE	232,9	4,051477598
Q5JSL3	DOCK11	232,6	3,714423541
Q4G0J3	LARP7	224,6	7,903780069
Q2TAZ0	ATG2A	217	3,457172343
Q9ULH0	KIDINS220	216,5	4,178430265
P02786	TFRC	205	6,842105263
O14795	UNC13B	201,4	4,022627278
Q14185	DOCK1	197,2	3,699731903
O76021	RSL1D1	195,1	11,83673469
Q5VT52	RPRD2	193,8	5,065023956
Q07157	TJP1	192,9	4,576659039
Q15648	MED1	188,6	3,6685642
Q9Y2X3	NOP58	188,5	10,96408318
Q14999	CUL7	181,3	4,299175501
Q14690	PDCD11	180,7	3,527525387
Q6YHU6	THADA	179,1	3,840245776
Q9NRY4	ARHGAP35	178,4	4,202801868
Q7Z401	DENND4A	176,6	3,381642512
Q93074	MED12	174,6	2,434542949
Q8NDI1	EHBP1	172,9	6,498781478
Q96P48	ARAP1	172,4	2,896551724
O60287	URB1	169,6	2,289740203
Q09472	EP300	167,4	2,775476388
Q9BY89	KIAA1671	164,5	4,208194906
Q96SN8	CDK5RAP2	162,5	2,588483888
Q9P2K8	EIF2AK4	162,4	3,214069133
Q96HP0	DOCK6	159,6	2,784562775
P16989	YBX3	158,7	23,38709677
Q8IZL8	PELP1	156,8	6,725663717
Q9ULT8	HECTD1	150	2,413793103
P46013	MKI67	148,7	1,074938575
Q6P2E9	EDC4	147,8	3,426124197
P10412	H1-4	139,7	22,37442922
Q96RG2	PASK	139,2	3,703703704

P38646	HSPA9	136,5	5,154639175
Q6R327	RICTOR	133,7	2,224824356
P31025	LCN1	130	12,5
P09884	POLA1	127,3	3,214774282
Q9BQS8	FYCO1	127,2	4,262516915
Q9Y3R5	DOP1B	114,4	1,305483029
O95071	UBR5	114	1,107538407
Q8IZH2	XRN1	113,9	2,461899179
Q7Z406	MYH14	113,5	2,255639098
Q2PPJ7	RALGAPA2	113,1	2,349172451
O15047	SETD1A	112,3	1,698886936
O43379	WDR62	110,5	2,108036891
O15085	ARHGEF11	108,9	2,23390276
P21359	NF1	108,6	1,408946812
Q9Y520	PRRC2C	106,2	1,553867403
Q9NQT8	KIF13B	96,3	1,642935378
P13942	COL11A2	95,6	1,036866359
P42858	HTT	95,2	1,591343094
P49792	RANBP2	94	1,395781638
Q96RT7	TUBGCP6	91,9	1,429356789
O60318	MCM3AP	86,8	2,121212121
Q5JRA6	MIA3	83,6	1,678028317
Q14191	WRN	80,6	1,466480447
O15027	SEC16A	80,5	0,975816716
Q8TEQ6	GEMIN5	80,2	2,188328912
Q08AD1	CAMSAP2	78,5	1,678979181
Q5SXM2	SNAPC4	77,1	1,769911504
Q14966	ZNF638	76,9	0,960566229
Q86VV8	RTTN	75,9	1,257861635
P42695	NCAPD3	75,6	0,934579439
Q7Z3U7	MON2	75,4	1,339545719
Q9H9Z2	LIN28A	74,7	11,96172249
Q14204	DYNC1H1	74,6	0,624192854
O60361	NME2P1	74	12,40875912
Q8IWV7	UBR1	69,9	0,971983991
O14497	ARID1A	69,9	1,487964989
Q96JI7	SPG11	65,8	1,064265248
Q5JSZ5	PRRC2B	65,1	1,121579183
P50851	LRBA	64,7	0,908138316

Q9P2E9	RRBP1	64,3	1,276595745
Q00839	HNRNPU	63,3	2,181818182
Q9UG01	IFT172	62,6	1,429388222
O94822	LTN1	62,2	0,792751982
Q9UIW2	PLXNA1	61,3	1,107594937
Q9C0D5	TANC1	59,5	0,967221924
Q14571	ITPR2	58,7	0,851536468
Q9NZ53	PODXL2	57,9	2,314049587
Q13017	ARHGAP5	55,4	1,664447403
Q05707	COL14A1	55,1	2,115812918
Q7Z6E9	RBBP6	55	0,892857143
O75592	MYCBP2	54,8	0,277896537
Q14573	ITPR3	54,2	0,636465743
P53621	COPA	53,2	0,571895425
O15078	CEP290	53,1	0,363049617
P08238	HSP90AB1	52,8	1,657458564
Q04656	ATP7A	51,8	1,4
P11717	IGF2R	51,5	0,481734243
Q9P2P1	NYNRIN	50,7	0,842992624
P23246	SFPQ	50,6	2,121640736
Q7Z2Z1	TICRR	50,2	0,471204188
Q9UKJ3	GPATCH8	48,6	0,932090546
P09651	HNRNPA1	48,5	4,301075269
O43426	SYNJ1	47,7	0,76287349
Q9BZ95	NSD3	44,4	0,626304802
Q96KK5	H2AC12	43,9	14,84375
Q8TER5	ARHGEF40	43,1	0,855826201
Q9Y4F5	CEP170B	42,6	1,006922593
P62805	H4C1	41,6	11,65048544
O14744	PRMT5	41,2	1,569858713
P22626	HNRNPA2B1	40,1	4,249291785
Q9BVV6	KIAA0586	39,2	1,826484018
P08865	RPSA	39,1	5,762711864
Q9P2E3	ZNFX1	38,3	0,834202294
Q7Z4S6	KIF21A	37,2	1,015531661
Q5T4S7	UBR4	37,1	0,540227667
Q7L2J0	MEPCE	36,5	1,596516691
P06454	PTMA	36,4	12,61261261
P40926	MDH2	36	4,733727811

Q8NDV7	TNRC6A	35,7	0,458715596
P51610	HCFC1	35,6	0,835380835
O75096	LRP4	35,6	0,682414698
O75376	NCOR1	34,2	0,409836066
A6NCN2	KRT87P	33,6	7,843137255
O00429	DNM1L	33,6	1,222826087
P04406	GAPDH	32,7	4,47761194
O60346	PHLPP1	31,9	1,688992429
Q562R1	ACTBL2	31,6	4,787234043
Q8IWV8	UBR2	31,3	0,797720798
P55268	LAMB2	30,9	1,112347052
P06576	ATP5F1B	30,5	3,59168242
Q70EL1	USP54	30,5	0,890736342
Q149N8	SHPRH	30,3	0,653594771
Q8WUW1	BRK1	30,1	9,333333333

6.5 Reactome Pathways terms enrichment analysis for genes detected in RIP-YTHDF2

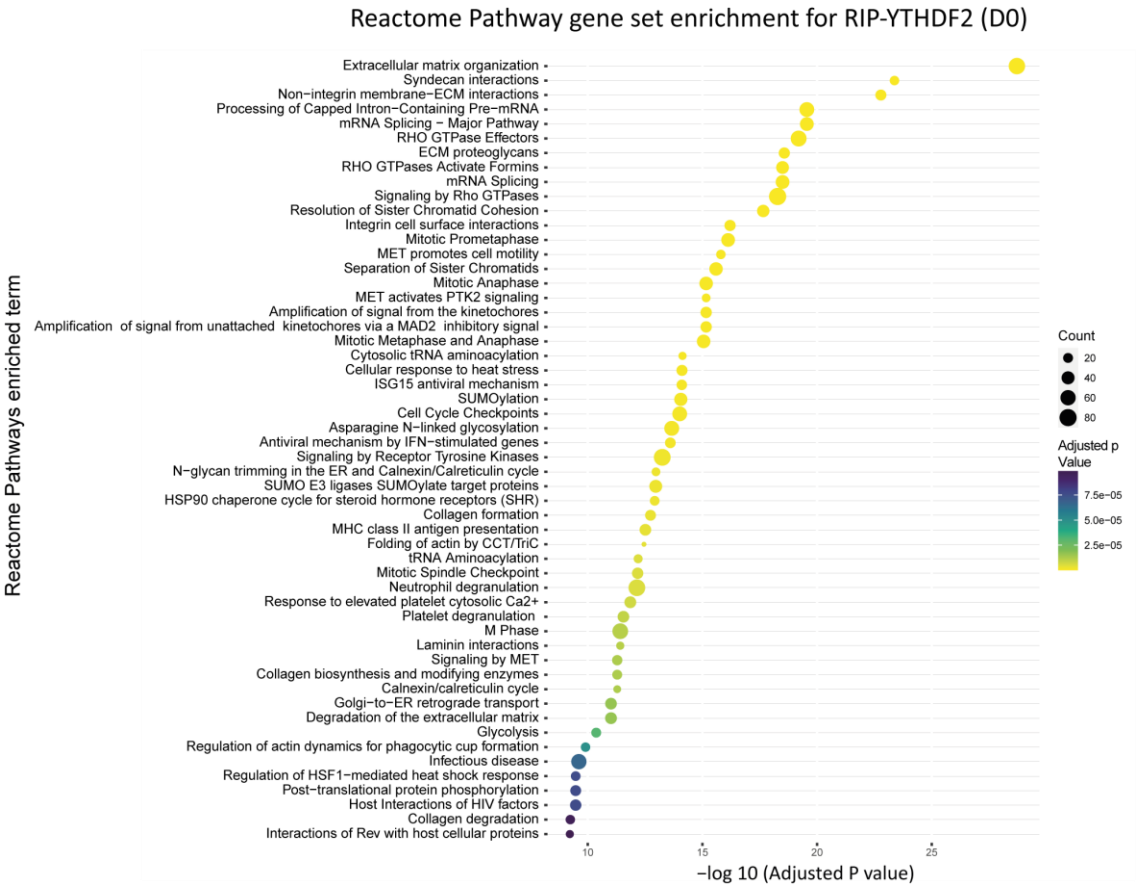

Figure 6.5.1. Term enrichment analysis of Reactome Pathways database. The main enriched terms are observed for the set of transcripts co-precipitated with YTHDF2 (RIP-YTHDF2) in proliferative human pulmonary artery smooth muscle cells (hPASMC D0, 70% confluence). The size of the dot represents the number of associated genes. The color scale represents the adjusted p value. The negative base 10 logarithm of the adjusted p value is depicted on the X axis. On the Y axis, the enriched terms ordered inversely to their adjusted p value are listed.

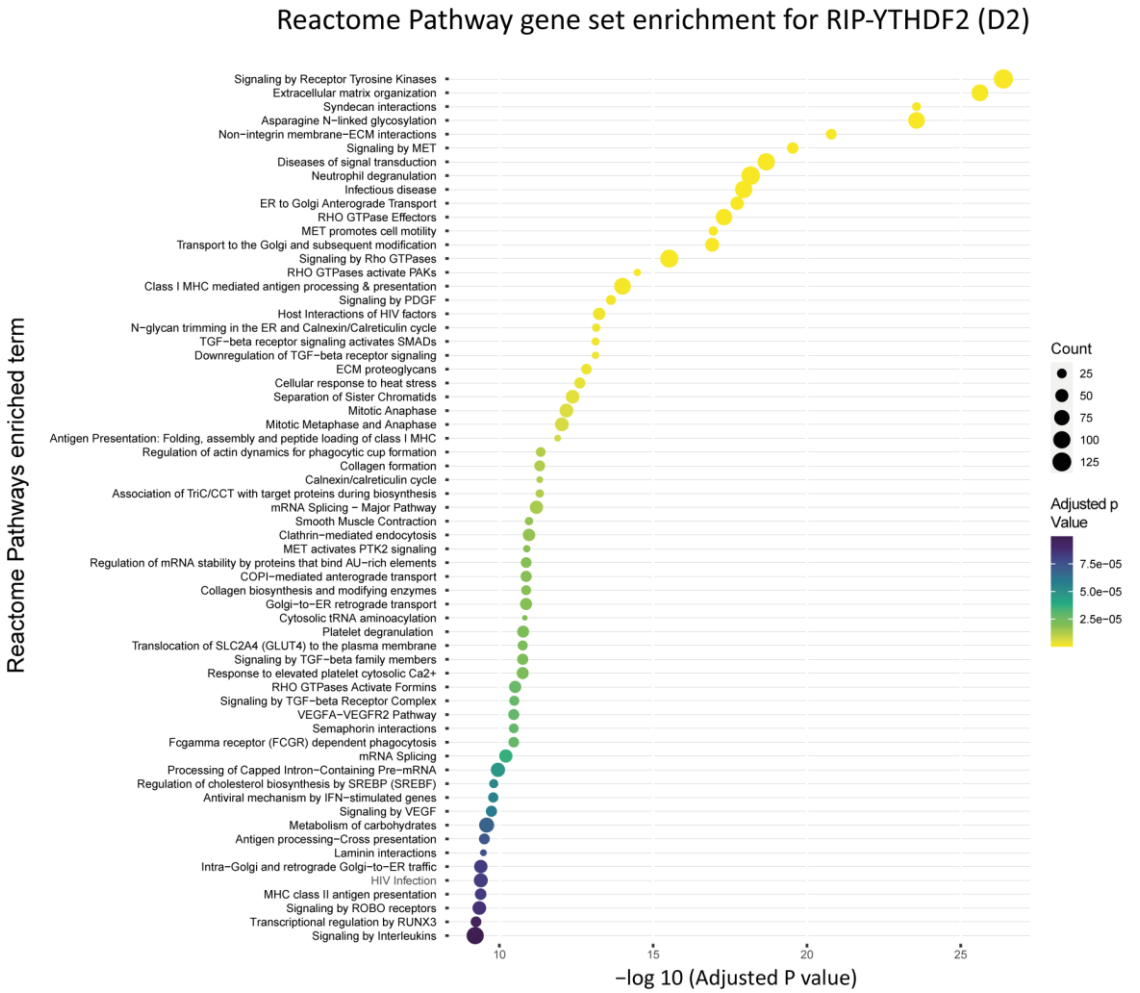

Figure 6.5.2. Term enrichment analysis of Reactome Pathways database. The main enriched terms are observed for the set of transcripts co-precipitated with YTHDF2 (RIP-YTHDF2) in human pulmonary artery smooth muscle cells at the beginning of differentiation (hPASMC D2, 100% confluence). The size of the dot represents the number of associated genes. The color scale represents the adjusted p value. The negative base 10 logarithm of the adjusted p value is depicted on the X axis. On the Y axis, the enriched terms ordered inversely to their adjusted p value are listed.

6.6 Disease Gene Network (DGN) terms enrichment analysis for genes detected in RIP-YTHDF2

Below are enrichment plots for disease-associated term gene sets from the *Disease Gene Network* database.

Disease Gene Network (DGN) gene set enrichment for RIP-YTHDF2 (D0)

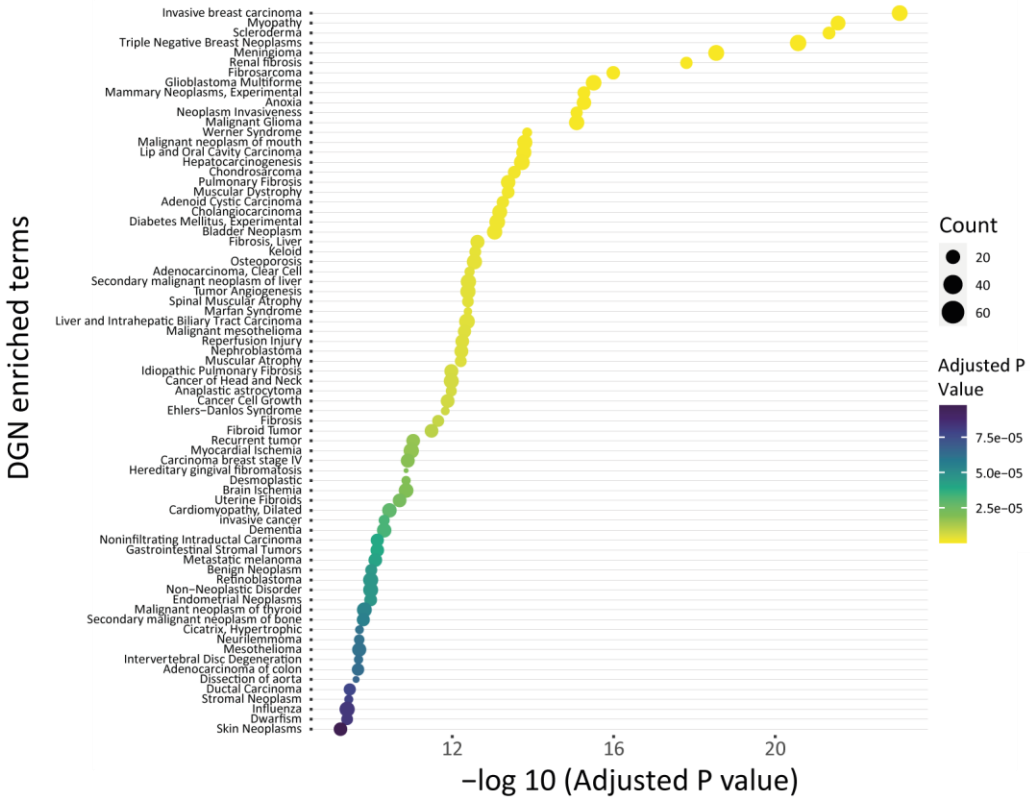

Figure 6.6.1. Term enrichment analysis of disease-associated terms from the Disease Gene Network (DGN) database. The main enriched terms for the set of transcripts co-precipitated with YTHDF2 (RIP-YTHDF2) in proliferative human pulmonary artery smooth muscle cells (hPASMC D0, 70% confluence). The size of the dot represents the number of associated genes. The color scale represents the adjusted p value. The negative base 10 logarithm of the adjusted p value is depicted on the X axis. On the Y axis, the enriched terms ordered inversely to their adjusted p value are listed.

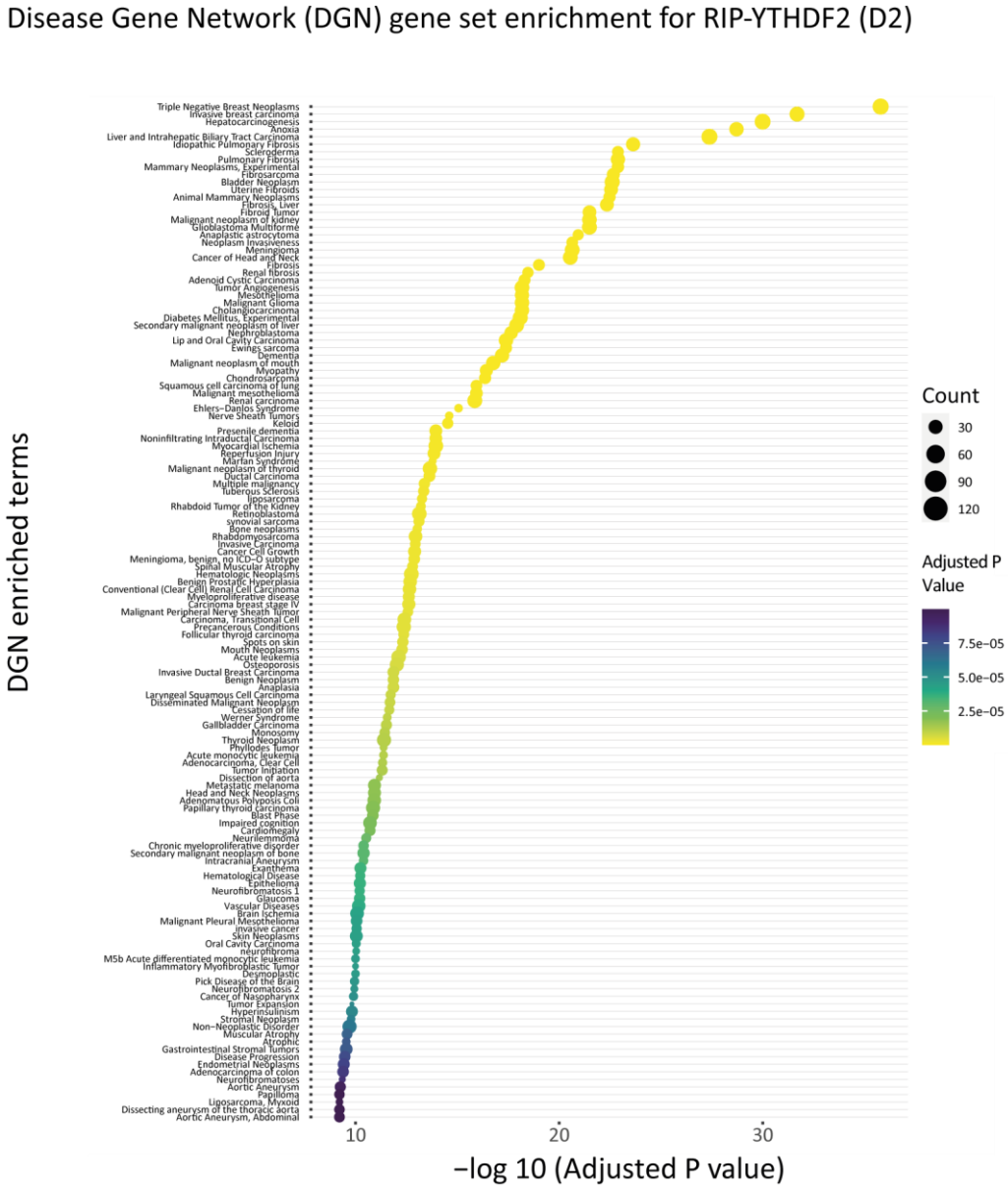

Figure 6.6.2. Term enrichment analysis of disease-associated terms from the Disease Gene Network (DGN) database. The main enriched terms for the set of transcripts co-precipitated with YTHDF2 (RIP-YTHDF2) in human pulmonary artery smooth muscle cells at the beginning of differentiation (hPASMC D2, 100% confluence). The size of the dot represents the number of associated genes. The color scale represents the adjusted p value. The negative base 10 logarithm of the adjusted p value is depicted on the X axis. On the Y axis, the enriched terms ordered inversely to their adjusted p value are listed.

6.7 Publications made in the context of the thesis

N. Col-Bonfill; **B. de la Cruz-Thea**; M. V. Pisano; M. M. Musri. **Noncoding RNAs in smooth muscle cell homeostasis: implications in phenotypic switch and vascular disorders**. PFLUGERS ARCHIV-EUROPEAN JOURNALOF PHYSIOLOGY.Berlin: SPRINGER. 2016 vol.468 n°6. p1071 - 1087. issn 0031-6768. doi: 10.1007/s00424-016-1821-x.

* #Melina M. Musri, * Núria Coll-Bonfill, Bradley A. Maron 4, Víctor I. Peinado, Wang Rui- Sheng, Jordi Altirriba, Isabel Blanco, William M. Oldham, Olga Tura-Ceide, Jessica García-Lucio, **Benjamín de la Cruz-Thea** , Gunter Meister , Joseph Loscalzo and Joan A. Barberà. **COPD- associated pulmonary vascular remodeling is linked to miRNA dysregulation**. Am J Respir Cell Mol Biol. 2018 May 14. doi: 10.1165/rcmb.2017-0040OC.

Ivana R Scolari, Ximena Volpini, María L Fanani, **Benjamín De La Cruz-Thea**, Lautaro Natali, Melina M Musri, Gladys E Granero. **Exploring the Toxicity, Lung Distribution, and Cellular Uptake of Rifampicin and Ascorbic Acid-Loaded Alginate Nanoparticles as Therapeutic Treatment of Lung Intracellular Infections**. Molecular Pharmaceutics. 2021 Mar 1. 18(3):807-821. doi: 10.1021/acs.molpharmaceut.0c00692.